Studies on Dynamical Mechanisms of the Reactions of Some Nitrogen-Containing Intermediates

Keiichi Yokoyama

Faculty of Engineering Science

Osaka University

1991

Preface

This thesis is a collection of the author's studies conducted to demonstrate usefulness of combining theoretical calculations with experimental observations for the investigations of chemical reactions. Specific aims have been to clarify the dynamic mechanisms of elementary reactions which some nitrogen-containing intermediates undergo in the gas phase. The studies have been carried out under the direction of Professor Takayuki Fueno at Osaka University during 1985 - 1991.

The thesis consists of two parts as follows:

I. Dynamisms of the reactions of the imino radical $NH(X^3\Sigma^-, a^1\Delta)$ with XO (X= N, O, and C).

II. Mechanisms of the disproportionation reaction of nitric oxide NO in the presence of the hydrogen atom.

In the first part, the reaction rates and products distributions as well as the dynamic paths were studied by theoretical approaches involving ab initio MO calculations with the MRD-CI method and by experimental approaches involving photolyses in the gas phase as well as argon matrices and pyrolysis behind incident shock waves. In the second part, a chain mechanism progressing in gaseous NO in the presence of a small amount of the H atom was elucidated by gas-phase experiments involving the flash photolysis technique and by theoretical calculations based on the APUMP2 method.

The author wishes to express his deepest gratitude to Professor Takayuki Fueno, who introduced him to this area of research, for his valuable guidance and direction, and for his continuous encouragement throughout his investigations.

He would like to express deep gratitude to Associate Professor Tadashi Okuyama for his kind advice and helpful direction. He is deeply grateful to Professor Kizashi Yamaguchi for his hearty encouragement. Deep appreciation should also be directed to Dr. Kunihisa Yoshida for his instructive suggestion.

The author thanks Messrs. Masayuki Fukuda, Shin-ya Takane, Hiroshi Kitaike, and Katsuji Miyake for their active collaboration and hot discussions. Without their technical aids this thesis would have never been completed. He also thanks Messrs. Masayoshi Nakano, Mitsutaka Okumura, Jun'ichi Kitagawa, Tsuyoshi Yorizane, and other members of the Fueno Laboratory for their friendly and continuous encouragement throughout the course of studies.

The numerical calculations were carried out on HITAC M680H, S810/10, and S820/10 computers at the Institute for Molecular Science.

Last but not least, the author is grateful to his parents, Tsutao and Yaeko Yokoyama, and his grandmother, Hiroko Yokoyama for their kindly encouragement and all kinds of support to everything he faced during the course of studies.

Keiichi Yokoyama

January, 1991

Contents

General Introduction

It is of fundamental important to chemistry to understand chemical reactions in dynamical terms. Chemical bondings arise from the electron-electron and nucleus-electron interactions as well as the internuclear repulsions , so that chemical reactivity of molecules is governed by their electronic structure. Generally, the potential energy of molecules involves the *electronic energy* as well as nuclear repulsion energy. An elementary reaction can thus be regarded as the motion of a mass-point on the potential energy surface, which spans geometries of the reacting molecular system. In particular, accurate characterizations of the stationary points (energy minima and saddle points) on the potential energy surfaces are essential in understanding the reactivity, such as reaction rate, product distribution and energy disposal in the products. The mechanism placing emphasis on the microscopic molecular-structural notion of reaction processes may be called "Dynamical Mechanism" or more simply "Dynamism".

The electronic energies differ depending on the electronic structures. Each electronic state individually owns its potential energy surface. In the course of reaction, the interactions between these surfaces such as intersystem crossing, avoided crossing and conical crossing often play important roles.

The author has felt much interest in such dynamical mechanisms of reactions of some systems containing the nitrogen atom. Nitrogen has an electronically curious character inherently. For example, there are some questions why gaseous NO and NO_2 having an unpaired electron can exist at room temperature under the atmospheric pressure. On the contrary, why is HNO unstable despite its closed-shell electronic structure? Chemical behavior of nitrogen still remains unexplored as compared to carbon and oxygen.

In the present study, kinetics and product distributions have been examined by the gas-phase and matrix experiments, which are appropriate for investigating elementary reactions under isolated conditions. For the initiation of reactions, the

author used the thermal decompositions in shock waves and the photo-decompositions in argon matrix as well as in the gas phase. Further, ab initio molecular orbital calculations have been performed to obtain the potential energy surfaces relevant to the reaction systems considered. Recent developments of theories, algorithms and equipments for the computational chemistry provide reliable tactics to investigate the reactions of small molecules containing at least 10 atoms. In fact, it has become available to apply a large-scale cofiguration-interaction (CI) method, complete-active-space self-consistent-field (CASSCF) calculations and the Møller-Plesset (MP) perturbation theory with fairly large basis sets including polarization functions. On account of the accuracy of such calculations, these theoretical approaches may be regarded as "computational *experiment*" rather than "approximate *prediction*".

Combinations of these experimental and theoretical approaches will hopefully present a great advantage to the understandings of reaction dynamism. The author will demonstrate the efficiency of such combinations in this thesis. In some cases (I - 1-4) the theories led the experiments, and in other cases (I - 5,6) the experimental results motivated the theoretical investigations. In a certain case (II - 1,2) both approaches were complementary and mutually indispensable.

In part I, the mechanisms of the reaction of $NH(^3\Sigma^-, {}^1\Delta)$ with XO (X = N, O, C) were investigated. Reactivity of the imino radical NH is interesting in view of the relation of the electronic structures to the reaction types. Its electronic ground state has the triplet spin multiplicity ($X^3\Sigma^-$) while the first excited state is a metastable singlet state ($^1\Delta$), as in the case of the isoelectronic oxygen atom. However, the reactivity of NH has not yet been studied as comprehensively as has been that of the O atom.

Nitric oxide $NO(X^2\Pi)$ has one odd electron. The reaction is expected to start with an association step to form HNNO intermediate in the case of both $NH(^3\Sigma^-)$ and ($^1\Delta$). The potential energy profiles for the NH-NO system has been calculated by the multi-reference single- and double-excitation CI (MRDCI)

method in chapter 1. The results have revealed that the reactions of both $NH(^3\Sigma^-)$ and $(^1\Delta)$ proceed without any activation energy and produce N_2O + H mainly and N_2 + OH subsidially. In order to examine the primary channel of the reaction $NH(^1\Delta)$ + NO, the N_2O quantum yield was measured in the photolysis of hydrazoic acid HN_3 in the presence of a controlled amount of NO (chapter 1). The same reaction was examined in 12 K argon matrix, in which the isolated molecules have little mobility, so that the reaction was expected to be trapped without subsequent reactions (chapter 2). The overall rate constant and the rate constant of the OH formation for the reaction $NH(^3\Sigma^-)$ + NO were measured in incident shock waves at high temperature (~3500 K) (chapter 3). A chemiluminescence of OH was also discovered. The results of these various kind of experiments at largely different temperatures have confirmed the validity of the theoretical results.

Molecular oxygen $O_2(X^3\Sigma_g^-)$ has two odd electrons. The first step of the reaction $NH(^3\Sigma^-)$ + O_2 is expected to be a non-barrier association step, as in the case of NH + NO. However, the potential energy profiles calculated by the MRDCI method have revealed that the subsequent unimolecular rearrangements of HNOO would require net activation energies. A novel reaction pathway involving an intermediacy of NOOH has been proposed (chapter 4). The non-Arrhenius behavior of the reaction has been reconciled by the tunneling effect operative at the rate-determining step.

Carbon monoxide $CO(X^1\Sigma^+)$ has no odd electrons. The addition step of $NH(^3\Sigma^-)$ + CO may have a significant activation barrier, while the reaction $NH(^1\Delta)$ + CO would form HNCO without any activation energy. HNCO is extremely stable. These two surfaces would cross at a certain CN distance in the course of addition. Thus, the former reaction would also form HNCO through the crossing. Formation of the CN radical was observed in the shock tube study of HNCO. The results indicate the occurrence of an isomerization from HNCO to HOCN (chapter 5). The potential energy surface for NH-CO system has been

obtained by the CASSCF and MRDCI methods. A possible isomerization path has been found (chapter 6).

In part II, chemical behavior of NO in the presence of the hydrogen atom has been studied both experimentally and theoretically. HNO, the initial adduct formed by the reaction H + NO, is known to be unstable in gaseous NO, but reaction products have not been established yet. Because of the rather modest radical character of NO, the reaction mechanism is intriguing. In chapter 1, product analyses based on the FTIR spectroscopy were carried out in the photodecompositions of HCHO and CH_3ONO and in the flash photolysis of NH_3 under rich NO conditions. the results have suggested a chain mechanism. In chapter 2, theoretical calculations involving the approximately projected unrestricted MP perturbation theory at the second order were carried out to unravel the complicated mechanism of the NO disproportionation in the presence of the H atom.

Part I

Dynamisms of the Reactions of the Imino Radical $NH(^3\Sigma^-,^1\Delta)$ with XO (X = N, O, C)

Chapter 1

Mechanism of the Reaction $NH(^1\Delta) + NO \longrightarrow N_2O + H$ in the Gas Phase

Hydrazoic acid HN_3 was photolyzed in the presence of a controlled amount of NO in the gas phase, to investigate the reaction of $NH(^1\Delta)$ with NO. Ab initio CI studies indicate that the ultimate product should be N_2O, which would arise via an intermediacy of the adduct radical $HNNO(^2A')$. Mass-spectrometric analyses of the reaction mixtures have shown that N_2O is indeed a principal product but that a sizable quantity of H_2O has been formed concurrently. Quantum yields of N_2O are found to increase in proportion to the initial molar fractions of NO in the reactant gas mixtures used. It is concluded that $NH(^1\Delta)$ enters into capture (no-barrier) reactions with NO and HN_3 in a competitive manner, to give N_2O and NH_2, respectively, the latter product eventually leading to H_2O through a rapid capture reaction with excess NO.

1. Introduction

The imino radical in its lowest singlet state NH($a^1\Delta$) can insert into a single bond of paraffins to give amines and, at the same time, directly abstracts a hydrogen atom giving rise to the amino radical [1]:

$$NH(^1\Delta) + H\text{-}R \longrightarrow H_2NR \qquad (1a)$$

$$NH(^1\Delta) + H\text{-}R \longrightarrow NH_2 + R \qquad (1b)$$

Obviously, reaction (1a) is a concerted process with virtually no activation energy, whereas reaction (1b) is an activation-controlled process. The activation barrier heights for reaction (1b) are, however, generally so low as to permit the hydrogen abstraction to compete with the insertion (1a), as has been demonstrated theoretically [2]. More important in this context is the notion that this dual chemical behavior of NH($^1\Delta$) is a consequence of the duality in its electronic structrue. Thus, the insertion capability is ascribable to the closed-shell-like character of the $^1\Delta$ state which can be represented by the two-configurational (x^2-y^2) wavefunction, while the abstraction mode is due to the diradical property arising from its open-shell (xy) character [3-5].

Inasmuch as NH($^1\Delta$) in its open-shell form can be regarded as a singlet diradical, its diradical character ought to be revealed most eminently when it is allowed to react with radical species. Thus, the association reactions of NH($^1\Delta$) with doublet radicals are thought to constitute another important type of elementary reactions possible to NH($^1\Delta$).

Motivated by the above-delineated perspective, we have undertaken to investigate the reaction of NH($^1\Delta$) with NO as a doublet radical. Ab initio SCF computations followed by the configuration-interaction (CI) treatments indicate that the association product HN-NO is liable to be collapsed into N_2O and H:

$$NH(^1\Delta) + NO \longrightarrow [HN\text{-}NO] \longrightarrow N_2O + H \qquad (2)$$

The possibility of a similar type of reaction for the case of $NH(^3\Sigma^-)$ has been suggested by Melius and Binkley [6].

The purpose of the present work is to clarify the dynamical mechanism of reaction (2) theoretically and to confirm the formation of nitrous oxide N_2O experimentally. To this end, the path as well as the energetics of reaction (2) has been examined theoretically and the quantum yields of N_2O under varying conditions have been determined experimentally. Rather unexpectedly, it has been observed that a sizable amount of H_2O is formed concurrently with N_2O. The overall mechanism of reactions will be discussed in the light of the theoretical as well as the experimental results obtained.

2. Methods

(A) Theoretical calculations

The potential energy profiles for the reactions of both $NH(X^3\Sigma^-)$ and $NH(a^1\Delta)$ with NO have been examined by ab initio MO calculations. The basis sets used are the conventional split-valence 4-31G functions [7] augmented with one set each of polarization functions for every atom involved. The exponents used for the polarization functions are $\zeta_p(H) = 1.1$ and $\zeta_d(N) = \zeta_d(O) = 0.8$ [8].

The minimum-energy paths for reactios were traced by the UHF SCF procedure, using the Gaussian-80 program package [9]. Geometries for the stable energy minima and the energy saddle points (transition states, TS) were all SCF-optimized. The transition state geometries were all checked with the vibrational normal-mode analyses.

All the transition states located as well as the relevant energy-minimum structures were subjected to the multireference double-excitation (MRD) configuration-

interaction (CI) computations (4-31G**//4-31G**). The Table MRD-CI program furnished by Buenker [10,11] was used. The configurations whose contributions $|c_i|^2$ to a state exceed 0.5 % were all regarded as the main (reference) configurations. The lowest configuration-selection threshold T was deliberately assigned a value between 1 and 10 μhartrees, so that the maximal dimension of the configurational space fell in the region 7000 - 9000. Four successive threshold values increasing stepwise by 5 μhartrees each were used to obtain the CI energy $E_{CI,T\rightarrow 0}$ extrapolated to $T = 0$ hartree. The generalized Langhoff-Davidson approximation [12,13] was used to correct for possible errors which might arise from the use of a limited number of reference configurations. The CI energies thus corrected are regarded as estimates of full CI values [13,14] and will be denoted as E_{CI}.

(B) Experimental

Mixtures of 1-7 Torr of HN_3 with 3-40 Torr of NO and 0-200 Torr of SF_6 were photolyzed for 0.5-4 h at room temperature. The light source used was a 450-W medium-pressure mercury lamp (Ushio UM-452). A combination of solution filters (aq. $NiSO_4$, aq. $CoSO_4$ and a cyclohexane solution of 1,4-diphenyl-1,3-butadiene) was used to isolate the 254 nm light for the photolysis. The effective band pass of the combined filters was 240 - 270 nm. The photolyzing light collimated with a quartz lens (f=110 mm) was led into a reaction cell. The reaction cell used was a quartz cylinder of 102 mm in length and 12 mm in diameter. The light that had passed through the cell was collected in a phototube (Hamamatsu Photonics R-840) for recording.

After the photolysis, the reaction mixture was kept at -196 °C for ca 1 h. The condensate was degassed at -196 °C and, after having been allowed to stand at room temperature for ca. 1 h, was subjected to gaschromatographic analysis. A 2.5-m column of Porapak Q was used at 25 °C with a stream (18 cm3/min) of He as carrier. The principal product was identified to be N_2O; the observed retention time 4.5 min agreed with that for an authentic gas sample of N_2O.

Determinations of N_2O formed were conducted on a quadrupole mass-spectrometer (ULVAC MSQ-150A). In preliminary experiments, it was found that the mass signal for SF+ (m/e = 51) as a fragment ion from SF_6 was stable enough to be used as a reference for the determination of N_2O. The relative peak heights for N_2O+ (m/e = 44) and SF+ were calibrated for gas mixtures of N_2O and SF_6 of known concentrations. It was confirmed that the peak-height ratios stayed invariant during the time interval (usually 10 min) required for the analysis. The nonvolatiles (at -196 °C) of the reaction gas mixtures were introduced into the ionization-room of the mass-spectrometer through a variable-leak bulb at room temperature. The mass spectra were recorded on a pen recorder.

The $NH(^1\Delta)$ radicals generated by the present photolysis are typically ca. 1 % the HN_3 sample used. The total amount of NH generated in each run can be assumed to equal the total number of photons absorbed in the photolysis, since the quantum yield of $NH(^1\Delta)$ from HN_3 by the 254 nm light is known to be nearly 1.0 [15]. The amount of photons absorbed were calculated from the amount of the incident photons, using the absorption coefficient of HN_3 previously determined, (254 nm at 23 °C) = 1.40×10^{-3} $Torr^{-1}cm^{-1}$ [1]. The intensity of the incident light was measured with a phototube calibrated by chemical actinometry. A $K_3Fe(C_2O_4)_3$ 1,10-phenanthrolin system was used for the chemical actinometry [16].

The quantum yields of N_2O were obtained from the total amount of N_2O formed and the amount of photons absorbed by the reaction mixture. The N_2O quantum yields are thus the molar yields of N_2O formed per one mol of $NH(^1\Delta)$ generated.

HN_3 was synthesized and purified by means of the trap-to-trap distillation at -80 °C and -196 °C. It was stored in a 5-l pyrex bulb. A portion of it was degassed each time immediately prior to use. Both NO and SF_6 of high purity were purchased and used after appropriate degassing.

3. Results

(A) Potential energy profiles

It is presumed intuitively that the primary step of the reaction between NH and NO is the association reaction giving a doublet adduct HN-NO. Under this presumption, the optimal structure for the adduct radical was explored by the UHF SCF procedure. Two planar doublet structures are conceivable. One is a doublet(^{2}A") of the allyl radical type with three π-electrons delocalized over the NNO skeleton, while the other is such a doublet(^{2}A') that four electrons are accommodated in the π orbitals, leaving the unpaired electron in an a' orbital of the skeleton:

^{2}A", ...(1a")^2(9a')^2(2a")(10a')^2

^{2}A', ...(1a")^2(9a')^2(2a")^2(10a')

For either of the two doublets, the cis and trans forms are possible. These four structures will be denoted as 3C, 3T, 4C and 4T. Thus, 4T, for example, should be read as indicating the four-π-electron form (2A') in the trans arrangement of the four atoms. The optimized geometries for the four radicals are given in Fig. 1.

Tracings of the minimum-energy paths by the SCF procedure have indicated that both 4C and 4T are connected with NH($^1\Delta$) + NO, whereas 3C and 3T with NH($^3\Sigma^-$) + NO. Clearly, NH($^3\Sigma^-$) attacks the singly occupied orbital (a') localized on the N atom of NO. The NH($^1\Delta$) radical, on the other hand, appears to attack the π bond orbital of NO.

MRD-CI calculations for the SCF optimized geometries have shown that the effects of electron correlation are much greater in the ^{2}A' radicals (4C and 4T) than in the ^{2}A" radicals (3C and 3T), as can be seen in Table 1. In terms of the CI energy E_{CI}, the former doublets are significantly more stable than the latter, the total energies of the four radicals relative to the NH($^3\Sigma^-$) + NO system as a common

reference being -77 (3C), 54 (3T), -252 (4C) and -254 (4T) kJ/mol. Thus, the association reaction of our present concern

$$NH(^1\Delta) + NO \longrightarrow HN\text{-}NO\ (^2A') \qquad (3)$$

is predicted to have an exothermicity of ca. 430 kJ/mol.

Possible pathways for the subsequent fragmentation of the $^2A'$ radical are

$$HN\text{-}NO\ (^2A') \begin{cases} \longrightarrow HNN(^2A') + O(^3P) & (4a) \\ \longrightarrow N_2O(^1\Sigma^+) + H & (4b) \\ \longrightarrow N_2 + OH(^2\Pi) & (4c) \end{cases}$$

Reaction (4a) is endothermic and has no activation barrier, whereas both reactions (4b) and (4c) should be elementary processes involving the activation energies [6]. Because reaction (4c) is possible only for the cis form of $HNNO(^2A')$, we have considered the reactions (4a)-(4c) for the 4C isomer primarily. The energy changes of reaction ΔE_{CI} calculated for reactions (4a)-(4c) are 278, 123 and -135 kJ/mol, respectively.

Geometries for the transition states, TS1 and TS2, for reactions (4b) and (4c), respectively, have been optimized by the 4-31G** SCF procedure. The optimal structures obtained are shown in Fig. 2. Both geometries closely resemble those that have recently been reported by Marshall, Fontijn and Melius [17] for the same reactions.

MRD-CI calculations were carried out for both TS1 and TS2 at their SCF optimized geometries. The activation barrier heights $\Delta E^{\ddagger}$ obtained for reactions (4b) and (4c) are 201 and 214 kJ/mol, respectively. It has been confirmed that use of the one-electron functions obtained by the quartet ($^4A'$) SCF calculations in place of the doublet ($^2A'$) SCF procedure does not alter the results appreciably (by no more than 5 kJ/mol). Reaction (4b) thus appears to be more favorable than reaction (4c), in

agreement with the feature demonstrated by Marshall et al. [17], even though both of our $\Delta E^{\ddagger}$ values are somewhat greater than theirs. At any rate, it is clear that the adduct radical 4C formed by reaction (3) is liable to decompose spontaneously in the gas phase, inasmuch as the exothermicity for reaction (3) (430 kJ/mol) far exceeds the activation barrier heights for the subsequent fragmentation processes. The most probable path of fragmentation should be reaction (4b), which gives $N_2O(^1\Sigma^+)$.

A few words seem to be in order regarding TS1. The optimal geometry located is in a planar cis form, as is shown in Fig. 2. Because TS1 is smoothly connected with 4C through the minimum-energy path over the potential energy surface, there is no doubt that 4C is subject to the N-H bond breaking reaction (4b). When the N-H bond of 4T is elongated, however, it is found that the bond angle ∠NNO increases progressively until the whole system takes on a cis structure to reach the same transition state (TS1) eventually.

In order to look into the dynamical mode of isomerization more closely, the path for the isomerization 4T→4C has been traced by the SCF procedure. As a result, it has proved that the minimum-energy path for the isomerization is such that the O atom migrates on the molecular plane. The transition state (TS3) located is planar in geometry with the bond angle ∠NNO being nearly 180 °, as is shown in Fig. 2. A similar (in-plane inversion) mode of the trans-cis isomerization has been noted with diazene HN=NH [18] and difluorodiazene FN=NF [19] theoretically. For the present instance of isomerization (TS3), CI calculations have given the barrier height $\Delta E^{\ddagger}$ = 83 kJ/mol, which is evidently lower than the activation barrier height $\Delta E^{\ddagger}$ = 201 kJ/mol calculated for the N-H bond braking reaction (4b) of 4C. No doubt, the N-H bond scission of 4T suffers the trans-cis isomerization before the scission is completed.

As for the fragmentation of the $^2A''$ radical, the energetically most favorable is the cleavage of the N-O bond:

$$HN\text{-}NO\ (^2A'') \longrightarrow HNN(^2A') + O(^3P) \qquad (5)$$

The HNN radical is liable to be decomposed into N_2 + H via the transition state (TS4). The barrier height calculated by the present CI procedure is 69 kJ/mol, which does not differ greatly from the value of ca. 46 kJ/mol reported by Pople et al. [20].

The overall potential energy profiles calculated for the NH + NO system are diagrammatically illustrated in Fig. 3. The energy gaps given in square brackets are the empirical estimates made on the basis of the experimental thermochemical data [21]. The calculated energy gaps shown in Fig. 3 will generally be accurate only to within 20 kJ/mol. Yet, they will be reliable enough to permit the conclusion that the reaction of $NH(^1\Delta)$ with NO will lead to the formation of N_2O as the principal product.

(B) Quantum yields of N_2O

In order to confirm that N_2O is the ultimate main product of reaction (2), we have attempted determinations of the quantum yields ϕ of N_2O under various conditions. By the quantum yields we mean the yields of N_2O per one mole of $NH(^1\Delta)$ generated photochemically. Determinations of ϕ_{N2O} entail quantitative determinations of $NH(^1\Delta)$ generated in given runs and of N_2O formed in the cell. Actinometry and mass-spectroscopy have been conducted for this purpose, as has been described in the experimental section.

Table 2 gives some representative data obtained under varying initial concentrations of HN_3 and NO at room temperature. The ϕ_{N2O} data listed inevitably involve experimental errors amounting to 0.05. Nevertheless, it does appear that ϕ_{N2O} is increased with the increase in the initial concentration of NO, even though the reactant NO has been used always in large excess over the $NH(^1\Delta)$ radicals generated.

In Fig. 4, the quantum yields ϕ_{N2O} are plotted against the initial molar fraction of NO:

$$x_{NO} = \frac{[NO]_0}{[HN_3]_0 + [NO]_0} \qquad (6)$$

for a total of 15 runs. Although the plotted points are somewhat scattered, ϕ_{N2O} does appear to be proportional, to a first approximation, to x_{NO} with the proportionality factor $\eta = 0.70$. η may be understood as a partial rate factor with which the adduct radical HNNO will select the decomposition channel (4b) to give N_2O; $\eta = k_{4b}/(k_{4a} + k_{4b} + k_{4c})$.

The observed proportionality, though somewhat crude, between ϕ_{N2O} and x_{NO} suggests that part of $NH(^1\Delta)$ has been consumed by reactions with the coexisting HN_3. The most probable is the hydrogen abstraction reaction as follows [22]:

$$NH(^1\Delta) + HN_3 \longrightarrow NH_2 + N_3 \qquad (7)$$

The quantum yield of N_2O should then be controlled by the competition between reactions (2) and (7). More precisely speaking, $NH(^1\Delta)$ is consumed by reactions (3) and (7), while N_2O is formed by reaction (2). Denoting the rate constants for reactions (3) and (7) by k_3 and k_7 and noting that the effective rate constant for reaction (2) should be $k_2 = \eta\, k_3$, we may write

$$\phi_{N_2O} = \eta \frac{(k_3/k_7)x_{NO}}{(k_3/k_7)x_{NO} + (1\text{-}x_{NO})} \qquad (8)$$

as a more reasonable expression of ϕ_{N2O} as the function x_{NO}. Equation (8) reduces to $\phi_{N2O} = \eta\, x_{NO}$, when $k_3/k_7 = 1$

Variations in ϕ_{N2O} as the function of x_{NO}, eq. (8), for the varying ratio k_3/k_7 are represented by the curves shown in Fig. 4. The ratio k_3/k_7 giving the best fits of the experimental data points to eq. (8) has been searched for by the least-squares treatment of the data under the constraint $\eta = 0.70$. The resulting k_3/k_7 ratio was found to be 0.79 + 0.06, the uncertainty limit indicating the probable error. The rate

ratio between reactions (2) and (7) will then be $k_2/k_7 = 0.55 \pm 0.05$. The result can be taken as an indication that, if reaction (2) is a collision-controlled (no-activation-barrier) process, so will reaction (7) be essentially. Reaction (7) should be about twice as fast as reaction (2).

Mass-spectrometric analyses of the product mixtures have indicated that, in the runs where x_{NO} is relatively small, a sizable amount of H_2O has been formed concurrently. Occurrence of H_2O must somehow be related to reaction (7). We assume that the formation of H_2O is ascribable to the reaction

$$NH_2 + NO \longrightarrow [H_2N\text{-}NO] \longrightarrow H_2O + N_2 \qquad (9)$$

which will immediately follow reaction (7). Because H_2O has been formed concurrently with N_2O and because both reactions (2) and (7) are likely to be collision-controlled, reaction (9) must also be a collision-controlled process.

4. Discussion

As has already been mentioned, the accuracy limit of the present CI calculations is at best 20 kJ/mol for stable energy minima. The situation requires particular cautions on the reliability of the energies calculated here for the various transition states.

The transition states of utmost importance in this work are TS1 and TS2. Some assessments of the energetics calculated for these states are possible in reference to the experimental kinetic results [17] for the reaction

$$N_2O + H \longrightarrow [HNNO] \longrightarrow N_2 + OH \qquad (10)$$

The transition states for the first and second steps of reaction (10) are nothing but our TS1 and TS2, respectively. According to the results of our CI calculations, the

barrier height for the first step is 78 kJ/mol while that for the second step relative to N_2O + H is 91 kJ/mol (see Fig. 3). When the vibrational zero-point energy corrections are made, these barrier heights are slightly enhanced to $\Delta H^{\ddagger}$ = 79 and 96 kJ/mol, respectively. The experimental study of reaction (10) shows that the second step is rate-controlling and that the net activation energy relative to N_2O + H is 81 kJ/mol [17]. Our predicted heats of activation ($\Delta H^{\ddagger}$) are in harmony with the experimental results, although $\Delta H^{\ddagger}$ = 96 kJ/mol for the second step is still 15 kJ/mol too high as compared to the experimental activation energy (81 kJ/mol). We believe that the accuracy of the present calculations is within a range of 20 kJ/mol even for the transition states. Incidentally, the MP4 calculations with the bond-additivity corrections (BAC) and spin contamination corrections by Marshall et al. [17] give the heats of activation 15 and 70 kJ/mol for the steps 1 and 2, respectively. Their results are significantly lower than the $\Delta H^{\ddagger}$ values (79 and 96 kJ/mol) obtained in the present study.

The theoretical expectation that the reaction between $NH(^1\Delta)$ and NO gives N_2O as the ultimate principal product has been corroborated experimentally. The reaction should be a two-step process involving the intermediacy of the adduct radical HN-NO ($^2A'$). Because the barrier top of the subsequent step, i. e., the N-H bond cleavage of the adduct radical (reaction (4b)), lies below the energy level for the initial binary system $NH(^1\Delta)$ + NO, the initial association step (3) should control the overall rate of reaction. Thus, reaction (2) as a whole should essentially be a collision-controlled process, which has no activation energy.

Under our experimental conditions, $NH(^1\Delta)$ should react with HN_3 also (reaction (7)). The bimolecular rate constant 5.6×10^{13} $cm^3mol^{-1}s^{-1}$ observed for reaction (7) [22] indicates that the reaction is indeed collision-controlled. Reaction (7) competes with reaction (2) thus affecting the quantum yield of N_2O. It is our feeling that reaction (7) is also a two-step process involving the initial insertion of $NH(^1\Delta)$ into the NH bond of HN_3.

The decrease in ϕ_{N2O} with the decreasing initial molar ratio of NO (Fig. 4) is counterbalanced by the increase in the yield of H_2O. We interpret this fact to be a consequence of the operation of reaction (9) which immediately follows reaction (7). So far as both HN_3 and NO are present in large excess over $NH(^1\Delta)$ as is actually the case, all the NH_2 radicals formed by reaction (7) will be led to H_2O if reaction (9) is assumed to be as rapid a process as the collision-controlled reaction (7). This last assumption seems to find support in the potential energy profiles calculated by Melius and Binkley [6]. The reaction is reported to be a multi-step process which involves the initial association of NH_2 with NO to form H_2NNO and the subsequent H-atom migrations, thereby ending up with the formations of H_2O and N_2 as stable products. They conclude that the various barriers which the adduct molecule has to overcome before reaching the final state $H_2O + N_2$ all lie below the energy level for the initial state NH_2 + NO. Reaction (9) can, therefore, be considered to proceed as rapidly as most association reactions which are basically collision-controlled. In fact, the rate constants observed for reaction (9) in the ordinary temperature region is on the order of 1×10^{13} $cm^3mol^{-1}s^{-1}$ [23].

The quantum yield of N_2O in the high NO fractional limit $x_{NO} = 1$ is 0.7. The remaining fraction 0.3 is probably ascribable to the operation of reaction (4c) as a less favorable fragmentation process of 4C. Although no special efforts have been made to determine the branching ratios of reaction (4) in this work, the partial rate factor as large as 0.3 for reaction (4c) is a likely possibility, since TS2 is calculated to be only slightly (by 13 kJ/mol) higher than TS1. Fragmentation to $NH(^3\Sigma^-)$ + NO will be much less favorable. Direct quenching of $NH(^1\Delta)$ to $NH(^3\Sigma^-)$ on collisions with NO will also be ignorable [1].

Finally, we would like to comment on the observed rate ratio $k_3/k_7 = 0.79$ briefly. Because reactions (3) and (7) are both collision- controlled, the relative rate constants k_3 and k_7 will be governed by the relative magnitudes of their preexponential factors. If so, the trend that $k_3/k_7 \leq 1$ is reasonable in view of the inherently smaller collision diameter for NO as compared to HN_3 which is apparently

a larger molecular species. In addition, the insertion of NH($^1\Delta$) into propane, a chemical reaction which is also a no-activation-barrier process, is reported to have the rate constant k_{1a} 0.30 times as large as k_7 [1]. The tendency that $k_{1a}/k_7 < k_3/k_7$ is also reasonable in view of the difference in type between reactions (1a) and (3); the former reaction is a concerted multi-site process, whereas the latter is essentially a simple association reaction, for which the activation entropy should be innately larger.

References

1) O. Kajimoto and T. Fueno, Chem. Phys. Lett., **80**, 484 (1981); O. Kondo, J. Miyata, O. Kajimoto and T. Fueno, Chem. Phys. Lett., **88**, 424 (1982).

2) T. Fueno, O. Kajimoto and V. Bonacic-Koutecky, J. Am. Chem. Soc.,**106**, 406 (1984).

3) T. Fueno, J. Mol. Struct. (Theochem), in press.

4) T. Fueno, V. Bonacic-Koutecky and J. Koutecky, J. Am. Chem. Soc., **105**, 5547 (1983).

5) M. K. Kasha and D. E. Brabham, in: Organic chemistry (NY©, Vol. 40 (Academic Press, New York, 1979) p.1.

6) C. F. Melius and J. S. Binkley, 20th Symposium (International) on Combustion (The Combustion Institute, Pittsburgh, 1984) p.575.

7) R. Ditchfield, W. J. Hehre and J. A. Pople, J. Chem. Phys., **54**, 724 (1971).

8) P. C. Hariharan and J. A. Pople, Theoret. chim. Acta (Berl.), **28**, 213 (1973).

9) J. S. Binkley, R. A. Whiteside, R. Krishnan, R. Seeger, D. J. DeFrees, H. B. Schlegel, S. Topiol, L. R. Kahn and J. A. Pople, Program No. 406, QCPE, Indiana Univ., Bloomington, Ind.

10) R. J. Buenker, in: Studies in physical and theoretical chemistry, Vol. 21, ed. R. Carbo (Elsevier, Amsterdam, 1982) p. 17.

11) R. J. Buenker and R. A. Phillips, J. Mol. Struct. (Theochem), **123**, 291 (1985).

12) S. R. Langhoff and E. R. Davidson, Int. J. Quant. Chem., **8**, 61 (1974).

13) P. J. Bruna and S. D. Peyerimhoff, in: Ab initio methods in quantum chemistry, Part I, ed. K. P. Lawley (Wiley-Interscience, New York, 1987) p. 1

14) R. J. Buenker, Int. J. Quant. Chem., **29**, 435 (1986).

15) R. S. Konar, S. Matsumoto and B. de B. Derwent, Trans. Faraday Soc., **67**, 1698 (1971).

16) C. G. Hatchard and C. A. Parker, Proc. Roy. Soc. (London), **A235**, 518 (1956).

17) P. Marshall, A. Fontijn and C. F. Melius, J. Chem. Phys., **86**, 5540 (1987).

18) J. Alster and L. A. Burnell, J. Am. Chem. Soc., **89**, 1261 (1967).

19) J. M. Howell and L. A. Kirschenbaum, J. Am. Chem. Soc., **98**, 877 (1976).

20) L. A. Curtiss, D. L. Drapcho and J. A. Pople, Chem. Phys. Lett., **103**, 437 (1984).

21) S. W. Benson, Thermochemical Kinetics, 2nd ed. (Wiley, New York, 1976).

22) R. J. Paur and E. J. Bair, J. Photochem., **1**, 255 (1972/73); Int. J. Chem. Kinet., **8**, 139 (1976).

23) L. J. Stief, W. D. Brobst, D. F. Nava, R. P. Borkowski and J. V. Michael, J. Chem. Soc. Faraday Trans. II, **78**, 1391 (1982).

Table 1.

Total energies calculated for various stationary structures

Structure		Energy (hartree)	
		SCF[a]	CI[b]
$NH(^3\Sigma^-) + NO$		-184.03215	-184.47594
$NH(^1\Delta) + NO$		183.99897	-184.40810
$HNNO(^2A'')$	3C	-184.03300	-184.50505
	3T	-184.03429	-184.45530
$HNNO(^2A')$	4C	-184.03595	-184.57196
	4T	-184.04175	-184.57241
TS1	$4C \rightarrow N_2O + H$	-183.97633	-184.49534
TS2	$4C \rightarrow N_2 + OH$	-183.97081	-184.49028
TS3	$4T \rightarrow 4C$	-183.99845	-184.52174
TS4	$HN_2 \rightarrow H + N_2$	-109.30067	-109.62258
$HN_2(^2A')$		-109.32304	-109.64895
$N_2O(^1\Sigma^+)$		-183.50573	-184.02704
$N_2(^1\Sigma_g^+)$		-108.83933	-109.15183
$NO(^2\Pi)$		-129.12300	-129.44450
$OH(^2\Pi)$		-75.31748	-75.47143

[a] UHF SCF (4-31G**) optimizations.

[b] MRD-CI (4-31G**//4-31G**) calculations.

Table 2.

Representative data for the product determinations

No	$[HN_3]_0$ Torr	$[NO]_0$ Torr	$[SF_6]$ Torr	x_{NO}[a]	$I\Delta t$ 10^{-8}mol	N_2O 10^{-8}mol	H_2O 10^{-8}mol	ϕ_{N2O}	ϕ_{H2O}
1	5.88	0.0	15.41	0.0	9.11	0.0	-	0.0	-
2	6.65	2.35	12.21	.261	0.99	0.22		.22	
3	4.89	3.81	10.56	.438	3.27	0.79	1.67	.24	0.51
4	5.16	4.10	18.58	.443	3.28	0.86	1.43	.25	.44
5	3.45	3.46	20.02	.501	2.33	0.73	0.83	.31	.36
6	5.59	7.17	10.99	.562	3.25	1.37	1.40	.36	.43
7	5.11	12.69	111.0	.713	1.72	0.72	0.56	.41	.32
8	6.21	29.69	8.32	.827	8.12	3.42	1.96	.42	.24
9	1.26	29.41	11.58	.953	1.92	1.31			.67

a $x_{NO} = \dfrac{[NO]_0}{[HN_3]_0 + [NO]_0}$

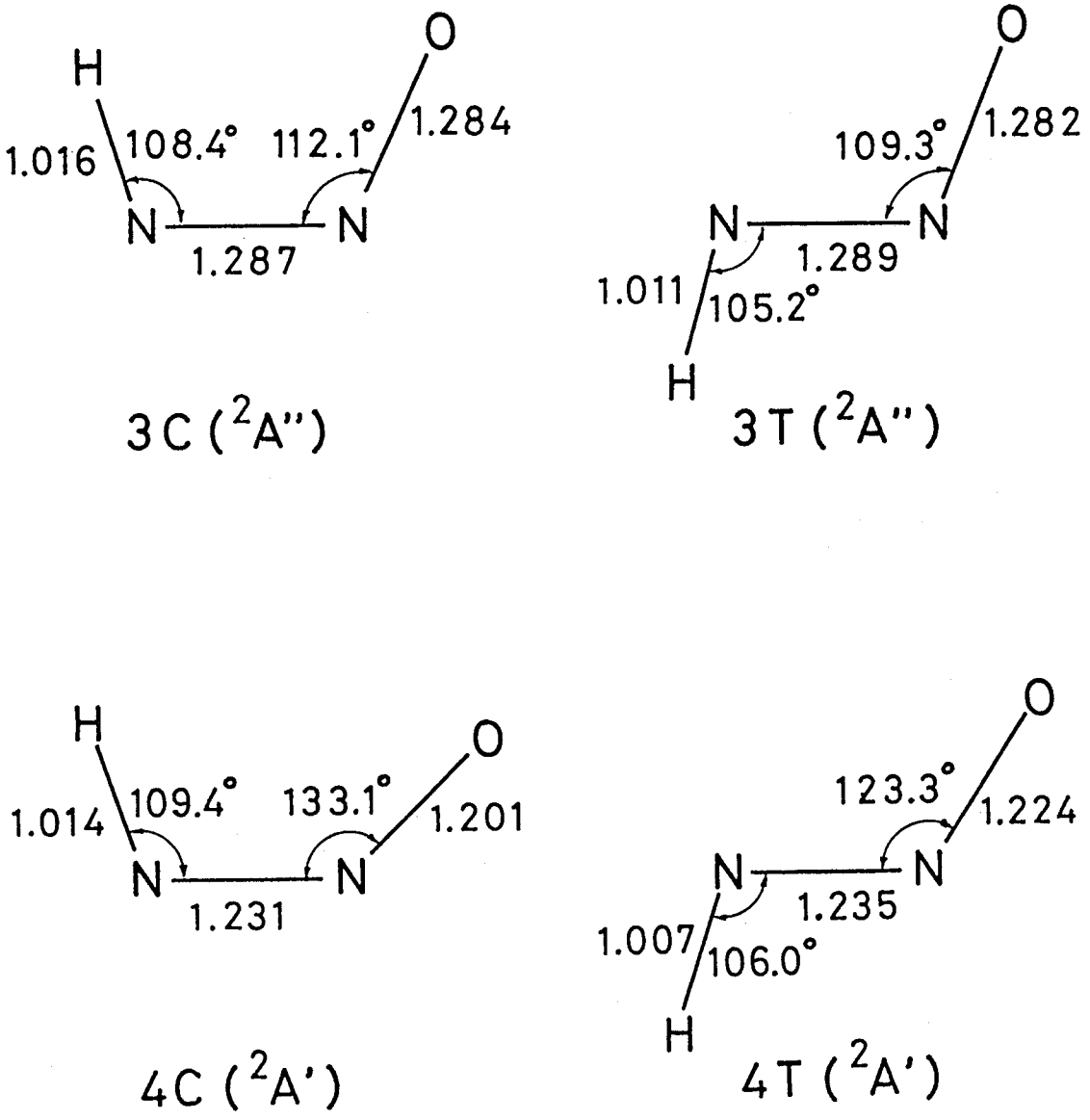

Fig. 1. Optimal geometries of the HNNO doublet radical.

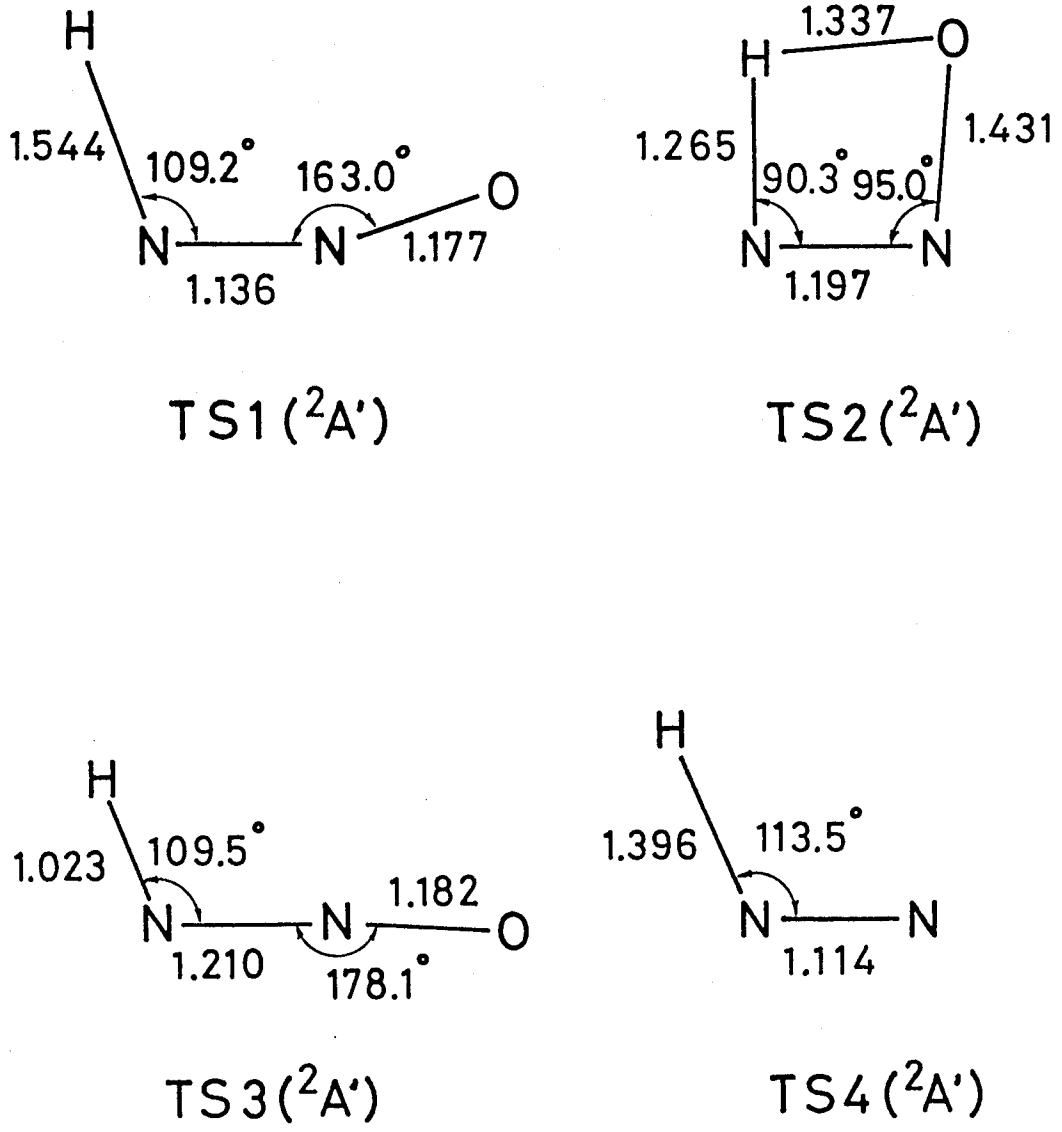

Fig. 2. Optimized transition state geometries.

TS1, N-H bond cleavage 4C ⟶ N_2O + H, reaction (4b);

TS2, 1,3-hydrogen migration 4C ⟶ N2 + OH, reaction (4c);

TS3, isomerization 4T ⟶ 4C;

TS4, N-H bond cleavage HN2 ⟶ H + N2 .

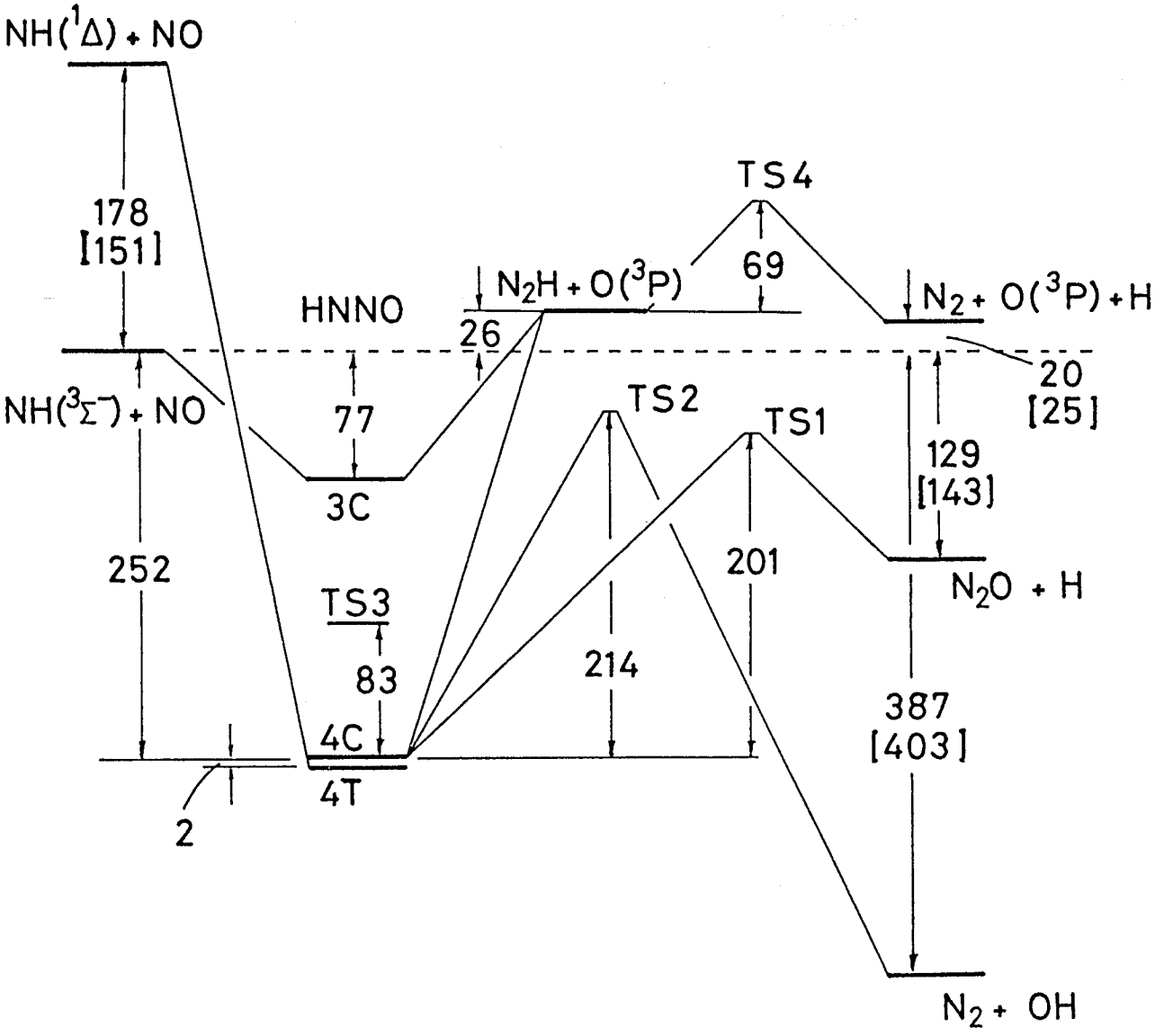

Fig. 3. Potential energy profiles calculated for the HN-NO system by the MRD-CI (4-31G**//4-31G**) procedure.

The energy gaps shown are in units of kJ/mol. The values given in [ ] are those obtained from the relevant thermochemical data [21].

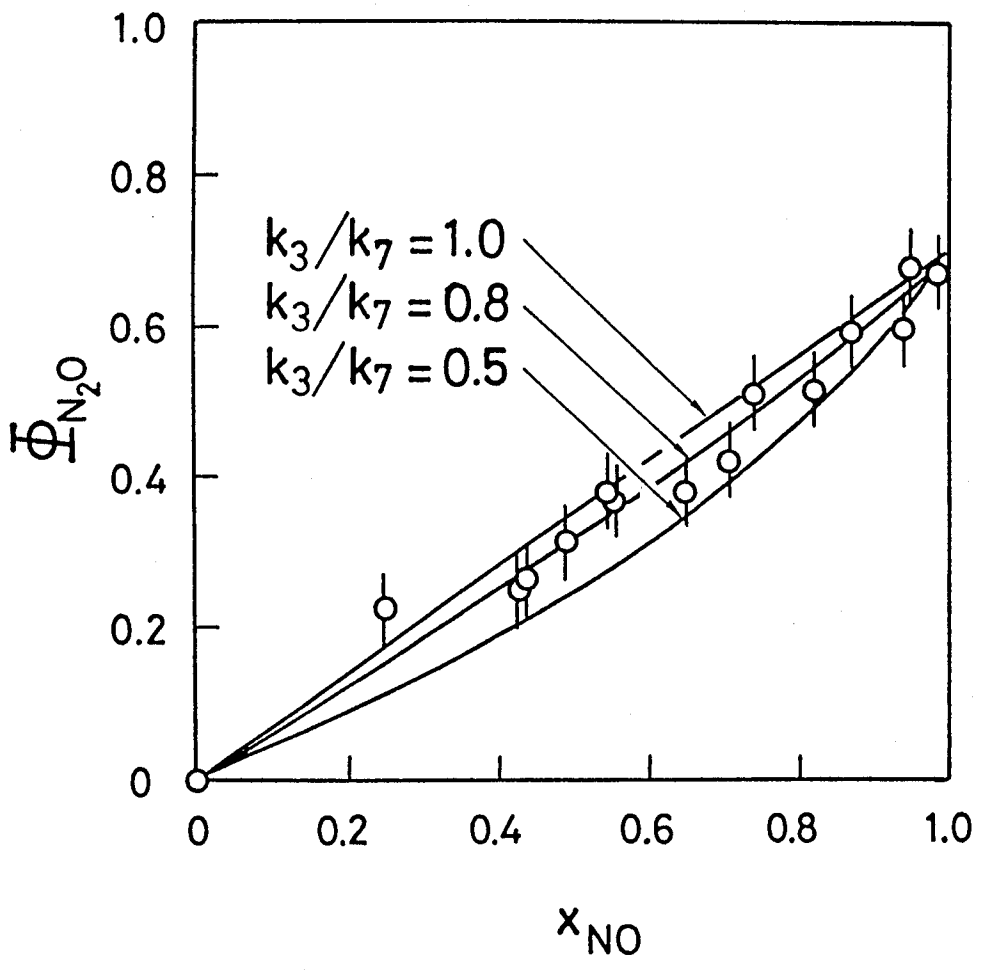

Fig. 4. Quantum yields (N_2O) as the functions of the initial fractional concentration of NO.

$$x_{NO} = \frac{[NO]_0}{[HN_3]_0 + [NO]_0}.$$

Chapter 2

Mechanism of the Reaction of NH($^1\Delta$) with NO in Argon Matrix

Matrix-isolated hydrazoic acid HN_3 admixed with NO was photolyzed by a low-pressure mercury discharge lamp. Product analysis based on the FTIR spectroscopy has revealed the formations of NH, N_2O, OH, HNO, and HONO as photoproducts. From the comparisons of the amount of HN_3 consumed with that of N_2O produced, we conclude that the reaction of NH($^1\Delta$) with NO proceeds mainly through the process NH($^1\Delta$) + NO $\longrightarrow$ N_2O + H. The quantum yield of N_2O is found to be $\phi_1 = 0.7 \pm 0.1$. The conclusion is in line with our previous results of the gas phase experiments at room temperature.

1. Introduction

We have previously investigated the gas-phase reaction $NH(^1\Delta)$ with NO both theoretically and experimentally.[1] The theoretical studies have shown that the reaction should proceed through an intermediacy of the HNNO adduct and that two channels are open for the unimolecular decomposition of the HNNO adduct:

$$NH(^1\Delta) + NO \longrightarrow [HNNO] \begin{cases} \longrightarrow N_2O + H & (1a) \\ \longrightarrow N_2 + OH & (1b) \end{cases}$$

The entire reaction is expected to be essentially collision-controlled, and the HNNO decompositions as the product-determining step have energy barrier heights lower than the heat of the adduct formation, with a marginal advantage of reaction (1a) over reaction (1b). The expectation that the primary product of the reaction should be N_2O was borne out by the experimental determination of the quantum yield of N_2O being ca 0.7, under the assumption that the quantum yield of $NH(^1\Delta)$ in the photodissociation is 1.0.

$$HN_3 \xrightarrow{h\upsilon} NH(^1\Delta) + N_2 \qquad \phi=1 \text{ at } 2537\text{Å} \qquad (2)$$

It is feared, however, that in the gas phase N_2O might well be formed by some routes other than the direct process (1a). Hack et al. carried out laser photolysis of HN_3 in the presence of NO in the gas phase at room temperature.[2] On the basis of the laser-induced fluorescence signal intensity of OH, they concluded that the primary product is $OH(X^2\Pi)$ to be formed by reaction (1b). They suggested the possibility that the formation of N_2O was rather a consequence of subsidiary reactions as follows:

$$NH(^1\Delta) + HN_3 \longrightarrow NH_2 + N_3 \quad (3)$$

$$N_3 + NO \longrightarrow N_2O + N_2 \quad (4)$$

In the present work, we have undertaken studies of the photo-induced reaction of HN_3 with NO in argon matrix. Our principal purpose here is to examine whether our previous gas-phase product determination study has indeed reflected the kinetics of reaction (1a). In a matrix there are not only isolated monomer but also dimer, polymer and complexes with other molecular species, but generally there are little mobilities for isolated molecules except for the H atom. Thus, photoinduced reactions are thought to be completed within single cages of argon matrix. Contributions of subsidiary processes to the overall reaction could be examined more closely in this study.

2. Experimental

The cryogenic aparatus used in the matrix experiments is schematically shown in Fig.1. A Cryomini D310 closed-cycle helium system (Iwatani Cryo-Techno Inc.) was used to refrigerate the deposition target made of CsI of 20mm in diameter and 2mm in thickness. An indium gasket was inserted between the CsI disk and a copper sample holder mounted on the cold head. Two pylex nozzles of 0.5 mm in internal diameter were placed at a distance of 3 cm from the target in the direction orthogonal to each other to spray sample gases onto the target. Only one of these nozzles was used in the present experiments. A thermocouple of Chromel vs Au-0.07%Fe was enbedded on the sample holder. The ordinary operating temperature was measured to be 12 K. A liquid nitrogen trap and an oil diffusion pump were used to evacuate all of these devices placed within a stainless steel envelope.

IR spectra were measured through two KRS-5 windows located on both sides of the target on the envelope. In the direction perpendiculer to the IR beam, there were two quartz windows for UV irradiation. The target was rotatable on a

holizontal plane for IR measurement and UV irradiation. The UV light source used was a 22W low-pressure mercury discharge lamp (Ultra Violet Prod. Inc.) placed just in front of the quartz window of 2 mm in thickness without lens nor filter. This alignment provided homogenious exposure of the target to the 2537 Å UV light. It is thought that another mercury line 1849Å will little influence the measurements because of the absorption by the quartz window (not suprasil) at this wavelength. A Fourier-transform infrared spectrometer FT/IR-5000 (Japan Spectroscopic Co., Ltd.) was operated with a resolution of 4 cm^{-1} and the spectra were calculated from the coaddition of 100 interferograms. The deposition rates of sample gases were controlled with a teflon needle valve and a capasitance manometer CMLB-1000 (Vacuum General Inc.).

HN_3/NO/Ar(= 0.1-1 / 0.08-1 / 100) gas mixtures were sprayed out through the nozzle at a rate of 2 mmol/hr for ca. 3.5 hs. After measurements of IR spectra for deposited samples, UV irradiation was started. Photolyzed matrix spectra were measured at the irradiation times of 0.5, 1, 2, 4, 6, 10, 20, 30, 60, and 120 mins. A single measurement took about 4 mins. The matrix temperature was monitored to be maintained at 12K during irradiation. A relative intensity of the N_2O υ_3 (2224 cm^{-1}) to the HN_3 υ_2 (2138 cm^{-1}) band was evaluated on the basis of the matrix spectra of N_2O/HN_3/Ar of known conpositions.

HN_3 was synthesized by the reaction of NaN_3 with excess stearic acid at 80~90 °C in a vacuum glass line. After the purification by means of trap-to-trap distilations at -80 °C, HN_3 gas was stored in a 6-l pylex bulb. NO(99.99%), Ar(99.9999%) and N_2O(99.999%) (Takachiho Kagaku Inc.) were used without further purification. Gas mixtures diluted in argon were kept in a 6-l pylex bulb overnight for mixing.

3. Results

(A) Assignment of complexes

The HN_3/NO/Ar matrix spectra have exhibited, in the vicinity of the HN_3 υ_2 band(2138 cm^{-1}), a perturbed υ_2 band at 2150 cm^{-1} due to the hydrogen-bonded HN_3 dimer.[3] More highly aggregated molecules may also conribute to this peak since annealing experiments broadened the υ_2 band. By contrast, the υ_2 band was not resolved by possible complexation of HN_3 with NO, which might reflect a weaker hydrogen bonding between the two components.

A new peak was observed at 1882 cm^{-1} near the isolated NO stretching (1874 cm^{-1}). It is assigned to the HN_3-NO *plus* $(HN_3)_2$-NO complexes on the basis of the following observations. First, this peak is observed in the HN_3/NO/Ar spectra but is absent in either of the HN_3/Ar and NO/Ar matrix spectra. Second, as can be seen in Fig.2, the relative peak heights of the complexes vs. NO remain constant, irrespective of the molar fraction of NO in the sample gas used.

(B) Photoproducts

Figure 3 shows a difference spectrum of an HN_3/NO/Ar matrix after photolysis for 1 h. The irradiation diminishes HN_3 and the complexes and gives rise to $NH(X^3\Sigma^-)$, N_2O, OH, HNO, HONO and NO_2. Little change was observed in absorbance of the peak due to the isolated NO monomer (1874 cm^{-1}). Assignments of the product peaks are listed in Table.1, together with literature values. In the vicinity of the NH_2 υ_2 band (1499 cm^{-1}), no significant peak was observed.

Evidently, N_2O is the primary product of the present matrix experiments also. As we believe, it has arisen from reaction (1a) directly, even though the mechanism proposed by Hack et al.[2], i.e., the succession of reactions (3) and (4), cannot wholly be negated at this stage. Importantly, the concurrent formation of HNO lends strong support to our belief. Namely, the H atom which should have

been formed together with N_2O by reaction (1a) could migrate in argon matrix cages to undergo recombination with NO:

$$NO + H + M \longrightarrow HNO + M \qquad (5)$$

Reaction (1a) followed by reaction (5) seems to be the only route for the formation of HNO under our experimental conditions.

(C) Time evolution

The HN_3 υ_2 band absorbances for monomer (2138 cm^{-1}) and dimer (2150 cm^{-1}) are plotted in Fig.4 as the functions of irradiation time. Two curves have apparently different time constants. Log plots of these decay curves manifest that the dimer is photodecomposed nearly twice as rapidly as is the monomer; the initial slope ratio for dimer to monomer is about 2. The results indicate that the dimerization does not perturb the IR intensity of the υ_2 band nor the UV dissociation cross section of HN_3. In addition, it seems that highly aggregated HN_3 molecules, if any, hardly contribute to the absorption at 2150 cm^{-1} because they should be photodecomposed further more rapidly.

Figure 5 shows the increases in the OH (3554 cm^{-1}) and NH (3136 cm^{-1}) absorbances with the elapsing irradiation time. For the purpose of comparisons in shape, measured absorbances have been arbitrarily normalized to a constant value at 300 min. Shown by the solid and dotted curves are the decrements in absorbance of HN_3 (2138 cm^{-1}) and $(HN_3)_2$ (2150 cm^{-1}), respectively, as the functions of time (Fig. 5). It can be seen that both the OH and NH increment curves fit the HN_3 monomer decrement curve. The results suggest that NH arises from the photolysis of the HN_3 monomer and that the precursor for OH is the 1:1 HN_3-NO complex.

The absorbance of N_2O $\upsilon 2$ band (2224 cm^{-1}) was also found to increase with time but to be fitted with neither of the HN_3 and $(HN_3)_2$ decay curves. The time

profile showed somewhat faster saturation curve. This is presumably due to a photodecomposition process of N_2O itself.[4)]

$$N_2O \xrightarrow{h\upsilon} N_2 + O(^1\Delta) \qquad \lambda < 2300\ \text{Å} \qquad (6)$$

Under such circumstances, we have decided to examine the initial rate of the formation of N_2O relative to that of the consumption of HN_3 monomer as the function of the molar fraction x_{HN_3} of HN_3 present in the sample gas deposited. Note that the word "initial" used here means such an early time region that the secondary photodecomposition does not affect $[N_2O]$, normally less than 4 min.

Figure 6 shows the initial production rate of N_2O (2224 cm^{-1}), $d[N_2O]/dt(t=0)$, relative to the initial decay rate of HN_3 monomer (2138 cm^{-1}), i.e., $-d[HN_3]/dt(t=0)$, at the varying initial molar fraction x_{HN_3}. It can be seen in Fig. 6 that the relative initial rate $-d[N_2O]/d[HN_3](t=0)$ is constant at 0.52, irrespective of x_{HN_3}. The results indicate that N_2O is produced from the HN_3 monomer complexes; i.e. HN_3-$(NO)_{1,2}$. In addition, the initial rate of the consumption of $(HN_3)_2$ (2150 cm^{-1}) was measured relative to $-d[HN_3]/dt(t=0)$. The relative rate $d[(HN_3)_2]/d[HN_3](t=0)$ was confirmed to be proportional to x_{HN_3}. Therefore, if the photolysis of $(HN_3)_2$-$(NO)_{1,2}$ had given rise to N_2O, the plots of $-d[N_2O]/d[HN_3]$ against x_{HN_3} would have shown a significant positive slope. Constancy of $-d[N_2O]/d[HN_3]$ indicates that the photolysis of the 2:1 or 2:2 complex $(HN_3)_2$-$(NO)_{1,2}$ has hardly contributed to the N_2O production. The results entirely negate the contribution of the succession of reactions (3) and (4) on the N_2O production under the present conditions.

(D) Yield of N_2O

We have evaluated the yield of N_2O formed by the photolysis of the 1:1 complex. In the measurements of the yield, there are two complexities. One is that N_2O is formed by the photolysis of both 1:1 and 1:2 complexes. The other is

that the absorption at 1882 cm^{-1}, which was used to measure the amount of the 1:1 complex, overlaps with that of the 2:1 complex. Therefore, appropriate corrections are needed in evaluating the yield from the rates of the N_2O production and the complex consumption.

Let the yields of N_2O arising from the photolyses of the 1:1 and 1:2 complexes be denoted as ϕ_1 and ϕ_2, respectively. Since N_2O is assumed to be formed from both complexes, we may write

$$d[N_2O] = - \phi_1 \, d[HN_3\text{-}NO] - \phi_2 \, d[HN_3\text{-}(NO)_2]. \qquad (I)$$

The apparent overall yield of N_2O, defined as $\Phi \equiv -d[N_2O]/d[HN_3\text{-}NO]$ is then expressed as

$$\Phi = \phi_1 + \phi_2 \, d[HN_3\text{-}(NO)_2]/d[HN_3\text{-}NO]. \qquad (II)$$

The second term $d[HN_3\text{-}(NO)_2]/d[HN_3\text{-}NO]$ is expected to be proportional to x_{NO}, which will be confirmed later. Thus, plots of Φ vs x_{NO} should provide the ϕ_1 value as the intercept at $x_{NO} \rightarrow 0$.

In order to evaluate the Φ value, the initial rate of the consumption of the 1:1 complex is needed. The complex peak at 1882 cm^{-1} which is the only peak distinguishable at the present resolution contains both the 1:1 and 2:1 complexes:

$$dC/dt = d[HN_3\text{-}NO]/dt + d[(HN_3)_2\text{-}NO]/dt \qquad (III)$$

where C is the amount of the complexes absorbing at 1882 cm^{-1}. Dividing both sides by $d[N_2O]/dt$;

$$dC/d[N_2O] = \Phi^{-1} + d[(HN_3)_2\text{-}NO]/d[N_2O] \qquad (IV)$$

where the second term $d[(HN_3)_2\text{-}NO]/d[N_2O]$ should be proportional to x_{HN_3} in view of the results illustrated in Fig. 6. Hence, by plotting $dC/d[N_2O]$ against x_{HN_3}, we obtain the reciprocal Φ from the intercept.

In practice, the values of dC/dt have been evaluated from the absorbance changes at 1882 cm^{-1} in the initial 4 min period. The initial decreasing rates of C have been divided by the initial production rates of N_2O (2224 cm^{-1}). Plots of the quotients against x_{HN_3} at a fixed x_{NO} value of 1.0 % , for instance, have indeed proved to be linear, as is shown in Fig. 7. The intercept 0.48 leads to Φ =2.08 at x_{NO} = 1.0 %.

The values of Φ at various x_{NO} values have been measured in a similar way. Figure 8 shows the plots of Φ vs x_{NO}. As has been anticipated in the form of Eq. II, the plots are linear. The intercept gives $\phi_1 = 0.7$.

On the absorption peaks of HN_3, N_2O and $(HN_3)_{1,2}$-NO the proportionalities between the concentrations and the absorbances have been assumed. Relative absorption coefficients are measured to be 1 : 1.15 : 0.225 for HN_3 (2136 cm^{-1}):N_2O (2224 cm^{-1}):$(HN_3)_{1,2}$-NO (1882 cm^{-1}). These values are obtained from the IR spectra of the matrices made of the sample gases of known compositions. The absorption coefficient of the complex peak (1882 cm^{-1}) has been assumed to be equal to that of isolated NO monomer, because the IR absorption intensity of the N-O stretching would not be perturbed largely by the complexation.

4. Discussion

Since $NH(a^1\Delta)$ formed by the photolysis of HN_3 is metastable, there may exist a physical quenching to $NH(X^3\Sigma^-)$:

$$NH(^1\Delta) + Ar \longrightarrow NH(^3\Sigma^-) + Ar. \qquad (7)$$

Ramsthaler-Sommer et al. measured the lifetime of NH($a^1\Delta$) in argon matrix.[5] Their reported value of ~0.7 s at 12 K is long enough to allow the barrierless reaction (1) to complete without an influence of the quenching process (7).

The photoinduced reaction of the 1:1 complex can be regarded as reaction (1) in argon matrix cages. The value 0.7 ± 0.1 obtained for ϕ_1 indicates that N_2O arises dominantly from reaction (1a) via the HNNO intermediacy. The result is perfectly compatible with the observation of HNO, whose production is inevitable as a fate of the H atom formed in reaction (1).

We have already noted the failure in detecting NH_2. For the purpose of more quantitative discussion, the infrared intensity of the NH_2 υ_2 band 1499 cm^{-1} is needed. Thus, we conducted separate photolysis experiments of NH_3/Ar and NH_3/CO in order to isolate the NH_2 radical.

$$NH_3 \xrightarrow{h\upsilon} NH_2 + H \qquad (8)$$

A low-pressure mercury discharge lamp with suprasil window provides 1849 Å UV light which should efficiently photodecompose NH_3. In the case of NH_3/Ar, the NH_2 υ_2 band at 1499 cm^{-1} showed only a slight absorption after an irradiation over a period of five hs, probably because of the recombination between the dissociated NH_2 and the H atom. In the NH_3/CO photolysis, on the other hand, effective productions of NH_2, HCO, and $HCONH_2$ have been observed.[6] Assuming that the amount of NH_2 produced is equal to that of NH_3 consumed, we have estimated a lower limit of the relative intensity of the NH_2 υ_2 band to the N_2O υ_3 band to be $I_{NH2}/I_{N2O} > 0.1$. Obviously, this value is underestimated owing to the production of a significant amount of $HCONH_2$. By appling this value to a spectrum for HN_3/NO/Ar, in which an absorbance ratio A_{NH2}/A_{N2O} is found to be less than 0.01 , we estimate an upper limit of the production ratio $[NH_2]/[N_2O]$ to be less than 0.1. Therefore, only less than 10% of N_2O might be formed via the succession of reaction (3) and (4), if any.

We have also been cautious of the possibility that N_2O may be formed directly from NO. Although isolated NO monomer cannot be decomposed by irradiation with a low-pressure mercury discharge lamp, the dimer is susceptible to the photodissociation:[7]

$$ONNO \xrightarrow{h\upsilon} N_2O + O \qquad \lambda < 2400\ \text{Å} \qquad (9)$$

However, in the present experiments, reaction (9) will not participate significantly, since the intense Hg resonance line at 1849 Å has been attenuated to a large extent through the window used in this study. In fact, the initial production rate $d[N_2O]/dt(t=0)$ in the photolysis of NO/Ar (1 / 100) was found to be less than 2 % that in the photolysis of HN_3/NO/Ar (1 / 1 / 100). Thus, N_2O formed in the photolysis of HN_3/NO/Ar has no doubt originated nearly exclusively from the photodecomposition of HN_3.

Our original aim of the present work was to detect the HNNO intermediate. This was unsuccessful, however. It is supposed that the nascent vibrationally excited HNNO has an extremely short lifetime compared to a period of time required for stabilization by collisions with Ar. Thus, fragmentation will take place prior to stabilization. Also, the photodecomposition might be so fast that the amount of HNNO could not reach the detection limit.

We have assigned a peak at 3554 cm^{-1} to the OH radical in the spectrum of a HN_3/NO/Ar matrix photolyzed. The infrared absorption of OH in argon matrix has not been established yet. There are some discrepancies among the reported values.[8-10] Acquista et al.[8] and Suzar et al.[9] conducted the photolysis of H_2O at 1218 Å and decomposition of H_2O by means of electron impact in argon matrix, respectively. Both of them assigned two absorptions near 3452 and 3428 cm^{-1} to the OH vibration. On the other hand, Cheng et al.[10] found a new peak at 3548.2 cm^{-1}, which was concluded to be due to the OH radical prepared in solid argon by means of the reactions of atomic H with NO_2, O_3 and atomic O. The shift of 21.4

cm^{-1} from 3569.6 cm^{-1} as the gas-phase fundamental band is within the common range of matrix shift.[11] They pointed out it possible that the absorptions at 3452 and 3428 cm^{-1} previously assigned to OH may be due to the hydroxyl radical in complex with either H_2O or one Ar atom. Our observation 3554 cm^{-1} supports the conclusion by Cheng et al. The difference of 6 cm^{-1} between their wavenumber and ours may have been caused by an interaction of OH with N_2 molecules, which is simultaneously formed with OH via reaction (1b). N_2 matrix experiments to isolate OH will be interesting.

The formation of HONO observed in a considerable amount probably stems from the 1:2 complex HN_3-$(NO)_2$. By virtue of weakness of the N-N bonding in $(NO)_2$, its photolysis will be apt to form the same intermediate HNNO as does reaction (1).

$$NH(^1\Delta) + ONNO \longrightarrow [HNNO]^* + NO \qquad (11)$$

If HNNO formed in this reaction has still enough excess energy, reaction (1b) will follow to give OH, which may in turn recombine with the other NO molecule to form HONO.

$$OH + NO + Ar \longrightarrow HONO + Ar \qquad (12)$$

Finally, in addition to the chemical channels (1a) and (1b), a quenching process must be considered.

$$NH(^1\Delta) + NO \longrightarrow NH(^3\Sigma^-) + NO \qquad (1c)$$

Hack et al. measured the rate constant of reaction (1c) in the gas phase, to claim that its branching ratio was as large as 0.4.[2] If so, the reaction of $NH(^1\Delta)$ with NO will inevitably be accompanied by the reaction of $NH(^3\Sigma^-)$ with NO under the

present conditions as well. Since N_2O may arise from $NH(^3\Sigma^-)$ as well as $NH(^1\Delta)$, the value of ϕ_1 (= 0.7) may not directly correspond to the branching ratio of the singlet reaction (1a) alone. This final point is still open to inquiry. Nevertheless, the conclusion that reaction (1a) is the most dominant channel of the reacion between $NH(^1\Delta)$ and NO will be basically correct.

5. Conclusions

Product analyses of the photochemical reactions in HN_3/NO/Ar matrices at 12 K were conducted to investigate the microscopic mechanism of the reaction of $NH(^1\Delta)$ with NO. NH, N_2O, OH, HONO and HNO were identified based on the IR spectra. The absolute yield of N_2O from the phtolysis of the 1:1 complex HN_3-NO was found to be $\phi_1 = 0.7 \pm 0.1$. Also, a considerable amount of N_2O was confirmed to arise from the 1:2 complex HN_3-$(NO)_2$. The photolysis of the 2:1 or 2:2 complex $(HN_3)_2$-$(NO)_{1,2}$ was found not to contribute to the production of N_2O, indicating that $NH(^1\Delta)$ fragmented from one of two HN_3 would react with the other HN_3 preferentially.

References

1) T. Fueno, M. Fukuda, and K. Yokoyama, Chem. Phys., **124**, 265 (1988).

2) W. Hack and K. Rathmann, private communication.

3) G. C. Pimentel, S. W. Charles, and K. Rosengren, J. Chem. Phys., **44**, 3029 (1966).

4) G. P. Kevopoulos and R. J. Cvetanovic, J. Am. Chem. Soc., **91**, 7572 (1969).

5) A. Ramsthaler-Sommer, K. E. Eberhardt, and U.Schurath, J. Chem. Phys., **85**, 3760 (1986).

6) D. E. Milligan and M. E. Jacox, J. Chem. Phys., **43**, 4487 (1965).

7) J. R. Sodeau and R. Withnall, J. P. Chem., **89**, 4484 (1985).

8) N. Acquista, L. J. Schoen, and D. R. Lide, Jr., J. Chem. Phys., **48**, 1534 (1968).

9) S. Suzer and L. Andrews, J. Chem. Phys., **88**, 916 (1987).

10) B. M. Cheng, Y. P. Lee, and J. F. Ogilvie, Chem. Phys. Lett., **151**, 109 (1988).

11) M. E. Jacox, J. Mol. Spectrosc., **113**, 286 (1985).

12) D. E. Milligan and M. E. Jacox, J. Chem. Phys., **41**, 2838 (1964).

13) M. E. Jacox and D. E. Milligan, J. Mol. Spectrosc., **48**, 536 (1973).

14) L. Andrews and G. L. Johnson, J. Chem. Phys., **76**, 2875 (1982).

15) W. A. Guillory and C. E. Hunter, J. Chem. Phys., **54**, 598 (1971).

Table 1. Infrared Absorption Frequencies for the Products Formed in the Photolyses of the HN_3/NO/Ar Matrices.

Frequency cm^{-1}	Assignment	Lit. value cm^{-1}	Ref.
3554	OH	3548.2	10
3136	NH	3133	12
2744			
2718	HNO	2717	13
2224	N_2O	2221	14
1758			
1686	trans-HONO	1690	15
1644			
1630	cis-HONO	1633	15
1609	NO_2	1610	15
1566	HNO	1563	13
1510			
1503			
1499 [a]	NH_2	1499	6
1317			
1286	N_2O	1284.9	14
1215			
856	cis-HONO	850	15
800	trans-HONO	800	15
719			
661			
588	N_2O	588	14

[a] observed in the photolysis of the HN_3/Ar matrix

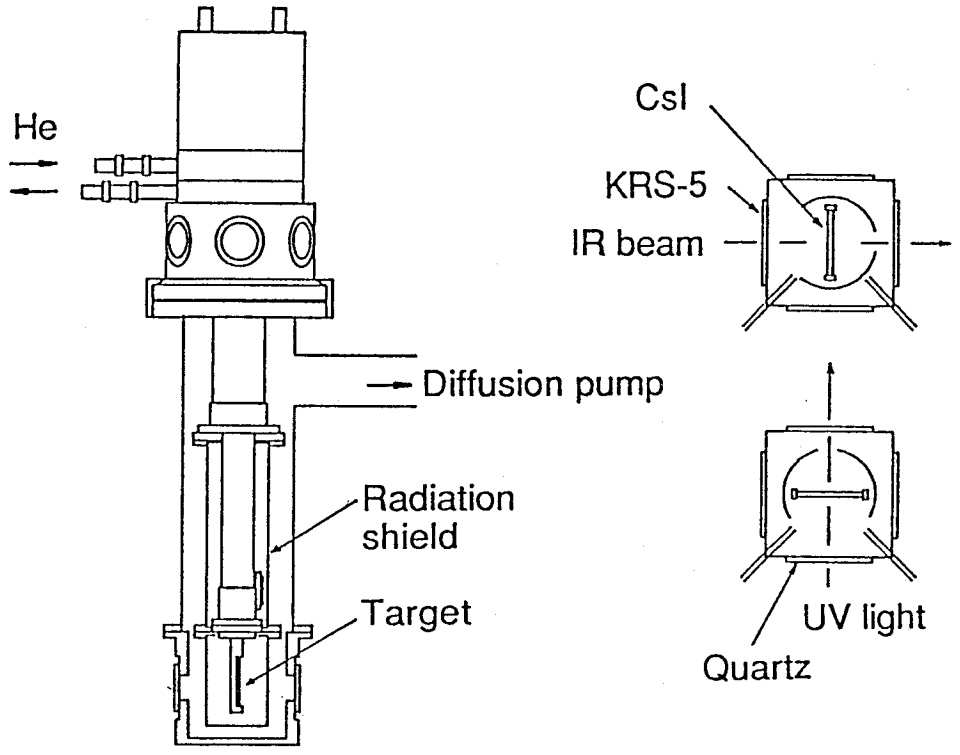

Fig. 1. Schematic drawing of the cryogenic aparatus.

Top right, target alignment for IR measurement.

Bottom right, that for deposition of the sample gases and UV photolyses.

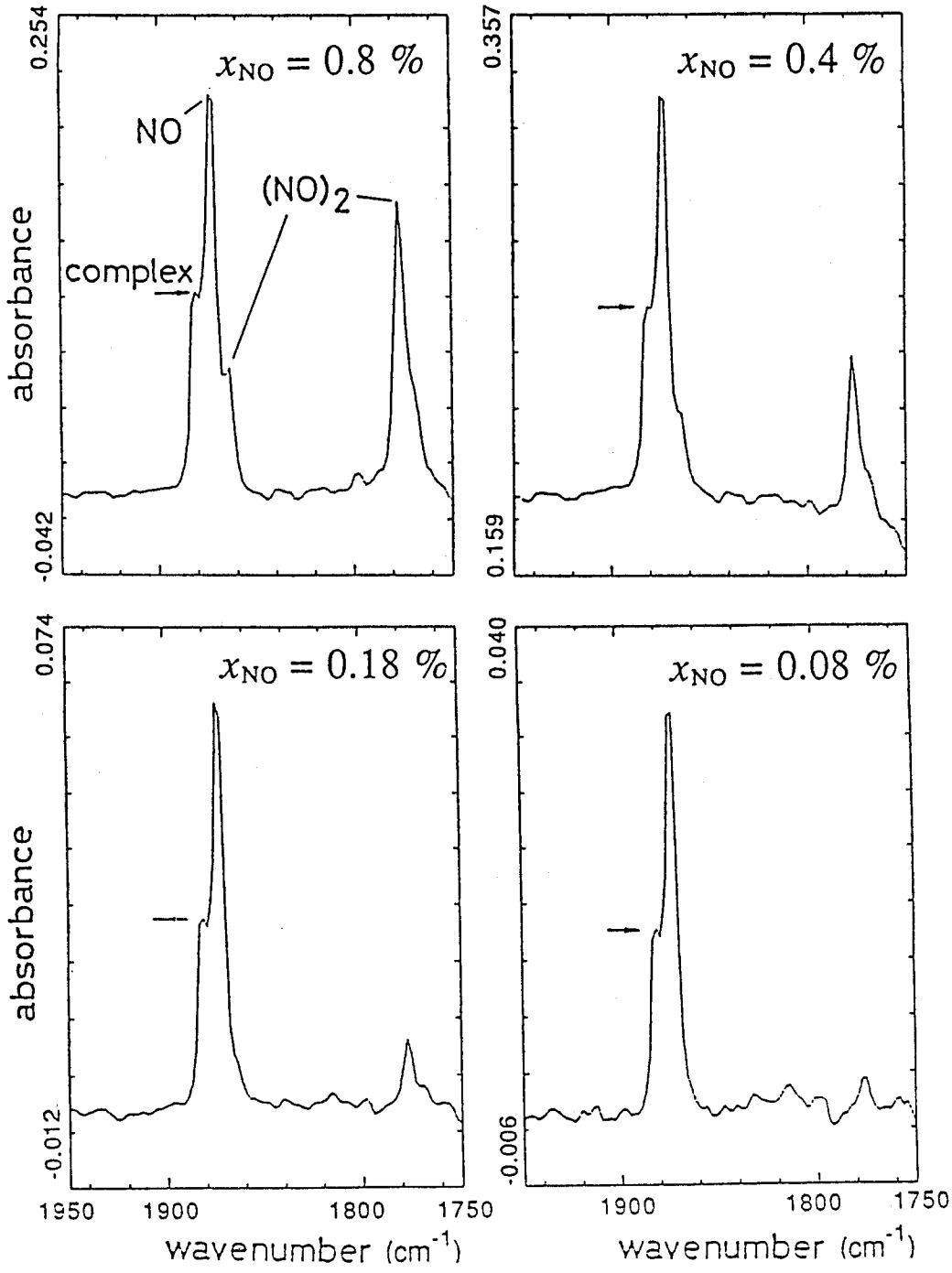

Fig. 2. Absorbance changes for the NO stretching bands of the NO monomer and dimer and for the complexes in the spectra of the HN_3/NO/Ar =1 / 0.08~0.8 / 100 matrices. The complex peak shows the same dependence as monomer, unlikely dimer.

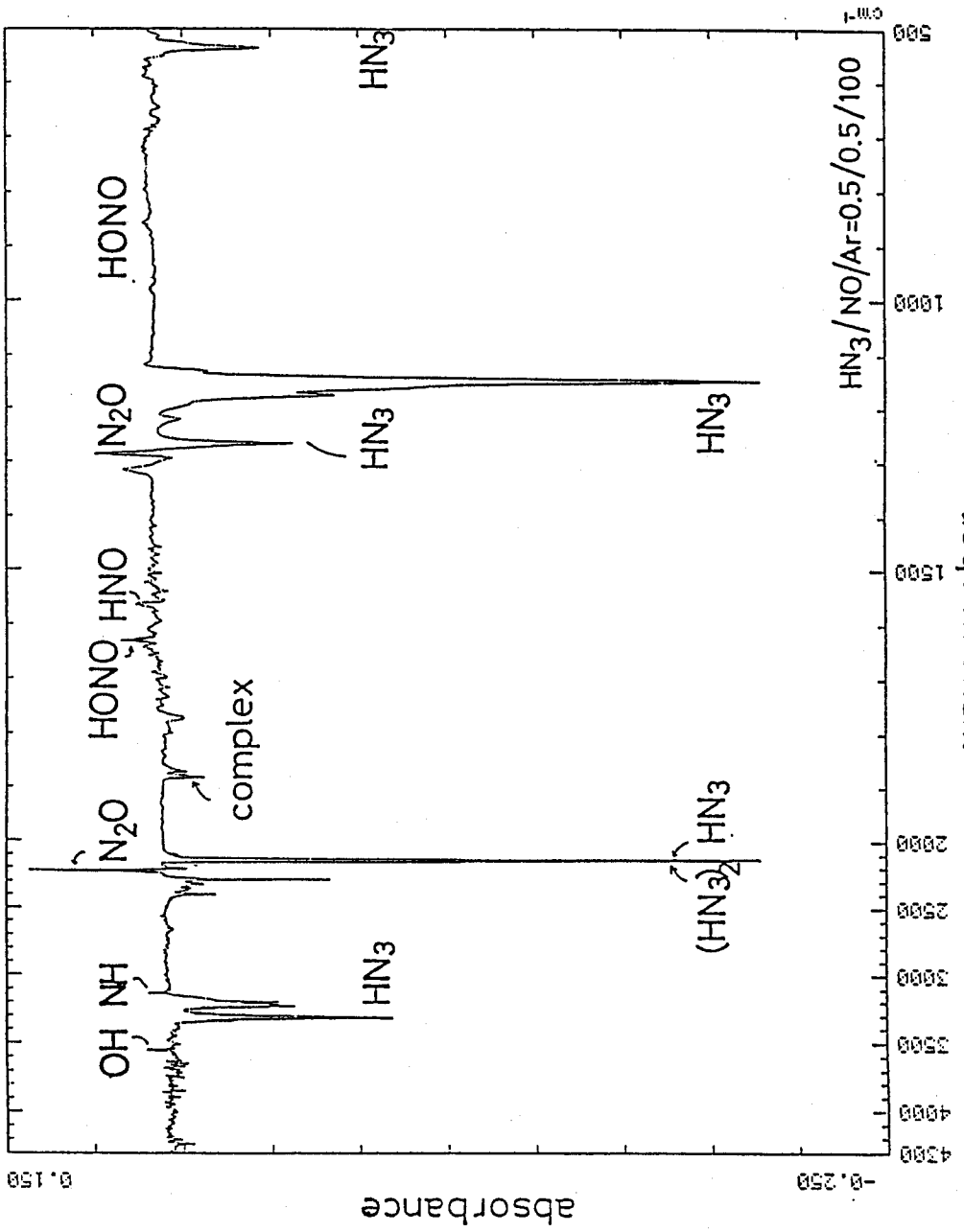

Fig. 3. FTIR difference spectrum of the HN_3/NO/Ar=0.5 / 0.5 / 100 matrix at 12 K after 1 h hotolvsis.

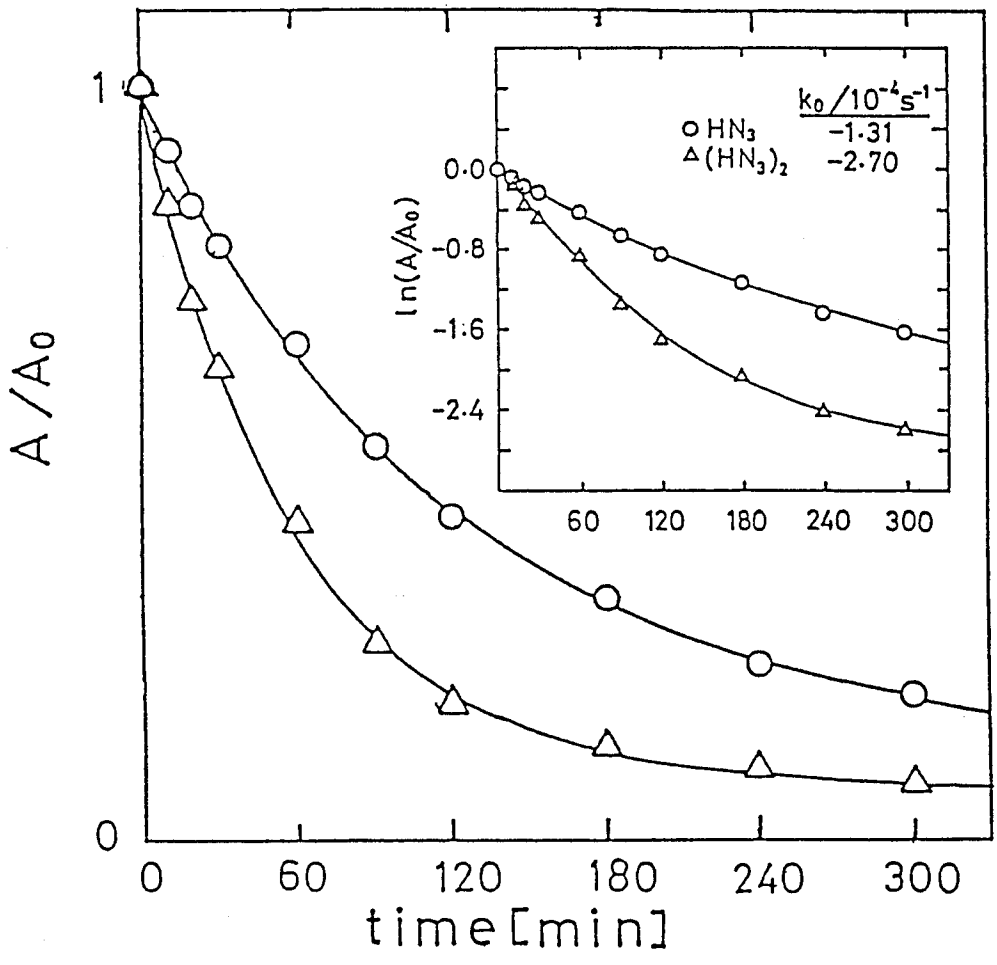

Fig. 4. Differernce between relative decay curves for the HN_3 monomer (2138 cm^{-1}) and dimer (2150 cm^{-1}) in the spectrum of HN_3/NO/Ar = 0.5 / 0.5 / 100. Solid curve is obtained from biexponential fitting. Insert is log plots of the decays. Note that initial slope ratio is about 1:2 (monomer:dimer).

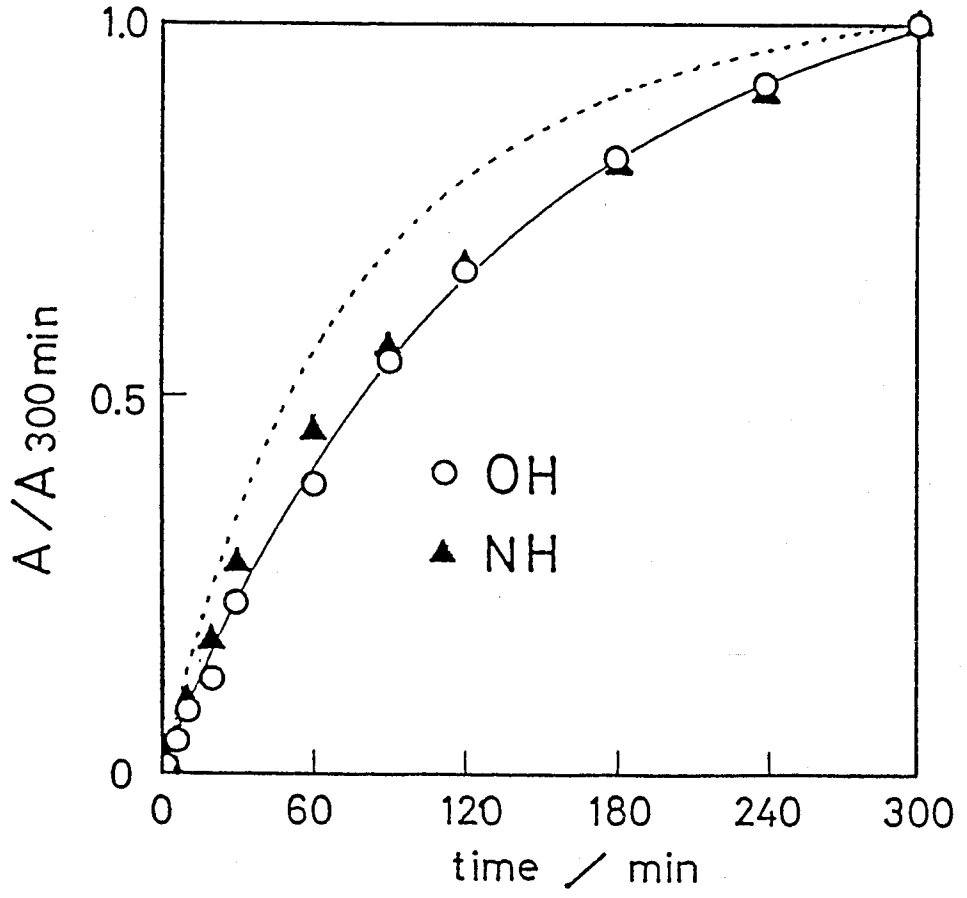

Fig. 5. Comparisons of the OH (3554 cm^{-1}) or the NH (3136 cm^{-1}) production profile with the HN_3 monomer and dimer decay profiles. The solid and dashed curves provide decrement in absorbanse at the HN_3 (2138 cm^{-1}) and $(HN_3)_2$ (2150 cm^{-1}) υ_2 band ,respectively. HN_3/NO/Ar = 1 / 1 / 100.

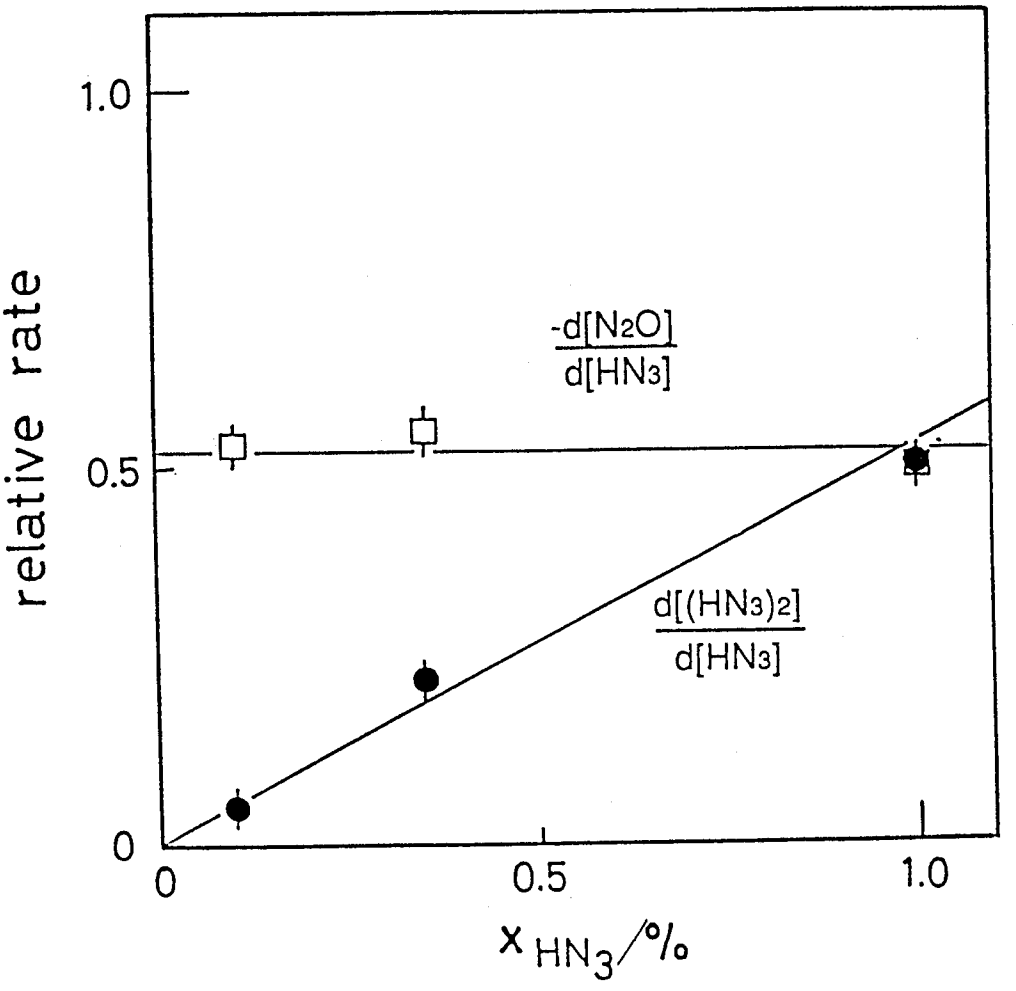

Fig. 6. Dependence of the production of N_2O on the fraction of HN_3. Dependence of the monomer:dimer ratio of HN_3 is also shown.

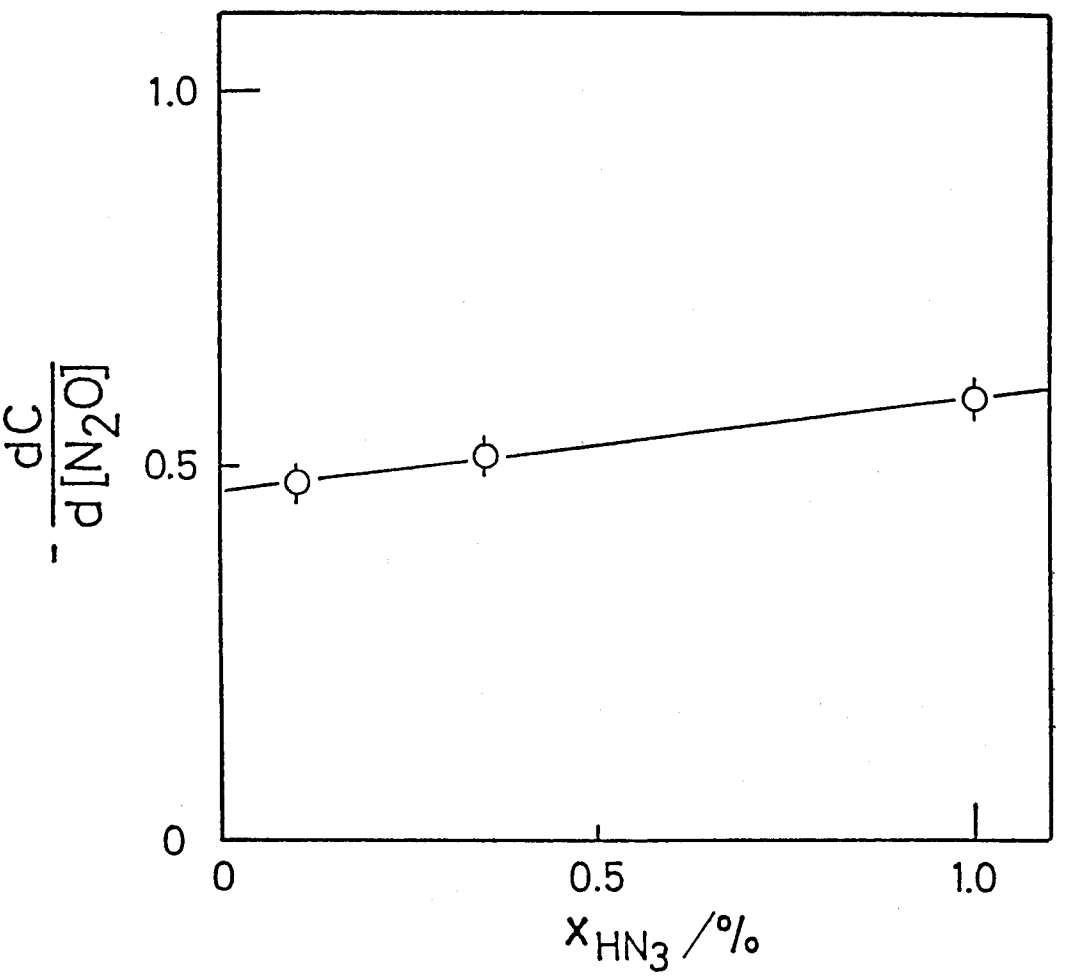

Fig. 7. x_{HN3} dependence of reciprocal yield, $-dC/d[N_2O]$, at a fixed x_{NO} value of 1.0 %. The intercept corresponds to the value of Φ^{-1}.

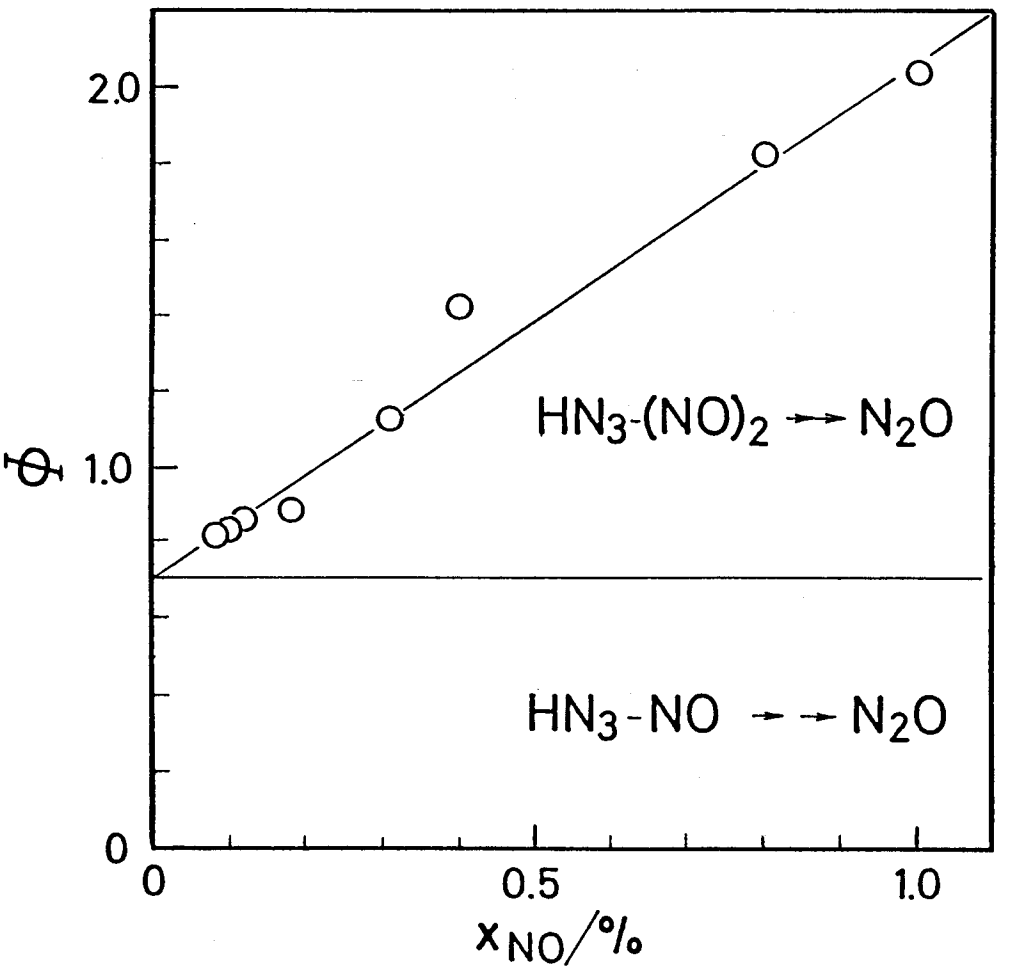

Fig. 8. [NO] dependence of the yield of N_2O from the photolysis of the 1:1 and 1:2 complexes HN_3-NO and HN_3-$(NO)_2$. The intercept is corresponding to the absolute yield of N_2O in reaction (1); ϕ_1.

Chapter 3

Formations of $OH(X^2\Pi, A^2\Sigma^+)$ in the Reaction of $NH(^3\Sigma^-)$ with NO in Incident Shock Waves

Gaseous mixtures of HNCO and NO diluted in Ar were heated by incident shock waves to about 3500 K to investigate the bimolecular reaction of $NH(^3\Sigma^-)$ with NO. Ultraviolet emissions from the excited $NH(A^3\Pi)$ and $OH(A^2\Sigma-)$ were monitored to determine the rate constants for the ground-state reaction $NH(^3\Sigma^-)$ + NO $\longrightarrow$ N_2 + $OH(X^2\Pi)$. The branching ratio defined as the rate constant for the formation of OH relative to that for the $NH(^3\Sigma^-)$ decay was found to be 0.32 ± 0.07 at the shock-wave temperature adopted. An intense spike of chemiluminescence due to $OH(A^2\Sigma^+ \rightarrow X^2\Pi)$ was observed, a finding which indicates a possible participation of the channel $NH(^3\Sigma^-)$ + NO $\longrightarrow$ N_2 + $OH(A^2\Sigma^+)$ at high temperatures.

1. Introduction

We have previously studied the reaction of $NH(^1\Delta)$ with NO in the gas phase at room temperature.[1] The results have been in essence (1) that the reaction should proceed through an intermediacy of an adduct radical HNNO and (2) that the subsequent decomposition of HNNO gives rise to N_2O + H in prevalence over the channel leading to N_2 + OH. Ab initio configuration-interaction (CI) calculations of the potential energy profiles [1] rationalized the experimental results.

Gas-phase reaction of $NH(^3\Sigma^-)$ with NO is intriguing in connection with the above-mentioned chemistry of $NH(^1\Delta)$ on one hand and with the issue of the process control for fuel combustions on the other. The reaction has already received interest by several groups of workers,[2-7] who unanimously claim that the $NH(^3\Sigma^-)$ decays essentially at the collision-controlled rate, the rate constant being on the order of 10^{13} $cm^3mol^{-1}s^{-1}$. However, product identification as the most important phase of chemical kinetics has remained unsettled.

In the present study, we intend to elucidate the kinetic feature of the $NH(^3\Sigma^-)$-NO system, paying due attention to the time-dependent behavior of products. For this purpose, we have shock-heated the HNCO/NO/Ar mixtures of varying composition to ca 3500 K, to let the $NH(^3\Sigma^-)$ entity generated by the thermal decomposition [8]

$$HNCO + Ar \longrightarrow NH(^3\Sigma^-) + CO + Ar \qquad (1)$$

react with the coexisting NO. In analogy to the case of $NH(^1\Delta)$, the reaction is expected to proceed in the following manner:

$$NH(^3\Sigma^-) + NO \longrightarrow [HNNO]^* \longrightarrow N_2O + H \qquad (2a)$$

$$[HNNO]^* \longrightarrow N_2 + OH \qquad (2b)$$

Unfortunately, however, N_2O if formed by reaction (2a) is liable to be readily decomposed into N_2 + O under the experimental conditions adopted. Thus, monitoring the OH radical to be formed by reaction (2b) will be a central issue of this study.

2. Experimental

The conventional incident shock tube described in a previous study [6] was used. Only the optical arrangement was altered. Time-resolved emission spectra were observed in the spectral region of 337.0 ± 3.0 nm for NH($A^3\Pi$-$X^3\Sigma^-$) and 309.1 ± 3.0 nm for OH($A^2\Sigma^+$-$X^2\Pi$). A Nikon-P250 grating monochromator with 1200 lines/mm and F=4.5 and a Hamamatsu 1P28 photomultiplier were used without lens or concave mirror. Time resolution arising from the observation volume was about 2 μs. The signals were amplified with an electronic rise time 2.2*RC* less than 1 μs and stored in a digital storage scope (Kawasaki electronica KDS-103). Sample gases were shock-heated to about 3500 K in the pressure range of 210~870 Torr. The compositions HNCO/NO/Ar of the samples used were 0.021 / 0.595 / 99.4 for the NH measurements and 0.048 / 1.10 / 98.9 and 0.053 / 0.616 / 99.3 for the OH measurements. The OH emission sensitivity was calibrated on the basis of the H_2/O_2/Ar experiments under the same conditions.

HNCO was synthesized by the reaction of potassium cyanate KCNO with excess stearic acid at 90 - 110 °C in a vacuum glass line. After removal of water using P_2O_5 and purification by means of trap-to-trap distillations at -80 °C, HNCO was stored at -196 °C and vaporized prior to use. NO(99.99%), H_2(99.999%), O_2(99.8%), N_2O(99.9%)(Takachiho Kagaku Inc.) and Ar(99.999%)(Seitetsu Kagaku Inc.) were used without further purification. Gas mixtures diluted in argon were stored in a 6-l pylex bulb for more than one day.

3. Results

(A) Decay of NH.

The NH emission-time profiles recorded have exhibited a rapid rise within 10 to 20 μs after the arrival of shock and subsequent decay during 40 to 100 μs. From these decay curves we have evaluated the rate constants k_2 of the overall reaction (2), assuming a pseudo first-order decay law in excess of NO. The rate constant was determined to be $k_2 = (7.1 \pm 0.5) \times 10^{12}$ $cm^3mol^{-1}s^{-1}$ at ca. 3500 K.

Figure 1 shows the Arrhenius plots of the reported experimental k_2 values at various temperatures including the value obtained in the present study. A negative temperature dependence is evident. The plotted points are best fitted by the Arrhenius equation, $k_2 = A \exp(-Ea/RT)$, with $A = (7.8 \pm 0.6) \times 10^{12}$ $cm^3mol^{-1}s^{-1}$ and $Ea = -(3.5 \pm 0.3)$ kJ mol^{-1}. The results indicate that the association step (HNNO formation) involving no potential energy barrier should be rate-controlling.

(B) Formation of OH

In the OH emission-time profiles, an intense emission was observed during a period of initial 30 μs, as is shown in Fig.2. We attribute this emission to the $OH(A^2\Sigma^+ \rightarrow X^2\Pi)$ chemiluminescence, as will be discussed later. After the intense spike, almost steady or slowly increasing emission profiles were observed. These latter emissions are due to $OH(A^2\Sigma^+)$ which is in thermal equilibration with $OH(X^2\Pi)$. Thus, the emission intensity of this steady part directly corresponds to the concentration of $OH(X^2\Pi)$.

In order to determine the rate constant k_{2b}, and hence the branching ratio $\beta \equiv k_{2b}/k_2$, we have decided to recourse to the computer simulation technique. Thus, we intend to search for the value of k_{2b} that will best reproduce the time-concentration profiles of OH observed under the varying experimental condition. To this end, we have invoked several elementary reactions to be considered concurrently at high temperatures. The elementary steps chosen for the simulation

are listed in Table 1, together with pertinent Arrhenius parameters. For reaction (1), we have chosen the most recent kinetic data obtained by Hanson et al. [9] For reactions (2a) and (2b) of our present interest, we use the rate constants $(1-\beta)k_2$ and βk_2, respectively, where k_2 is the above-mentioned rate constant for the net decay of NH. Reactions 3 through 6 are those elementary processes which are known to be important in simulating the time-concentration profile of $NH(^3\Sigma^-)$ after its generation by reaction (1).[8] The remaining reactions are all those that are related somehow with the OH radical. Reaction 7 in particular is the key reaction which has turned up to be of importance in the high temperature region above 2300 K.[10] The rate constants for reactions 8 through 13 were all taken from the literature.[11]

An example of the curve-fittings by simulation is shown in Fig. 2. As can be seen in Fig. 2, the calculated OH concentration first tends to increase with the decaying NH concentration. The OH concentration observed in this sample run stays at a nearly constant level of 3×10^{-10} mol/cm3 over the time period of 25 - 125 μs. The curve simulated under the assumption that $\beta = 1.0$ definitely overestimates the OH concentration. It appears that the best fit of the calculated curve to the observed is attainable when β is assigned a value of 0.28. Note that the OH concentration approaches the experimentally observed steady level even when reaction (2b) has been assumed to make no contribution at all, i.e., $\beta = 0$. This is simply because of the situation that reactions 7 and 12 can make significant contributions in the prolonged time region considered.

Computer simulations as delineated above have been conducted for a total of 9 runs. Results for typical runs are summarized in Table 2, together with the relevant experimental data. The values of β appear to be nearly constant at 0.32 ± 0.07 on the average, the allowance limit attached being the probable error. Taking this branching ratio as granted, the branching ratio for reaction (2a) is estimated to be 0.68 ± 0.07 which is in good agreement with the ratio deduced previously for the case of the reaction of $NH(^1\Delta)$.

4. Discussion

(A) Branching Ratio

The branching ratio depends on the excess energy and temperature. We have calculated the branching ratio at 3500 K on the basis of the RRKM theory. Since the reactions to be taken into account are only (2a) and (2b), it is enough to calculate only the ratio k_{2a}/k_{2b}. In the basic RRKM theory, the ratio of the specific rate constants is given by

$$\frac{k_{2a}(E)}{k_{2b}(E)} = \frac{N_a(E-E_a)}{N_b(E-E_b)} \qquad \text{(I)}$$

Here, $k_{2i}(E)$, i being a or b, is the rate constant at a specific energy E, which is measured from the potential energy minimum for HNNO; $N_i(E-E_i)$ is the number of available states for the respective transition states with an energy in excess over E_i, and Ei is the barrier height for reaction ($2i$). In order to obtain the ratio k_{2a}/k_{2b} Eq.I need be integrated over the energy distribution. We assume that chemically activated HNNO upon its formation by the association of NH with NO would undergo fragmentation, before collisional stabilization affects the internal energy distribution. Thus, we may write approximately,[12)]

$$\frac{k_{2a}}{k_{2b}} = \int_{E_0}^{\infty} \frac{N_a(E-E_a)}{N_b(E-E_b)} F(E)dE \qquad \text{(II)}$$

where E_0 is the reactant potential energy level and where $F(E)$ is the energy distribution function:

$$F(E) = \frac{N(E-E_0)\exp(-E/kT)}{\int_0^{\infty} N(E-E_0)\exp(-E/kT)dE} \qquad \text{(III)}$$

with $N(E)$ as the number of available states for HNNO having energy in excess over E_0.

In calculating the ratio k_{2a}/k_{2b} according to Eq. II, the energy humps E_0, E_a and E_b were all taken from the results of our previous CI calculations (Fig. 3). Thus, they are 252, 201 and 214 kJ/mol, respectively. The values of N, N_a and N_b were all evaluated by the Whitten-Rabinovitch approximation,[13] using the fundamental vibrational frequencies obtained from the ab initio SCF calculations. At 3500 K, k_{2a}/k_{2b} has come out to be 3.2. It follows that $\beta = 0.24$, in reasonable agreement with the experimental value of 0.32. The small discrepancy between the calculated and observed values may be due to the uncertainty attached to the calculated potential energies of the transition states as well as the dynamically preferential formation of $OH(X^2\Pi) + N_2$, i.e. the non-statistical behavior of HNNO. Either way, it is confirmed that a sizable amount of OH can arise from reaction (2), although it may not innately be the main product. Further, we have obtained β = 0.31 and 0.19 for $NH(^1\Delta) + NO$ and $NH(^3\Sigma^-) + NO$, respectively, both at 300 K. The former value is in good accord with our previous results of the N_2O quantum yield measurements [$\phi_{N2O} \equiv 1-\beta = 0.7$].[1]

Incidentally, the above discussions presume that the HNNO adduct to be formed from $NH(^3\Sigma^-) + NO$ be in its ground electronic state (X^2A_1), just as in the case of the $NH(^1\Delta) + NO$ system. The presumption will be acceptable in view of the possibility of an effective "conical" crossing between the two doublet surfaces of the interacting HN ----NO system.

(B) OH Chemiluminescence

The initial spike in the OH emission profiles is attributed to the $OH(A^2\Sigma^+ \rightarrow X^2\Pi)$ chemiluminescence on the basis of the following observations. First, the emission was observed in the absorption experiments as well. That is, in order to monitor the OH concentration, we applied also the absorption technique using a $He-H_2O$ microwave-discharge lamp as a light source of the OH absorption.

Obtained profiles were of course quite different from the emission profiles. However, the initial spike was still an intense emission in contrast to the subsequent steady part which was observed as absorption. Second, we have examined a wavelength-dependence of the peak height of the spike. The result was that a maximum was found near 308 nm, which is consistent with the OH(A-X) band. Third, when temperature was raised from 3500 K to 4100 K, the peak height did not increase correspondingly as did the subsequent steady part. Fourth, when $N_2O/H_2/Ar$ gas mixtures were shock-heated, a similar intense spike was observed. In addition, when O_2 or H_2O, instead of NO, was added to the HNCO/Ar gas mixtures, no emission spike was observed. These observations imply that the initial spike arises from both the reaction NH + NO and the reaction N_2O + H. The latter may occur as follows:

$$N_2O + Ar \longrightarrow N_2 + O + Ar \qquad (13)$$

$$H_2 + O \longrightarrow OH + H \qquad (14)$$

$$N_2O + H \longrightarrow [HNNO]^* \longrightarrow OH(A^2\Sigma^+) + N_2 \qquad (15)$$

It should be noted that the initial step of reaction (15) is nothing but the reverse process of the unimolecular step of reaction (2a).

The formation of $OH(A^2\Sigma^+)$ is formally represented as

$$NH(^3\Sigma^-) + NO \longrightarrow [HNNO] \longrightarrow N_2 + OH(A^2\Sigma^+) \qquad (2c)$$

The branching ratio of reaction (2c) has been estimated from the comparison of the chemiluminescence intensity with the thermal emission intensity. We assume that the relative intensity is equal to the rate of the $OH(A^2\Sigma^+)$ formation through reaction (2c) relative to that through the excitation of $OH(X^2\Pi)$ on collisions with Ar:

$$\frac{I_{chem.}}{I_{therm.}} = \frac{k_{2c}[NH(^3\Sigma^-)][NO]}{k_{ex}[OH(X^2\Pi)][Ar]} \qquad (IV)$$

Here, k_{ex} denotes the rate constant for the collisional excitation, which may be assumed to be equal to k_{quench} K_{ex}, in which k_{quench} is the quenching rate constant [14] and K_{ex} is the equilibrium constant between $OH(X^2\Pi)$ and $OH(A^2\Sigma^+)$. As a result, we have estimated $k_{2c} \leq 7 \times 10^{10} cm^3 mol^{-1} s^{-1}$. The branching ratio for reaction (2c) is thus less than 0.01. Considering that reaction (2c) is only slightly exothermic, the reaction is expected to have a significantly high barrier.

Hoffmann et al. have already reported on the same chemiluminescence arising from the reaction of N_2O with the H atom having a kinetic energy of ca. 2.5 eV under bulk conditions (single collision and arrested-relaxation).[15] At lower H-atom kinetic energies (ca. 1.8 eV), however, there was no chemiluminescence. Since the N_2O + H system lies about 1.5 eV below the $NH(^3\Sigma^-)$ + NO system, the threshold energy for the production of $OH(A^2\Sigma^+)$ + N_2 from $NH(^3\Sigma^-)$ + NO should lie 0.3 to 1.0 eV above the energy level for $NH(^3\Sigma^-)$ + NO.

Previous ab initio MO calculations[1] have revealed that the ground state $HNNO(\mathbf{1}^2A')$ surface is correlated to $OH(X^2\Pi)$ + N_2 adiabatically. Therefore, it is most likely that for the first excited state $HNNO(\mathbf{2}^2A')$ an adiabatic potential energy surface correlates to $OH(A^2\Sigma^+)$ + N_2. The virtual excitation energy of the $HNNO(\mathbf{2}^2A')$ at the equilibrium geometry of cis-$HNNO(\mathbf{1}^2A')$ has been calculated by MRD-CI method to be 105 kJ/mol, as has been shown in Fig.3. Geometry optimization and MRD-CI (two roots) calculations were carried out using the 4-31G** basis set. This excitation energy seems to be low enough for the internal conversion from $\mathbf{1}^2A'$ to $\mathbf{2}^2A'$ to occur. Additionally, in the $\mathbf{1}^2A'$ state, the odd electron is localized on the oxygen in-plane p-orbital directing to the hydrogen atom side, whereas the orbital is almost doubly occupied in the $\mathbf{2}^2A'$ state. These features lead us to a speculation that the 1,3 hydrogen migration occurs in the manner of a hydrogen atom abstraction by the oxygen atom in the $\mathbf{1}^2A'$ state, while

in the $2^2A'$ state this will proceed by way of a proton transfer onto the lone pair of oxygen. For the purpose of clearer discussion on the mechanism of the formation of $OH(A^2\Sigma^+)$, ab initio MCSCF calculations on the excited state surface are required.

5. Conclusions

From the time-concentration profiles of the OH radicals formed in the shock-heated HNCO/NO/Ar mixtures, the branching ratio of the reaction, $NH(^3\Sigma^-) + NO \longrightarrow OH(X^2\Pi) + N_2$, was determined to be 0.32 ± 0.07. The experimental result was rationalized by the RRKM treatments of the product-determining step.

A new chemiluminescent reaction; $NH(^3\Sigma^-) + NO \longrightarrow OH(A^2\Sigma^+) + N_2$ was found, although it is a minor channel.

References

1) T. Fueno, M. Fukuda, and K. Yokoyama, Chem. Phys., **124**, 265 (1988).

2) J. A. Harrison, A. R. Whyte, and L. F. Phillips, Chem. Phys. Lett., **129**, 346 (1985).

3) I. Hansen, K. Hoinghaus, C. Zetzsch, and F. Stuhl, Chem. Phys. Lett., **42**, 370 (1976)

4) S. Gordon, W. Mulac, and P. Nangia, J. Phys. Chem., **75**, 2087 (1971).

5) J. W. Cox, H. H. Nelson, and J. R. McDonald, Chem. Phys., **96**, 175 (1985).

6) A. M. Dean, M. S. Chou, and D. Stern, Int. J. Chem. Kinet., **16**, 633 (1984).

7) O. Kondo, Doctoral Dissertation, Osaka University (1982).

8) O. Kajimoto, O. Kondo, K. Okada, J. Fujikane, and T. Fueno, Bull. Chem. Soc. Jpn., **58**, 3469 (1985).

9) J. D. Mertens, A. Y. Chang, R. K. Hanson, and C. T. Bowman, Int. J. Chem. Kinet., **21**, 1049 (1989).

10) K. Yokoyama and T. Fueno, Bull. Chem. Soc. Jpn., to be published.

11) F. Westley, "Table of Recommended Rate Constants for Chemical Reactions Occurring in Combustion," National Bureau of Standards, Washington, D. C. (1980).

12) W. N. Olmstead and J. I. Brauman, J. Am. Chem. Soc., **99**, 4219 (1977).

13) G. Z. Whitten and B. S. Rabinovitch, J. Chem. Phys., **38**, 2466 (1963).

14) K. H. Becker, D. Haaks, and Tatarczyk, Chem. Phys. Lett., **25**, 564 (1974).

15) G. Hoffmann, D. Oh, and C. Wittig, J. Chem. Soc., Faraday Trans. 2, **85**, 1141 (1989).

16) M. W. Chase, Jr., C. A. Davies, J. R. Downey, Jr., D. J. Frurip, R. A. McDonald, and A. N. Syverud, "JANAF thermochemical Tables," 3rd ed, National Bureau of Standards, Washington, D. C. (1985).

Table 1. Elementary Reactions Used for the Simulations of the Time-Concentration Profiles of the OH radical.

No.	Reaction [a]	log A ($cm^3mol^{-1}s^{-1}$)	n	Ea ($kJ\ mol^{-1}$)	ref.
1	$HNCO + Ar \longrightarrow NH + CO + Ar$	35.51	-5.11	460	8
2a	$NH + NO \longrightarrow N_2O + H$	$(1-\beta)k_2$	0	0	this study
2b	$NH + NO \longrightarrow OH + N_2$	βk_2	0	0	this study
3	$NH + NH \longrightarrow N_2 + 2H$	13.65	0	0	8
4	$NH + Ar \longrightarrow N + H + Ar$	14.42	0	316	8
5	$H + HNCO \longrightarrow NH_2 + CO$	14.04	0	223	8
6	$NH_2 + Ar \longrightarrow NH + H + Ar$	23.50	-2.0	382	9
7	$NH + CO \longrightarrow CN + OH$	13.00	0	0	10
8	$OH + H \longrightarrow H_2 + O$	9.90	1	29	11
		10.26 [b]	1 [b]	37 [b]	11
9	$OH + O \longrightarrow O_2 + H$	13.40	0	0	11
		14.34 [b]	0 [b]	70.3 [b]	11
10	$OH + H_2 \longrightarrow H_2O + H$	13.34	0	21.7	11
11	$OH + Ar \longrightarrow O + H + Ar$	18.90	-1	439	11
12	$NO + H \longrightarrow OH + N$	12.40	0.5	201	11
13	$N_2O + Ar \longrightarrow N_2 + O + Ar$	14.70	0	243	11

a) The rate constant $k = AT^n\exp(-Ea/RT)$ $cm^3mol^{-1}s^{-1}$.

b) For the reverse processes.

Table 2. Run Conditions and the Branching Ratio β for the Reaction $NH(^3\Sigma^-) + NO \longrightarrow OH + N_2$.

No.	[Ar]	$[HNCO]_0$	$[NO]_0$	P_2	T_2	ρ_{21}	β
	10^{-6}mol cm^{-3}	10^{-9}mol cm^{-3}		Torr	K		
1	1.26	0.61	13.9	279	3539	3.69	0.29
2	1.12	0.59	6.9	233	3355	3.67	0.25
3	1.79	0.95	11.0	380	3404	3.68	0.29
4	1.80	0.95	11.1	359	3207	3.66	0.38
5	3.73	1.98	23.0	846	3637	3.70	0.28
6	4.05	2.15	25.0	871	3444	3.68	0.44

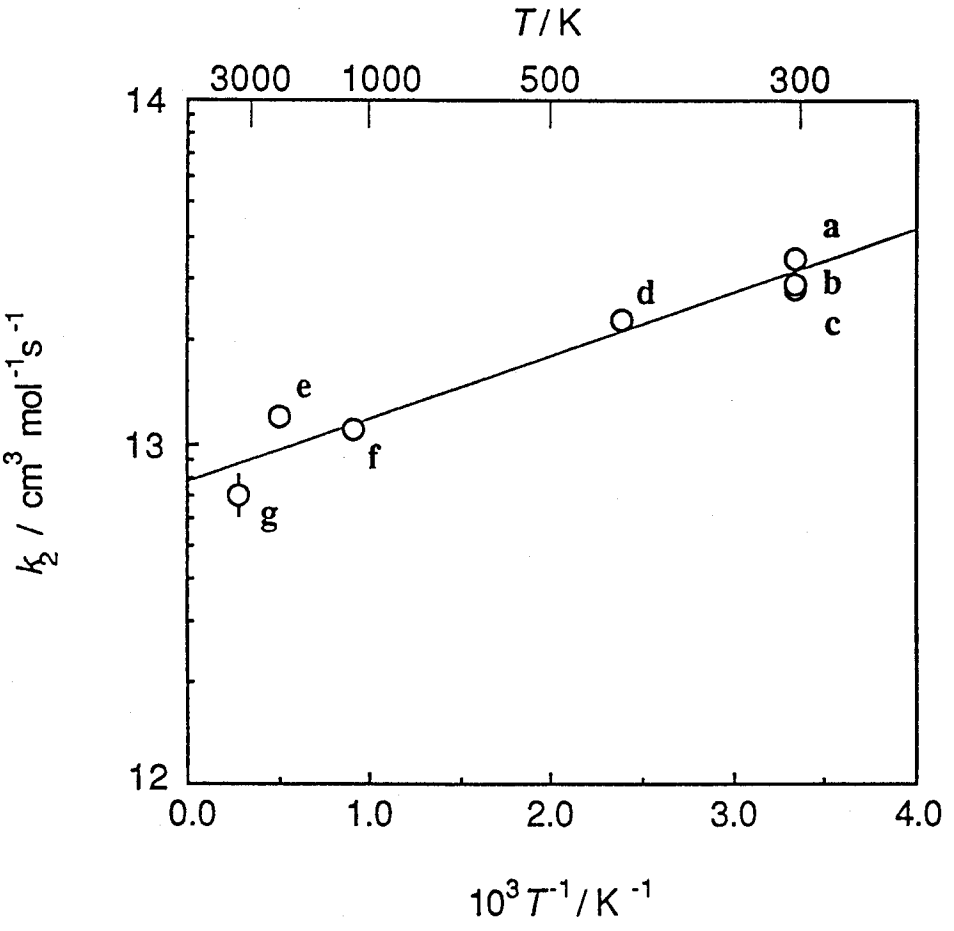

Fig. 1. Arrhenius plots of k_2. **a**, Harrison et al.[2]; **b**, Hansen et at.[3]; **c**, Cox et al.[5]; **d**, Gordon et al.[4]; **e**, Dean et al.[6]; **f**, Kondo [7]; **g**, the present work.

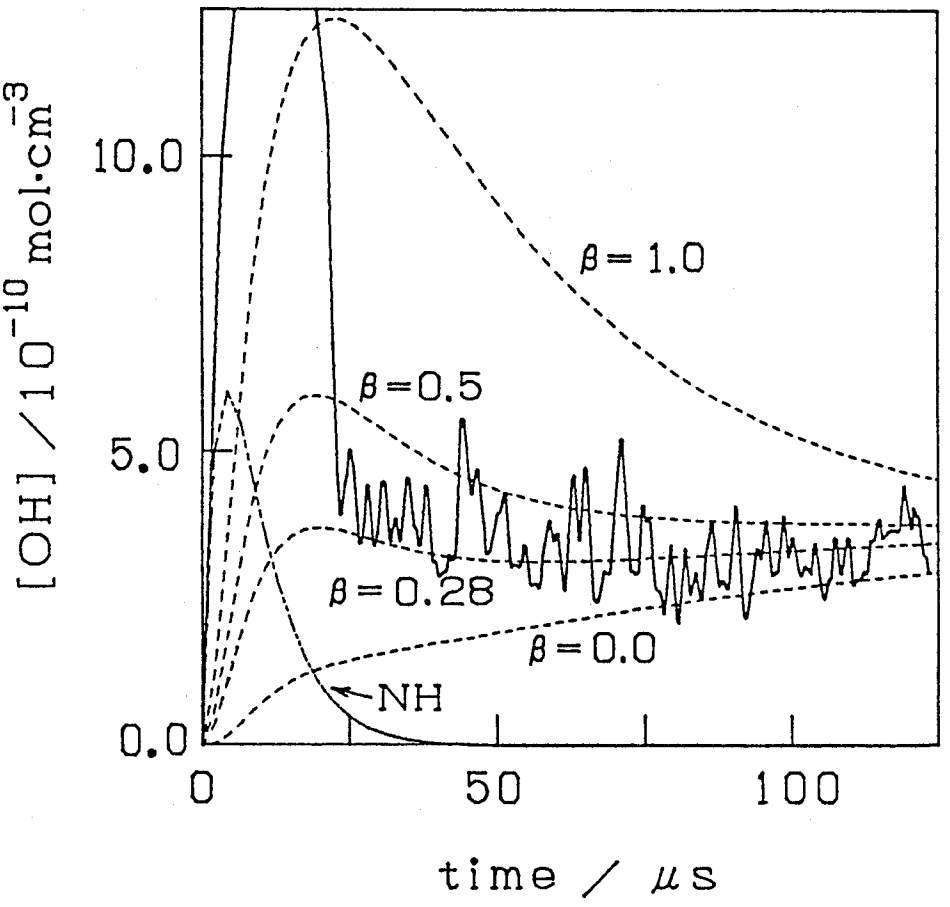

Fig. 2. Comparisons of the computed OH concentration profiles (----) with the observed (–). T_2= 3637 K, P_2= 846 Torr, HNCO/NO/Ar = 0.053 / 0.613 / 99.33.

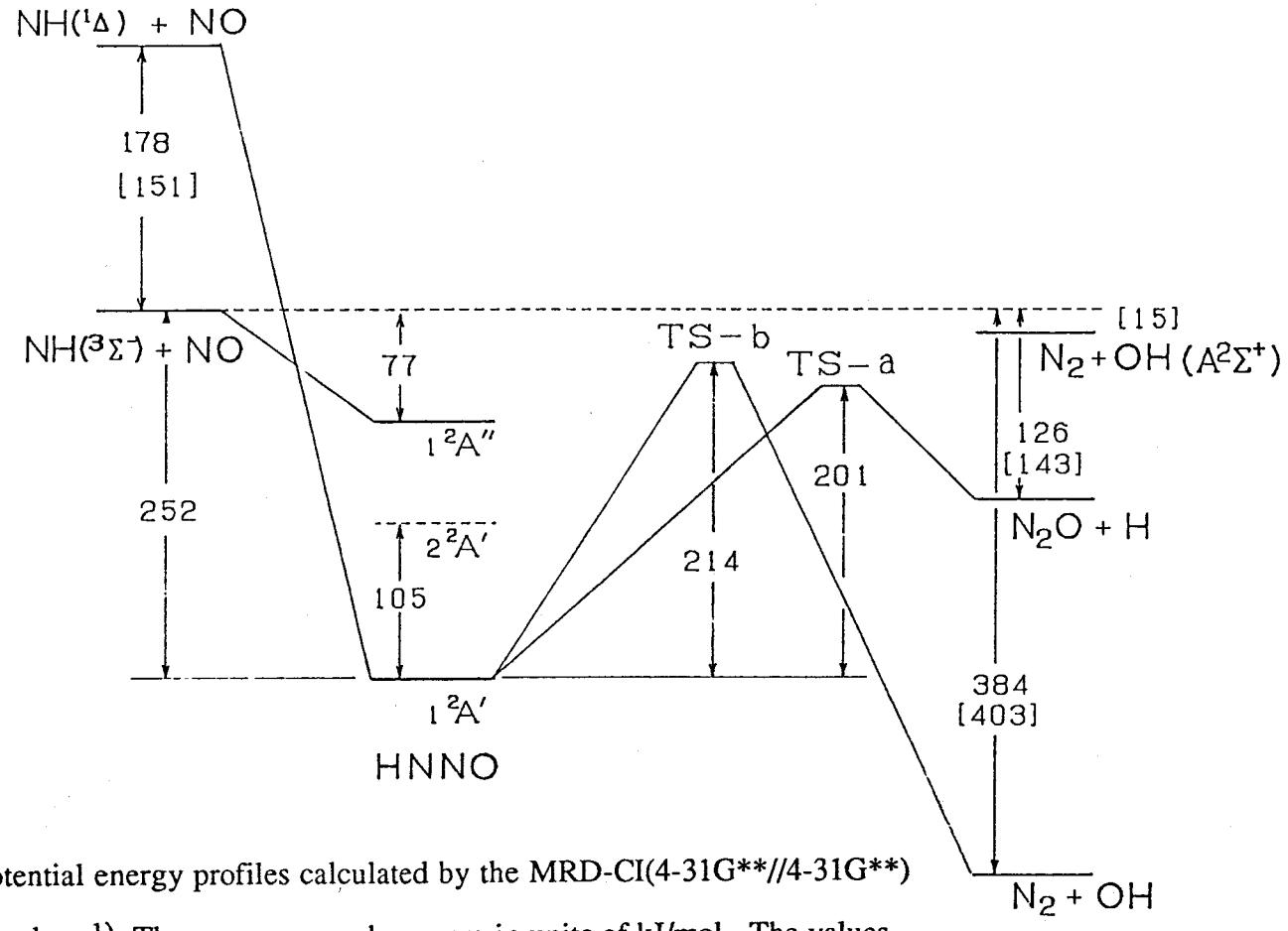

Fig. 3. Potential energy profiles calculated by the MRD-CI(4-31G**//4-31G**) procedure.[1)] The energy gaps shown are in units of kJ/mol. The values given in brackets are those obtained from the relevant thermochemical data.[16)] TS-a and TS-b denote the transition states located for the unimolecular steps of reactions (2a) and (2b), respectively.

Chapter 4

Electronic Structure and the Unimolecular Reaction Pathways of HNOO

Electronic structure and possible unimolecular reaction paths of a linear four-atom molecule HNOO to be formed by the addition of $NH(^3\Sigma^-)$ toward $O_2(^3\Sigma_g^-)$ are investigated by the SCF and MRD-CI calculations employing the 6-31G** basis functions. Geometries and excitation energies of various one-electron excited states, both singlet and triplet, are examined. The isomerization paths of the ground-state $HNOO(^1A_1)$ are traced, by a multi-configuration (MC) SCF procedure. It has proved that the energetically most favorable is the 1,3-hydrogen migration to give hydroperoxynitrene $NOOH(^1A_1)$ with the activation barrier of 96 kJ/mol. The nitrene should be extremely unstable; it is liable to be readily decomposed to NO + OH with virtually no activation barrier.

1. Introduction

In these past years, we have concerned ourselves with the investigations of the reactions of the imino radical NH theoretically [1] as well as experimentally. The reaction of NH with O_2 in the gas phase is of interest along this line and seems to be of importance as well in relation to the chemistry of fuel combustions. The reaction has already received interest of experimental kineticists. Thus, Zetzsch and Hansen were the first group of workers, who measured the rate of the reaction between $NH(^3\Sigma^-)$ and $O_2(^3\Sigma_g^-)$.[2] The reaction has long been known to give NO and OH simultaneously during the decay of $NH(^3\Sigma^-)$.[3] Recently, Hack et al. traced the same reaction by monitoring the laser-induced fluorescence of OH as well as $NH(^3\Sigma^-)$, to conclude that the activation energy is 6.4 kJ/mol in the temperature range 286-543 K.[4]

Naively, the reaction is expected to involve an initial association.

$$NH + O_2 \longrightarrow HNOO \qquad (1)$$

Little is known, however, as to the structural characteristics of HNOO, except for the possibility that there can exist various conformations for its diradical form.[5] Still less has been noted regarding the dynamical path of its isomerization / fragmentation process.

$$HNOO \longrightarrow NO + OH \qquad (2)$$

In the present work, we examine reactions (1) and (2) by ab initio computations. We will first optimize geometries of the various diradical (excited) states of HNOO as well as the singlet ground state, and estimate the electronic excitation energies. The paths of isomerization reactions of the

ground-state HNOO will then be traced by the multi-configuration (MC) SCF procedure. The activation barrier heights are calculated by the multi-reference double-excitation (MRD) configuration-interaction (CI) method. In the light of the results of theoretical calculations, possible pathways for reaction (2) will be discussed.

2. Method of calculation

Geometry optimizations of HNOO diradicals were carried out by the UHF SCF procedure using the Gaussian 82 program package.[6] For the ground state of HNOO ($^1A_1$) in particular, multi-configuration (MC) SCF method has been adopted, since its electronic structure is basically of the closed-shell type and yet involves contributions of doubly-excited configurations to an unignorable extent. In practice, we used for the sake of convenience the limited-configuration formalism in which six electrons are accommodated in six frontier orbitals with the remaining electrons are frozen in the low-lying molecular orbitals. Paths of the isomerization of HNOO ($^1A_1$) were traced by the same MC SCF procedure. The basis sets employed are throughout the conventional 6-31G functions [7] augmented with one set each of d or p polarization functions for every atom involved.

MRD-CI calculations were performed for all the stationary geometries located.[8,9] The TABLE MRD-CI program furnished by Buenker was used. The configuration-selection and extrapolation routines were followed.[10] The extrapolated CI energies were all subjected to the Langhoff-Davidson corrections,[11] to estimate the full CI limit values. Since the corrected CI energies are relatively insensitive to the number of the reference configurations chosen, we adopt them as the ultimate CI energies and will denote them as E_{CI}. Other technical details of the MRD-CI calculations carried out here are

exactly the same as those described in our previous work on S_2O [12] and CH_2CH_2NH.[1e]

3. Results

3.1. Ground singlet state

The HNOO molecule in its ground electronic state is a planar four-π-electron system (A_1) . Preliminary MRD-CI calculations have revealed that it involves the contribution (squared weight $|c_i|^2$) of the ground configuration

$$X^1A_1 \; ; \; (1a')^2...(10a')^2 \, (1a'')^2 \, (2a'')^2$$

amounting only to 0.80. The contribution of the configuration arising from the two-electron transition $(2a'')^2 \rightarrow (3a'')^2$ is as large as 0.09. The state is thus regarded as a diradicaloid as in the case of O_3 and hence cannot be described properly by the conventional RHF formalism.

Under such circumstances, the ground $^1A_1$ state was subjected to the limited-space (6-electron / 6-orbital) MC SCF calculations to optimize its geometry. The structures, cis and trans, thus optimized are shown in Fig. 1. Results of MRD-CI calculations at these geometries are included in Fig. 1. Both of them may be regarded as zwitter-ionic O-oxides with a certain extent of biradical character. The cis isomer is predicted to be 1.6 kJ/mol more stable than the trans counterpart. Incidentally, the binding energy for the cis isomer against its decomposition into $NH(^3\Sigma^-) + O_2(^3\Sigma_g^-)$, is calculated to be 20 kJ/mol.

3.2. Diradical (excited) states

The low-lying excited states are all diradical in character. The most of these is a diradical such that the two odd electrons are localized on the pπ

orbitals of the nitrogen and the oxygen atom, which may be termed the $\pi\pi$ state.[5] Above the $\pi\pi$ state, those diradical states in which either one $p\pi$ orbital of the N and O atom is occupied by an electron, leaving the other electron in an in-plane n orbital of N or O. The states having one pi-electron localized on the N and O atoms will be referred to as the $\pi\sigma$ and $\sigma\pi$ states, respectively.[5] The state in which both $p\pi$ orbitals are occupied by a pair of electrons so that both the in-plane n orbitals constitute the radical sites is also conceivable. This last state may be referred to the $\sigma\sigma$ state.[5] Taking the ground configuration as the standard, the principal configurations of these various states are represented as follows;

$$\pi\pi\ (A')\ ;\ (2a'') \rightarrow (3a'')$$
$$\pi\sigma\ (A'')\ ;\ (10a') \rightarrow (3a'')$$
$$\sigma\pi\ (A'')\ ;\ (9a')\ (2a'') \rightarrow (3a'')^2$$
$$\sigma\sigma\ (A')\ ;\ (9a')\ (10a') \rightarrow (3a'')^2$$

Note that the $\pi\pi$ state is a four-π-electron (4π) system, while both the $\pi\sigma$ and $\sigma\pi$ have five π-electrons (5π). By the same token, the $\sigma\sigma$ state may be called a six-π-electron (6π) system.

Each diradical state can be either singlet or triplet. Besides, cis and trans configurations are possible for every state. Geometries of all these sixteen diradicals were optimized by the UHF SCF procedure. They were all confirmed to be planar in structure. The geometrical parameters are given in Tables 1 and 2 for the cis and trans configurations, respectively.

The total energies of the various diradical states were calculated by the MRD-CI procedure. The results expressed by taking the energy of the ground-state cis-HNOO as the standard are listed in Tables 1 and 2. Shown in Fig. 2 are the energy levels of these states. The levels for various combinations of the Σ and Δ states of the NH + O_2 system are also shown to illustrate the

state correlations. The lowest excited state is apparently the triplet $\pi\pi$ state ($^3A'$) of the cis isomer. Further, for both the cis and trans isomers, the $\pi\sigma$ states are no doubt more stable by ca. 2 eV than the $\sigma\pi$ states. However, it does not seem possible to make any generalization as to the relative stabilities between the singlet vs triplet excited states. Nor is it possible to conclude that the cis form of a given electronic state is generally more stable than the corresponding trans form.

3.3. Unimolecular reaction paths

Binkley et al.[13] considered theoretically the unimolecular decomposition pathway involving the ring closure of HNOO (**1**) followed by the O-O bond cleavage to give a symmetric (C_{2v}) HNO_2, hydrogen nitryl (**2**), a yet never identified entity. **2** would then suffer the isomerization into nitrous acid (**3**) as a direct precursor of NO and OH which are to be formed in equal amounts.

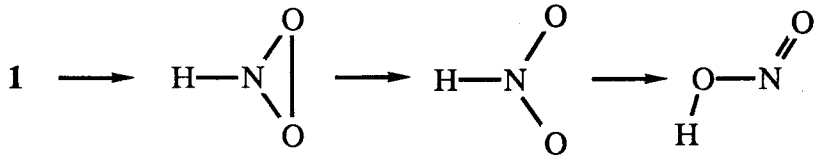

2 **3** (3)

The reaction sequence broached resembles the notable mechanism by which the methylene peroxide CH_2OO is believed to isomerize into formic acid HCOOH.[14]

We here assume that another pathway of decomposition involving the 1,3-hydrogen migration giving rise to hydroperoxynitrene (**4**) :

4 (4)

The singlet nitrene **4**, which has hitherto never been identified either, could also be a direct precursor of an equimolar mixture of NO and OH.

The minimum-energy path of reaction (3) as well as reaction (4) have been traced by the 6-electron / 6-orbital MC SCF procedure. The optimal geometries of the transition states located, TS1 and TS2, respectively for the initial ring closure in reaction (3) and the 1,3-hydrogen migration (4) are illustrated in Fig. 3, together with those for the resulting ring isomer and singlet nitrene. It should be noted that TS1 was found to be connected with the trans form of the reactant HNOO, whereas TS, with the cis structure by necessity.

The TS geometries were then dealt with by the MRD-CI procedure. The activation barrier heights were calculated to be 159 and 96 kJ/mol for TS1 and TS2, respectively. Clearly, the 1,3-hydrogen migration (4) is energetically more favorable than the ring closure in reaction (3).

The subsequent isomerization / fragmentation processes were treated likewise. The overall potential energy profiles obtained are illustrated in Fig. 4. The ring-opening reaction of the cyclic intermediate and the O-O bond cleavage of the nitrene (**4**) have both proved to have extremely low barriers (less than 10 kJ/mol). The transition state for the isomerization process **2** $\rightarrow$ **3** was found to be located ca. 90 kJ/mol below the ring entity. Thus, both the isomerization reactions related to TS1 and TS2 are the rate-determining step for the unimolecular decompositions of **1** giving NO + OH as ultimate products.

4. Discussion

As has already been mentioned, the binding energy of cis-HNOO in the ground states 20 kJ/mol. Therefore, the more favorable pathway of the HNOO decomposition involving the intermediary of **4** is predicted to have an effective activation barrier height of 76 kJ/mol against the initial binary system $NH(^3\Sigma^-)$ + $O_2(^3\Sigma_g^-)$. The net activation energy corrected for the vibrational zero-point energy comes out to be 70 kJ/mol. This is much greater than the experimental activation energy of 6.4 kJ/mol reported by Hack et al.[4] for the reaction :

$$NH(^3\Sigma^-) + O_2(^3\Sigma_g^-) \longrightarrow NO + OH \qquad (5)$$

Interestingly enough, the temperature dependence of the rate constants for reaction (5) observed in the high temperature region (~3500 K) corresponds to an empirical activation energy amounting to ca. 60 kJ/mol, in better agreement with the present result of theoretical calculations. Most likely, the non-Arrhenius character of the rate constants for reaction (5) is a consequence of the tunneling effect operative in the region of TS2.

The lowest triplet state of $HNOO(a^3A')$ will be formed by the addition of $NH(^3\Sigma^-)$ to $O_2(^1\Delta)$ with an activation barrier of 56 kJ/mol. With an additional energy of 9 kJ/mol, it will be collapsed into HNO + O :

$$NH(^3\Sigma^-) + O_2(^1\Delta) \longrightarrow HNO + O(^3P) \qquad (5)$$

Also, the reaction between $NH(^1\Delta)$ and $O_2(^1\Delta)$ will be a concerted cycloaddition to give the cyclic HNO_2. It is to be readily isomerized into nitrous acid (**5**) via hydrogen nitryl (**4**), an intriguing planar symmetric isomer of **5**.

5. Conclusions

$HNOO(^1A_1)$ to be formed by the association between $NH(^3\Sigma^-)$ and $O_2(^3\Sigma_g^-)$ is a zwitter-ionic diradicaloid with a binding energy of only 20 kJ/mol. The exchange reaction $NH(^3\Sigma^-) + O_2(^3\Sigma_g^-) \longrightarrow NO + OH$ is predicted to proceed through the rate-determining isomerization of $HNOO(^1A_1)$ into hydroperoxynitrene. The net activation barrier height was calculated to be 76 kJ/mol.

References

1) (a) T. Fueno, V. Bonacic-Koutecky, and J. Koutecky, J. Am. Chem. Soc., **105**, 5547 (1983)

(b) T. Fueno, O. Kajimoto, and V. Bonacic-Koutecky, J. Am. Chem. Soc., **106**, 406 (1984)

(c) T. Fueno, M. Fukuda, and K. Yokoyama, Chem. Phys., **124**, 265 (1988)

(d) T. Fueno, J. Mol. Struct. (Theochem), **170**, 143 (1988)

(e) T. Fueno, K.Yamaguchi, and O. Kondo, Bull. Chem. Soc. Jpn., **63**, 901 (1990)

2) C. Zetzsch and I. Hansen, Ber. Bunsen-Ges. Phys. Chem., **82**, 830 (1978)

3) G. M. Meaburn and S. Gordon, J. Phys. Chem., **72**, 1592 (1968)

4) W. Hack, H.Kurzke and H. Gg. Wagner, J. Chem. Soc., Faraday Trans. 2, **81**, 949 (1985)

5) K. Yamaguchi, S. Yabushita, and T. Fueno, J. Chem. Phys. , **71**, 2321 (1979)

6) J. S. Binkley, E. J. Frisch, D. J. DeFrees, K. Rahgavachari, D. J. DeFrees, H. B. Schlegel, R. A. Whiteside, E. M. Fluder, R. Seeger, J. A. Pople, J. H. Yates and K. K. Sunil, GAUSSIAN 82, Carnegie-Mellon University, IMS version.

7) W. J. Hehre, R. Ditchfield, and J. A. Pople, J. Chem. Phys., **56**, 2257 (1972); P. C. Hariharan and J. A. Pople, Theor. Chim. Acta (Berl.), **28**, 213 (1973)

8) R. J. Buenker, "Studies in Physical and Theoretical Chemistry", R. Carbo, ed., Elsevier, Amsterdam (1982), Vol. 21, pp. 17-34

9) R. J. Buenker, and R. A. Phillips, J. Mol. Struct. (Theochem), **123**, 291 (1985)

10) R. J. Buenker and S. D. Peyerimhoff, Theor. Chim. Acta (Berl.), **35**, 33 (1974); **39**, 217 (1975)

11) S. R. Langhoff and E. A. Davidson, Int. J. Quant. Chem., **8**, 61 (1974)

12) T. Fueno and R. J. Buenker, Theor. Chim. Acta (Berl.), **73**, 123 (1988)

13) C. F. Melius and J. B. Binkley, ACS Symp. Ser. , **249** (1984); cited in ref. 4

14) W. R. Wadt and W. A. Goddard III, J. Am. Chem. Soc., **97**, 3004 (1975)

15) K. Yokoyama, H. Kitaike, and T. Fueno, to be published.

Table 1. Optimized Geometries and the Relative Energies of the Diradical States for HNOO(cis)

	Singlet				Triplet			
	$^1\pi\pi$ (4π)	$^1\pi\sigma$ (5π)	$^1\sigma\pi$ (5π)	$^1\sigma\sigma$ (6π)	$^3\pi\pi$ (4π)	$^3\pi\sigma$ (5π)	$^3\sigma\pi$ (5π)	$^3\sigma\sigma$ (6π)
Geometry [a]								
R(N-O) / Å	1.339	1.333	1.374	1.396	1.365	1.338	1.368	1.396 [c]
R(O-O) / Å	1.290	1.386	1.273	1.365	1.317	1.374	1.271	1.365 [c]
R(H-N) / Å	1.014	1.013	0.999	0.999	1.012	1.014	1.000	0.999 [c]
∠NOO / °	114.7	110.3	108.6	98.2	111.4	110.2	108.7	98.2 [c]
∠HNO / °	105.6	107.0	127.7	129.7	104.0	106.8	127.0	129.7 [c]
Relative energy [b]								
ΔE_{CI} / eV	4.69	1.61	3.81	4.45	1.43	1.69	3.64	5.22

a) 1Å = 0.1 nm

b) Relative to cis-HNOO(X^1A'), for which E_{CI} = -205.03443 hartree

c) No stable UHF SCF minimum exists. The geometry parameters for $^1\sigma\sigma$ are assumed for CI calculations.

Table 2. Optimized Geometries and the Relative Energies of the Diradical States for HNOO(trans)

	Singlet				Triplet			
	$^1\pi\pi$ (4π)	$^1\pi\sigma$ (5π)	$^1\sigma\pi$ (5π)	$^1\sigma\sigma$ (6π)	$^3\pi\pi$ (4π)	$^3\pi\sigma$ (5π)	$^3\sigma\pi$ (5π)	$^3\sigma\sigma$ (6π)
Geometry [a]								
R(N-O) / Å	1.343	1.336	1.374	1.390	1.365	1.340	1.366	1.377
R(O-O) / Å	1.290	1.378	1.274	1.372	1.315	1.367	1.268	1.380
R(H-N) / Å	1.012	1.011	0.997	0.997	1.014	1.011	0.997	0.995
∠NOO / °	111.4	106.7	111.9	105.6	108.1	106.6	113.4	104.1
∠HNO / °	100.4	100.3	125.0	124.4	100.4	100.4	123.9	125.4
Relative energy [b]								
ΔE_{CI} / eV	5.05	1.48	3.48	5.19	1.64	1.60	3.41	4.99

a) 1Å = 0.1 nm

b) Relative to cis-HNOO(X^1A'), for which E_{CI} = -205.03443 hartree

HNOO(X^1A')

Geometry:

Limited-active-space(MC)-SCF/6-31G**

(2-configuration SCF)

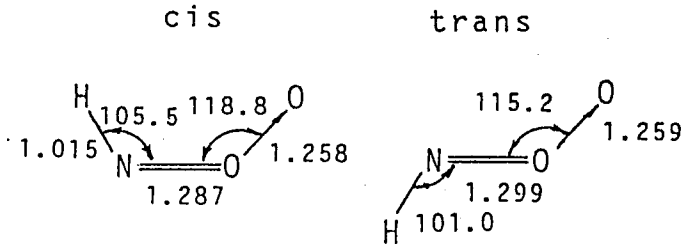

	cis	trans
E_{MC-SCF} =	-204.55251	-204.55170

Energy(CI):

MRD-CI/6-31G**//MC-SCF/6-31G**

T =	20 μh(9392/439806)	20 μh(9227/439806)
$E_{CI,T\rightarrow 0}$ =	-205.00525	-205.00436
$E_{full-CI}$ =	-205.03443	-205.03381

Configurations:

	$\lvert C_i \rvert^2$	$\lvert C_i \rvert^2$
Closed [a]	0.8083	0.7993
(2a'') → (3a'')	0.0852	0.0942
(8a')(1a'') → (12a')(3a'')	0.0062	0.0059

[a] Closed: $(1a')^2 \ldots (10a')^2 (1a'')^2 (2a'')^2$

Fig. 1 Geometries of cis- and trans-HNOO optimized by an MC SCF procedure.

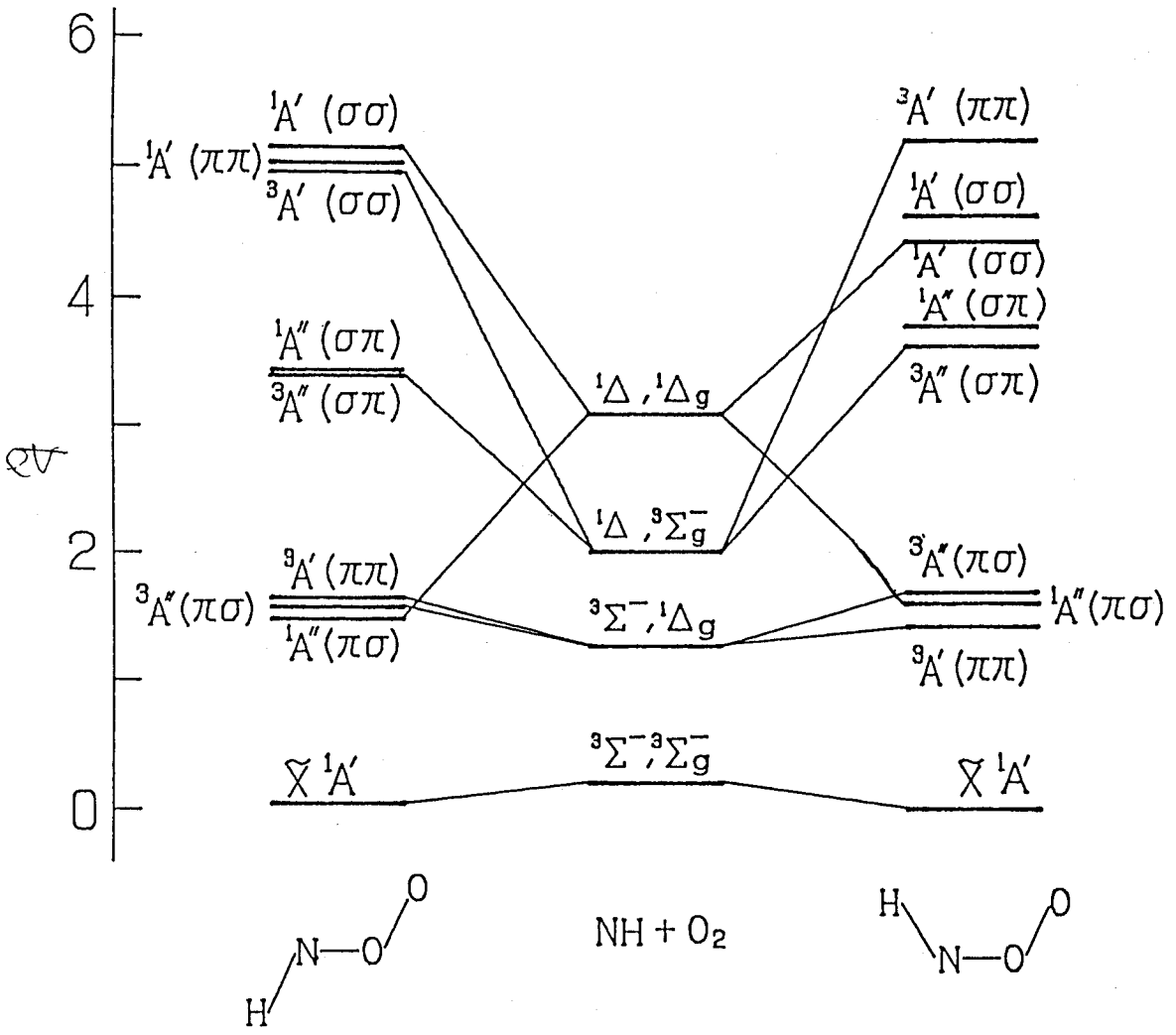

Fig. 2 Adiabatic excitation energies of singlet and triplet HNOO diradicals. cis-HNOO(X^1A_1) is taken as the standard.

Ring closure

LAS(MC)-SCF/6-31G**

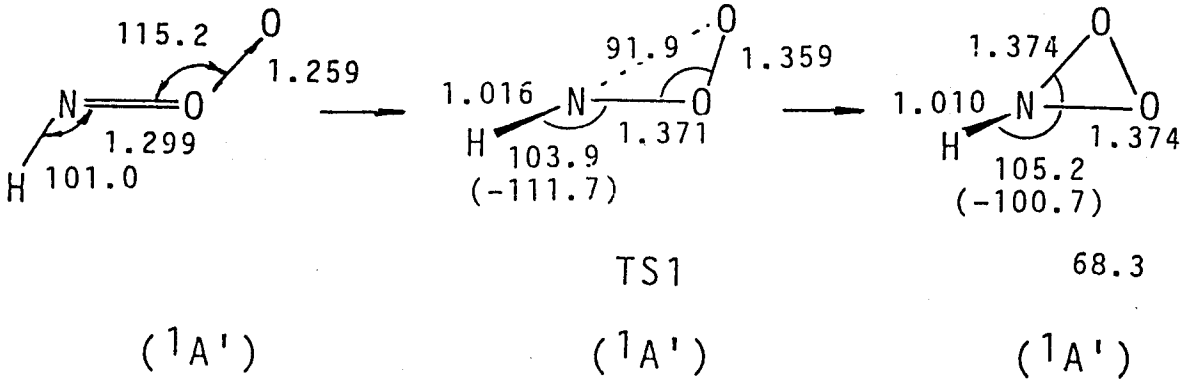

1,3-Hydrogen migration

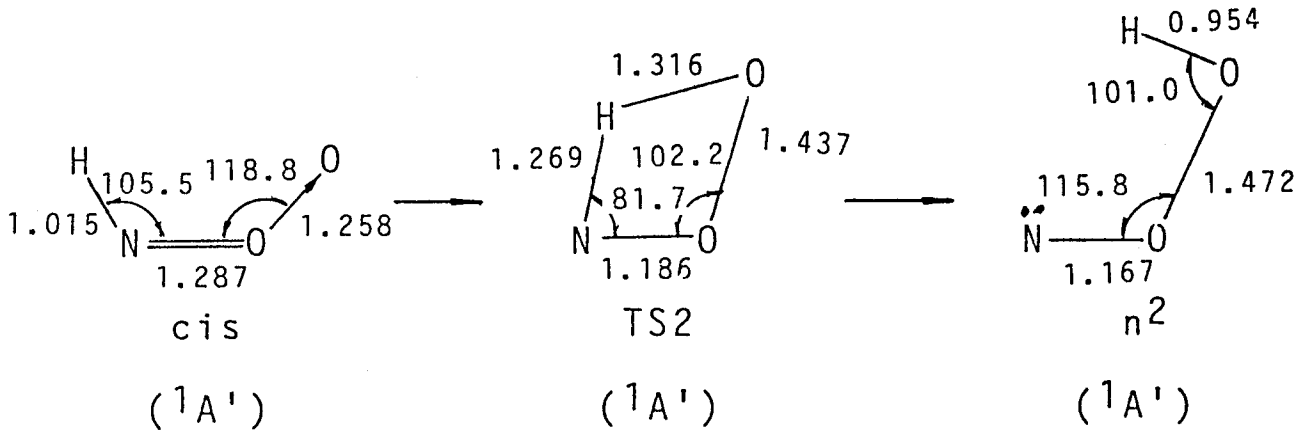

Fig. 3 Optimized geometries for the transition states and products of the ring closure in reaction (3) and the 1,3-hydrogen migration reaction (4) of HNOO(X^1A_1).

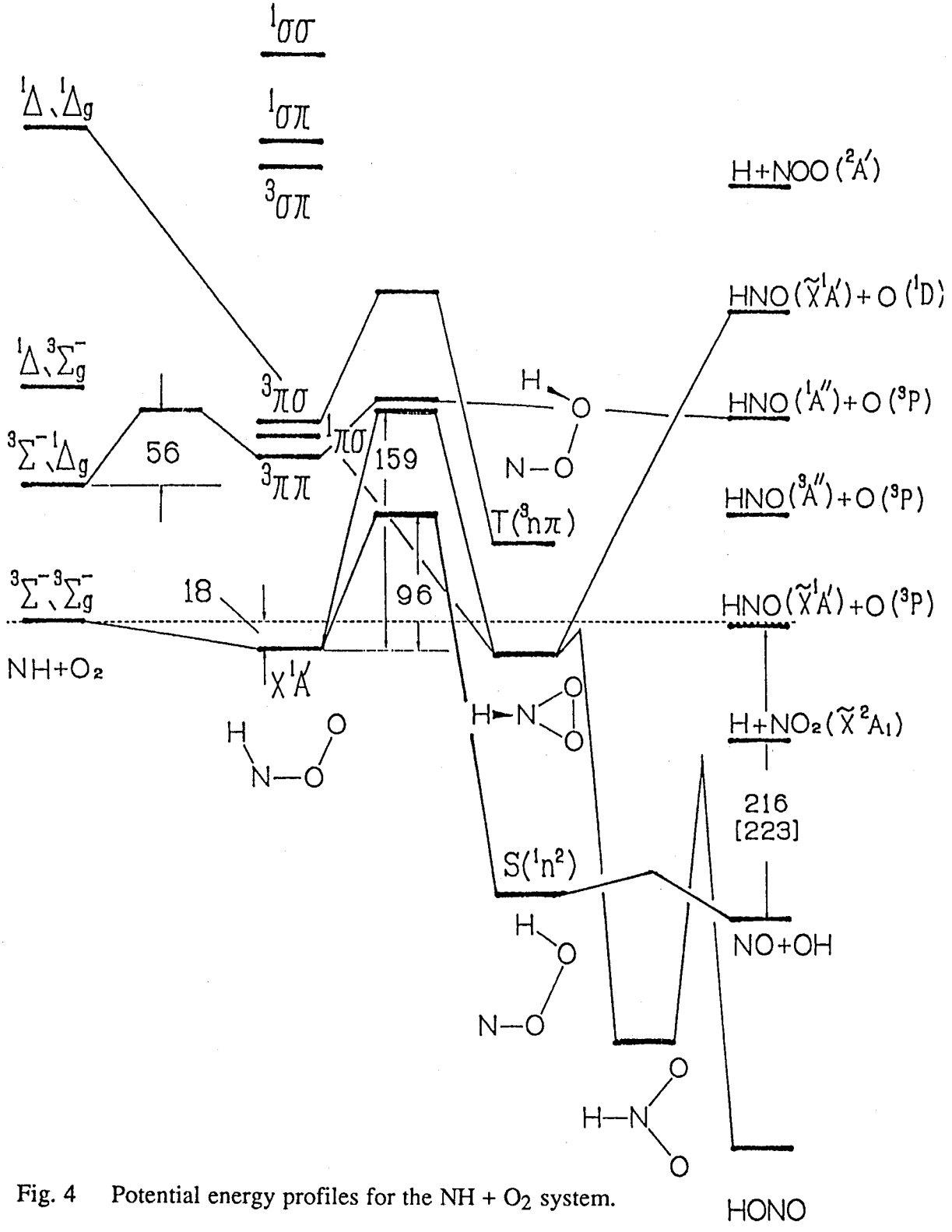

Fig. 4 Potential energy profiles for the NH + O_2 system.

Chapter 5

Kinetics and Mechanism of the Formation of the CN Radical in the Thermal Decomposition of Isocyanic Acid in Incident Shock Waves

Isocyanic acid HNCO diluted in argon was thermally decomposed behind incident shock waves in a temperature range of 2300 - 3600 K. The course of the cyano radical formation was traced by monitoring the emission of CN ($B^2\Sigma^+ \rightarrow X^2\Sigma^+$) at 388 ± 3 nm. From the CN concentration-time profiles, two types of reaction mechanisms for the CN production were inferred. One is a direct decomposition HNCO + Ar $\longrightarrow$ CN + OH + Ar (1c) while the other is a subsequent bimolecular reaction $NH(^3\Sigma^-)$ + CO $\longrightarrow$ CN + OH (2). From the initial slopes of the CN concentration-time profiles the rate constant of reaction (1c) was determined to be $k_{1c}=10^{12.97\pm0.73}\exp[-(266\pm40)\text{kJ mol}^{-1}/RT]$ $\text{cm}^3\text{mol}^{-1}\text{s}^{-1}$. From comparisons of the subsequent CN growth curves observed with those computed with a 17-reaction mechanism, the rate constant of reaction (2) was estimated to be $k_2 = 1.0 \times 10^{13}$ $\text{cm}^3\text{mol}^{-1}\text{s}^{-1}$ with little temperature dependence. Both reactions appear to involve the isomerization from HNCO to HOCN or HONC. In the lower temperature range the isomerization may compete with the main decomposition channel into $NH(^3\Sigma^-)$ + CO.

1. Introduction

Decomposition of isocyanic acid HNCO has been investigated photolytically or thermally by several groups.[1-7] In the photolysis at 193 nm the predominant products are $NH(^1\Delta)$ + CO,[1-4] whereas the pyrolysis gives rise to $NH(^3\Sigma^-)$ + CO,[5-7] exclusively. Small amounts of NCO and H detected in shock tube experiments indicate a minor contribution of reaction (1b) to the pyrolysis of HNCO. Wu et al. estimated the contribution to be only 5 % at 2100 - 2500 K.[7] Judging from the relatively low ΔH value,[8] the third channel which produces CN and OH appears to be worth exploring.

		ΔH_{3000} (kJ mol^{-1})	
HNCO + Ar	→ $NH(^3\Sigma^-)$ + CO + Ar	359	(1a)
	→ NCO + H + Ar	496	(1b)
	→ CN + OH + Ar	366	(1c)
	→ $NH(^1\Delta)$ + CO + Ar	510	(1d)

In this study, we will present some evidence for the ccurrence of reaction (1c). Unlike reactions (1a) and (1b), it cannot be a single-step reaction. The most probable will be a two-step reaction involving an initial isomerization as follows:

$$\text{HNCO} \longrightarrow \text{HOCN (or HONC)} \longrightarrow \text{CN + OH}$$

2. Experimental

The incident shock tube used was a conventional one that was used in a previous study.[5] Only the detection system will be described here. The emission light was detected through a quartz window (0.6 mm width slit), a grating monchromator (Nikon P250) and a photomultiplier (Hamamatsu 1P28). The observed spectral range was 388 ± 3 nm fitted to the CN ($B^2\Sigma^+ \rightarrow X^2\Sigma^+$) emission band. The transit

time of shock wave is less than 1.5 μs. Signals were amplified with the electronic rise time $2.2RC < 1$ μs and stored in a digital storage scope (Kawasaki electronica KDS-103). Sample gases of HNCO/Ar 0.2 - 0.5 mol% were shock-heated in a temperature range of 2300 - 3600 K and a pressure range of 300 - 700 Torr behind incident shock waves. HNCO was synthesized by the procedure as described elsewhere.[5] Impurity was checked by means of the IR and mass spectrometries to be less than 1%. The amount of hydrogen cyanide HCN in particular was ascertained to be less than 0.1%. Synthesized HNCO was stored at -196 °C and volatiled before use. Diluent Ar (Seitetsukagaku 99.9995%) was used without further purification.

To confirm that the observed emission was due to the CN (B→X) band, we measured this transient emission at three different wavelengths in the vicinity of 388 nm. As a result, the relative intensities of this emission peak height were found to be 0.8, 1.0 and 0.0 at 385.0, 388.0 and 391.0 ± 0.15 nm, respectively. This roughly accords to the CN (B→X) band shape at high temperatures. In addition, product analysis of shock-heated sample gases exhibited a sizable amount of hydrogen cyanide HCN, which should not be formed without an intermediacy of the CN radical.

The CN emission sensitivity was calibrated by means of the thermal decomposition of hydrogen cyanide HCN.

$$HCN + Ar \longrightarrow CN + H + Ar$$

Its decomposition rate constants have already been measured to be $k = 1.26 \times 10^{16}\exp(-417.1\ \text{kJ mol}^{-1}/RT)\ \text{cm}^3\text{mol}^{-1}\text{s}^{-1}$ in this laboratory.[9] The CN (B→X) emission intensity can be assumed to be approximately proportional to the concentration of CN (X). Therefore, initial slopes of the CN emission-time profiles can be linearly related to the initial CN production rate:

$$\left(\frac{d[\mathrm{CN}]}{dt}\right)_{t=0} = c(T)\left(\frac{dI_{\mathrm{CN}}}{dt}\right)_{t=0} = k[\mathrm{HCN}]_0[\mathrm{Ar}] \qquad \text{(I)}$$

where $c(T)$ is an instrumental constant depending on the temperature and where I_{CN} is the emission intensity of CN in units of volt. Practically, sample gases of HCN 0.039, 0.089 and 0.172 mol% diluted in Ar were shock-heated in the temperature range of 2800 - 3450 K and the pressure range of 630 - 740 Torr. The values of $c(T)$ were obtained from Eq. I. with the adis of the initial slopes in the emission-time profiles observed. Figure1 shows an Arrhenius-like plot of $\log(c(T))$ vs $1/T$. The solid line is expressed as $c(T) = 9.46 \times 10^{15}\exp(-27769\ /T)$ mol $cm^{-3}V^{-1}$. Applying this expression to the HNCO/Ar experiments, we have converted the intensities of the CN emission to the concentrations.

3. Results

(A) CN production mechanism

Figure 2a shows a typical CN emission profile for ca. 80 μs after the shock arrival in an HNCO/Ar experiment. The initial rise of the emission cannot be fitted with a simple first-order rise curve expressed by a single exponential function. This implies the existence of more than one route for the CN production. To examine the mechanism for the CN production, we performed three experiments by adding NO or CO to gas samples and by changing the initial concentration of HNCO. The results were as follows: (a) Addition of NO to the sample gases suppressed the CN emission but it did not affect the initial slopes at all (Fig. 2b); (b) addition of CO, by contrast, enhanced the the emission without affecting the initial slopes (Fig. 2c); (c) lowering in HNCO molar fraction of sample gases allowed the CN emission-time profile to approach a first-order (single exponential) growth curve (Fig. 3).

These results can be interpreted as indicating an additional participation of an exchange reaction:

$$NH(^3\Sigma^-) + CO \longrightarrow CN + OH \qquad (2)$$

in the presence of CN. Thus, in experiment (a), most of $NH(^3\Sigma^-)$ formed by reaction (1a) would be consumed by excess NO, which is known to react with $NH(^3\Sigma^-)$ rapidly,[10] thereby being converted only to N_2 plus OH or N_2O plus H. On the contrary, in experiment (b), the addition of CO would directly acceralate reaction (2) with reaction (1c) littled perturbed, in experiment (c), the low concentrations of NH and CO rendered reaction (2) ineffective, to permit reaction (1c) alone to be effective in producing CN.

The two reactions, (1c) and (2), will proceed presumably through the identical dynamical path. Difference between reaction (1c) and (2) should be in the way to activate the HNCO entity. It is collisional in reaction (1c), whereas it is chemical in reaction (2).

(B) k_{1c} measurement

Initial slopes of the CN emission-time profiles are determined in the first 2-3 μs region. The shock wave transit time (ca. 1.5 μs) may affect the initial slopes. However, because the CN emission-concentration calibration was conducted by using initial rates of the HCN decomposition observed in the same early time region, errors arising from the shock wave transit time are expected to be cancelled.

The initial slope of the CN concentration-time profile is expressed as follows.

$$\left(\frac{d[\mathrm{CN}]}{dt}\right)_{t=0} = k_{1\mathrm{C}}[\mathrm{HNCO}]_0[\mathrm{Ar}] \qquad \text{(II)}$$

Values of k_{1c} were calculated by the Eq. II at various temperatures. The resluts are listed in Table 1, together with relevant experimental conditions.

Figure 4 shows Arrhenius plots of k_{1c} for HNCO/Ar, HNCO/NO/Ar, and HNCO/CO/Ar gas mixtures. Variations in total pressure caused no significant systematic change to the values of k_{1c}. As mentioned before, addition of NO or CO did not alter the values of k_{1c} appreciably.

Least-squares fits of the experimental data to the Arrhenius equation resulted in

$$k_{1c} = 10^{12.97\pm0.73}\exp[-(266\pm40)\ \text{kJ mol}^{-1}/RT] \qquad \text{cm}^3\text{mol}^{-1}\text{s}^{-1}$$

The uncertainty corresponds to 3 σ. The temperature dependence of k_{1a} is also shown in Fig. 4. Over the temperature range studied here, the contribution of channel (1c) to the whole decomposition is apparantly small, $k_{1c}/k_{1a} < \sim 0.1$. In the lower temperature region (ca.1500 K), however, it may not be the case. The activation energy for reaction (1c) is lower than that for reaction (1a) by 90 kJmol^{-1}. The A-factor is lower by three orders of magnitude than for k_{1a}. These values seem to be too small as compared to the rate constants for decompositions of usual 4-atom molecules. We will discuss later what these small values are likely to indicate.

(C) k_2 measurement

The CN concentration-time profiles in the initial 50 μs region are computed with a 17-reaction mechanism given in Table 2. The simulation curves can well reproduce the S-shaped increases of the CN concentrations. Initial slopes are governed by the value of k_{1c} exclusively, whereas the later concave-up region involves the dominant influence of k_2. Therefore, the values of k_2 were determined by fitting the computed curves to those observed in this latter region. A typical best fit is shown in Fig. 5, where the attached curves illustrate the effects of ± 30 % variations on k_2.

The resulting k_2 values are listed in Table 3, together with relevant experimental conditions. Temperature dependence is inappreciable in the temperature range studied. We estimate $k_2 = (1.0 \pm 0.3) \times 10^{13}$ cm^{3}mol^{-1}s^{-1} (3σ) in the temerature range of 2820 - 3380 K.

Sensitivity analyses of the rate constants used in the 17-reaction mechanism were conducted as follows. We define a sensitivity coefficient *ai*,

$$a_i = k_i \frac{d[\mathrm{CN}]}{dk_i}$$

where k_i is the rate constant of the i-th reaction. Figure 6 shows typical examples of calculated a_i-time profiles only for important reactions. It is clear that at an early stage (~10 μs) the CN concentration is sensitive only to k_{1c}, while in the subsequent CN growth region (10-50 μs) it is sensitive to k_2 and k_{1a} as well. Large contributions of k_{1a} are inevitable under our conditions. We have deliberately chosen the recent k_{1a} data for use, which have been determined by Mertens et al. by means of the narrow-linewidth laser absorption technique.[6] Their minimum and maximum rate constant factors defining the lower and upper uncertainty limits are 0.56 and 1.60, respectively. These values correspond to the uncertainty in k_2 to be 0.62 and 2.1 for the lower and upper limits, respectively.

4. Discussion

There exist four isomers for HNCO, i.e. fluminic acid HCNO, cyanic acid HOCN and isofluminic acid HONC. The latter two species are unstable and observed only in rare gas matrices.[11,12] A complicated potential energy surface for the isomerizations among these isomers were illustrated by Poppinger et al. by using ab initio calculations with the 4-31G or STO-3G basis sets at the RHF SCF level of theory.[13] In that potential energy surface various kinds of intermediates were shown to have potential wells.

On the other hand, the reaction of hydrogen cyanide HCN with the $O(^1D)$ atom has been found to give rise to both $NH(^1\Delta)$ + CO and CN + OH in the gas phase [14] and to form both HNCO and HOCN in argon matrix.[15] For the sake of rationalization of the appearance of these products, an intermediacy of oxazirine was proposed:

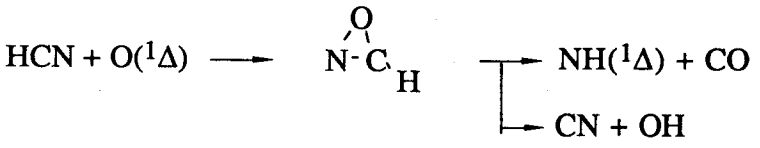

These two lines of information join to assist our mechanismistic considerations of the reactions of our present concern. Presumably, both reaction (1c) and (2) also involve the isomerization from HNCO to HOCN or HONC via the oxazirine intermediacy.

The idea of participation of reaction (2) in producing CN is supported strongly by the CN concentration-time profiles obtained from the experiments in which CO is added to the HNCO/Ar gas mixtures. The observed rapidity of reaction (2) is compatible with the characteristics that there should be no high potential energy barrier on the way from $NH(^3\Sigma^-)$ + CO to CN + OH. Namely, if the preexponential factor is assumed to be 10^{14} $cm^3mol^{-1}s^{-1}$ (the upper limit for bimolecular reactions), the activation energy is estimated to be 57 kJ/mol . Reaction (2) is expected to form vibrationally hot HNCO first. If collisional stabilization of this hot species takes place rapidly, the entire process is just the reverse reaction of (1a). Several groups have measured the activation energy for reaction (1a) to be 402,[5] 377,[7] and 358 kJ/mol.[6] Taking the enthalpy change at 3000 K ΔH_{3000} = 359 kJ/mol into account, the activation energy for the reverse reaction of (1a) is calculated to be ca. 20 kJ/mol. Therefore, the rate of reaction (2) may be controlled mainly by the entrance barrier.

The occurence of reaction (1c) has been confirmed by the NO- and CO-added experiments, in which the initial slopes of the CN emission-time profiles did not change markedly compared to those observed in the HNCO/Ar experiments (see Fig. 4). It is also supported by the above-mentioned large k_2 value, which implies the potential energy barrier for the isomerization lying below the entrance barrier. The small activation energy of k_{1c} may reflect this isomerization barrier height.

Inferioriy of reaction (1c) to (1a) may be explained by its tight transition state. If the rate-determining step for reaction (1c) is the isomerization, its activation

entropy should be much lower than in the dissociation to $NH(^3\Sigma^-)$ + CO. The preexponential factor of the overall rate constant for reaction (1c) would be small accordingly.

The activation energy (266 kJ mol^{-1}) for reaction (1c) obtained here is much lower than the enthalpy changes 359 and 366 kJ mol^{-1} for reaction (1a) and (1c), respectively. In the case of successive two-step reactions with the first-step barrier being lower than the second, it is usual to assume that an equilibrium for the first-step is reached before the second step proceeds. But this is not generally the case. Cases should exist where the first step, isomerization, controls the whole reaction rate, with the reverse reaction being much slower compared to the succeeding second step.

For an example of the thermal decomposition process in which the activation energy observed is definately smaller than the dissociation energy, we can take the decomposition of CO_2:

	ΔH_{3000} (kJ mol^{-1})	
$CO_2 \longrightarrow CO_2(^3B_2) \longrightarrow CO + O(^3P)$	530	(17)

The recent value of the activation energy for reaction (17) is 341 kJ mol^{-1},[16] whereas the enthalpy change at 3000 K, ΔH_{3000}, is 530 kJ mol^{-1}. In order to explain the anomaly, Fishburne et al. took into account a triplet excited state of $CO_2(^3B_2)$ as an intermediate.[17] They suggest that the first spin inversion step from singlet to triplet controls the whole decompositon rate. The bent $CO_2(^3B_2)$ has been suggested to lie near 340 kJ mol^{-1} above the linear $CO_2(X^1\Sigma^+)$ both experimentally [18-20] and theoretically.[21,22]

Other candidates of the mechanism for the CN production have been considered. First, the NCO radical produced by reaction (1b) might also contribute to the CN profile through reaction (19).

	ΔH_{3000} (kJ mol^{-1})	
$NCO(^2\Pi) + M \longrightarrow CN + O(^3P)$	321	(19)
$\longrightarrow N(^4S) + CO$	198	(20)

However, a spin-forbidden but energetically favorable channel (20) is supposed to dominate over reaction (19).[23] Hence, this possibility can be ruled out. Second, a hydrogen-catalyzed isomerization reaction (21)

	ΔH_{3000} (kJ mol^{-1})	
HNCO + H ⟶ HOCN + H	96	(21)
HNCO + H ⟶ NH_2 + CO	-63	(22)

might produce HOCN, which would decompose directly into CN + OH. However, The rate constantsof an alternate channel (22) were measured to be $k_{22} = 1.1 \times 10^{14}\exp(-6400/T)$ $cm^3mol^{-1}s^{-1}$ by Mertens et al.[6], which are enough large to let reaction (22) dominate over reaction (21). The activation energy for reaction (22) is evidently much lower than the enthalpy change of reaction (21), thus negating the possibility of reaction (21) participating in the CN formation.

5. Conclusions

On the basis of the CN emission-time profiles observed in the shock tube studies for the HNCO decomposition, occurence of a minor decomposition channel HNCO + Ar ⟶ CN + OH + Ar has been confirmed. The rate constants have been determined to be $k_{1c} = 10^{12.97\pm0.73}\exp[-(266\pm40)$ kJ mol^{-1}/RT] $cm^3mol^{-1}s^{-1}$ over the temperature ragne of 2300-3600 K. It is inferred that an exchange reaction NH + CO ⟶ CN + OH may also contribute to the production of CN, whose rate constant is estimated to be $k_2 = (1.0 \pm 0.3) \times 10^{13}$ $cm^3mol^{-1}s^{-1}$ with little temperature dependence. These results indicate that the potential energy barrier for the isomerization from HNCO to HOCN (or HONC) lies below the threshold energy for the primary decomposition channel into $NH(^3\Sigma^-)$ + CO and controls the overall rate of reaction (1c).

References

1) T. A. Spiglanin, R. A. Perry, and D. W. Chandler, J. Phys. Chem., **90**, 6184 (1986).

2) K. Uno, T. Hikida, A. Hiraya, and K. Shobatake, Chem. Phys. Lett., **166**, 475 (1990).

3) T. A. Spiglanin and D. W. Chandler, Chem. Phys. Lett., **141**, 428 (1987).

4) W. S. Drozdoski, A. P. Baronavski, and J. R. McDonald, Chem. Phys. Lett., **64**, 421 (1979).

5) O. Kajimoto, O. Kondo, K. Okada, J. Fujikane, and T. Fueno, Bull. Chem. Soc. Jpn., **58**, 3469 (1985).

6) J. D. Mertens, A. Y. Chang, R. K. Hanson, and C. T. Bowman, Int. J. Chem. Kinet., **21**, 1049 (1989).

7) C. H. Wu, H.-t. Wang, M. C. Lin, and R. A. Fifer, J. Chem. Phys., **94**, 3344 (1990).

8) M. W. Chase, Jr., C. A. Davies, J. R. Downey, Jr., D. J. Frurip, R. A. McDonald, and A. N. Syverud, "JANAF thermochemical Tables," 3rd ed, National Bureau of Standards, Washington, D. C. (1985).

9) K. Tabayashi, T. Fueno, K. Takasa, and O. Kajimoto, and K. Okada, Bull. Chem. Soc. Jpn., **50**, 1754 (1977).

10) K. Yokoyama, Y. Sakane, and T. Fueno, Bull. Chem. Soc. Jpn., submitted.

11) J. H. Teles, G. Maier, B. A. Hess, Jr., L. J. Schaad, M. Winnewisser, and B. P. Winnewisser, Chem. Ber., **122**, 753 (1989).

12) V. E. Bondybey, J. H. English, C. W. Mathews, and R. J. Contolini, J. Mol. Spectrosc., **92**, 431 (1982).

13) D. Poppinger, L. Radom, and J. A. Pople, J. Am. Chem. Soc., **99**, 7806 (1977).

14) B. K. Carpenter, N. Goldstein, A. Kam, and J. R. Wiesenfeld, J. Chem. Phys., **81**, 1785 (1984).

15) J. N. Crowley and J. R. Sodeau, J. Phys. Chem., **93**, 3100 (1989).

16) S. Fujii, private communication.

17) E. S. Fishburne, K. R. Bilwakesh, and R. Edse, J. Chem. Phys., **45**, 160 (1966).

18) H. H. Mohammed, J. Fournier, J. Deson, and C. Vermeil, Chem. Phys. Lett., **73**, 315 (1980).

19) Y. Zhu and R. J. Gordon, J. Chem. Phys., **92**, 2897 (1990).

20) B. B. Brady, G. B. Spector, L. Chia, and G. W. Flynn, j. Chem. Phys., **86**, 3245 (1987).

21) V. Y. Simkin, A. I. Dementev, and V. I. Pupyshev, Russ. J. Phys. Chem., **56**, 1739 (1982).

22) N. W. Winter, C. F. Bender, and W. A. Goddard III, Chem. Phys. Lett., **20**, 489 (1973).

23) M. Y. Louge and R. Y. Hanson, Combust. Flame, **58**, 291 (1984).

24) F. Westley, "Table of Recommended Rate Constants for Chemical Reactions Occurring in Combustion," National Bureau of Standards, Washington, D. C. (1980).

25) B. S. Haynes, Combust. Flame, **28**, 113 (1977).

Table 1. The Rate Constant for the Reaction: HNCO + Ar ⟶ CN + OH + Ar (1c), with Relevant Experimental Conditions.

No.	T_2 / K	P_2 / Torr	ρ_{21}	[Ar] / 10^{-9}molcm^{-3}	[HNCO] / 10^{-9}molcm^{-3}	[NO]/[CO]	k_{1c} / 10^{7}cm^{3}mol^{-1}s^{-1}
0801	3230	690	3.66	3420	1.13		71.6
0901	3045	736	3.64	3870	1.28		22.1
1001	2994	721	3.63	3860	1.27		18.3
1002	2817	678	3.61	3860	1.27		13.8
1003	2803	681	3.61	3900	1.29		11.0
1201	3429	650	3.68	3040	1.00		83.9
1202	2614	636	3.58	3900	1.29		4.56
1301	3362	662	3.67	3160	1.04		76.2
1401	3339	449	3.67	2150	1.98		45.0
1402	3025	493	3.63	2610	2.40		16.5
1501	2894	536	3.62	2970	2.73		13.5
1502	2908	481	3.62	2650	2.44		12.9
1601	2308	410	3.52	2850	2.62		1.04
1602	2762	779	3.60	4520	4.16		6.96
1701	2544	709	3.57	4470	4.11		0.87
2001	2606	468	3.57	2880	2.65		4.12
2002	2331	463	3.53	3180	2.93		1.70
2201	2558	513	3.57	3220	0.45		4.66
2301	2519	504	3.56	3210	3.85		2.31
2302	2405	525	3.54	3500	4.20		1.89
2401	3307	422	3.67	2050	0.29		95.6
2701	3551	610	3.69	2760	0.39		120.5
2101	3016	726	3.63	3860	6.98	14.04 a)	20.4
2102	3351	659	3.68	3150	5.71	11.48 a)	98.7
2201	2697	643	3.59	3820	6.92	13.91 a)	6.92
2202	2828	690	3.61	3910	7.08	14.23 a)	12.9
2203	3194	692	3.65	3470	6.29	12.65 a)	41.6
2204	3301	690	3.67	3350	6.06	12.19 a)	44.0
2701	2973	740	3.63	3990	7.10	34.08 b)	22.6
2702	3365	637	3.67	3030	5.40	25.92 b)	53.9
2703	2829	699	3.61	3960	7.05	33.85 b)	24.0

a) Concentration of NO in the incident shock waves.

b) Concentration of CO.

Table 2. Reaction Mechanism Used for Determination of k_2 in the HNCO/Ar Mixtures.

No.	Reaction [a]	log A	n	E_a	Ref.
1a	$HNCO + Ar \rightarrow NH(^3\Sigma^-) + CO + Ar$	35.51	-5.11	460	6
1b	$\rightarrow NCO + H + Ar$	15.99	0.0	498	b)
1c	$\rightarrow CN + OH + Ar$	12.97	0.0	266	This study
2	$NH + CO \rightarrow CN + OH$	13.0	0.0	0	This study
3	$NH + NH \rightarrow N_2 + 2H$	13.65	0.0	0	6
4	$NH + OH \rightarrow N + H_2O$	11.70	0.5	8.4	24
5	$CN + OH \rightarrow NCO + H$	13.75	0.0	0	25
6	$HNCO + H \rightarrow NH_2 + CO$	14.04	0.0	54	6
7	$NCO + Ar \rightarrow N + CO + Ar$	16.80	-0.5	200	23
8	$NH + Ar \rightarrow N + H + Ar$	14.42	0.0	316	6
9	$N + NH \rightarrow N_2 + H$	11.80	0.5	0	6
10	$H + NH \rightarrow H_2 + N$	11.80	0.5	33	24
11	$CN + N \rightarrow N_2 + C$	11.80	0.5	0	24
12	$CO + N \rightarrow CN + O$	12.51	0.5	323	24
13	$C + NH_2 \rightarrow CN + 2H$	13.48	0.0	0	b)
14	$NH_2 + Ar \rightarrow NH + H + Ar$	23.50	-2.0	381	6
15	$C + NH \rightarrow CN + H$	11.80	0.5	0	24

a) The rate constant $k=AT^n\exp(-E_a[kJ/mol]/RT)$ $cm^3mol^{-1}s^{-1}$.

b) Estimated.

Table 3. The Rate Constant for the Reaction: NH + CO ⟶ CN + OH (2), with Relevant Experimental Conditions.

No	T_2 / K	P_2 / Torr	ρ_{21}	[Ar] / 10^{-9}molcm^{-3}	[HNCO] / 10^{-9}molcm^{-3}	x_{HNCO} / mol%	k_2 / 10^{13}cm^{3}mol^{-1}s^{-1}
2401	3382	644	3.67	3050	2.75	0.090	0.65
2801	3246	667	3.66	3290	5.86	0.178	0.7
2802	3376	659	3.67	3130	5.57	0.178	0.6
2803	3141	710	3.65	3630	6.45	0.178	1.0
2804	2885	698	3.62	3880	6.90	0.178	1.5
1101	3246	673	3.66	3320	9.57	0.288	1.56
1102	3254	676	3.66	3330	9.59	0.288	1.3
1401	3264	665	3.66	3270	12.41	0.380	1.3
1402	3370	644	3.67	3070	11.65	0.380	1.6
1601	2823	682	3.61	3870	14.72	0.380	1.0
1701	2920	477	3.62	2620	9.96	0.380	1.0
1702	3259	283	3.66	1390	5.29	0.380	0.8

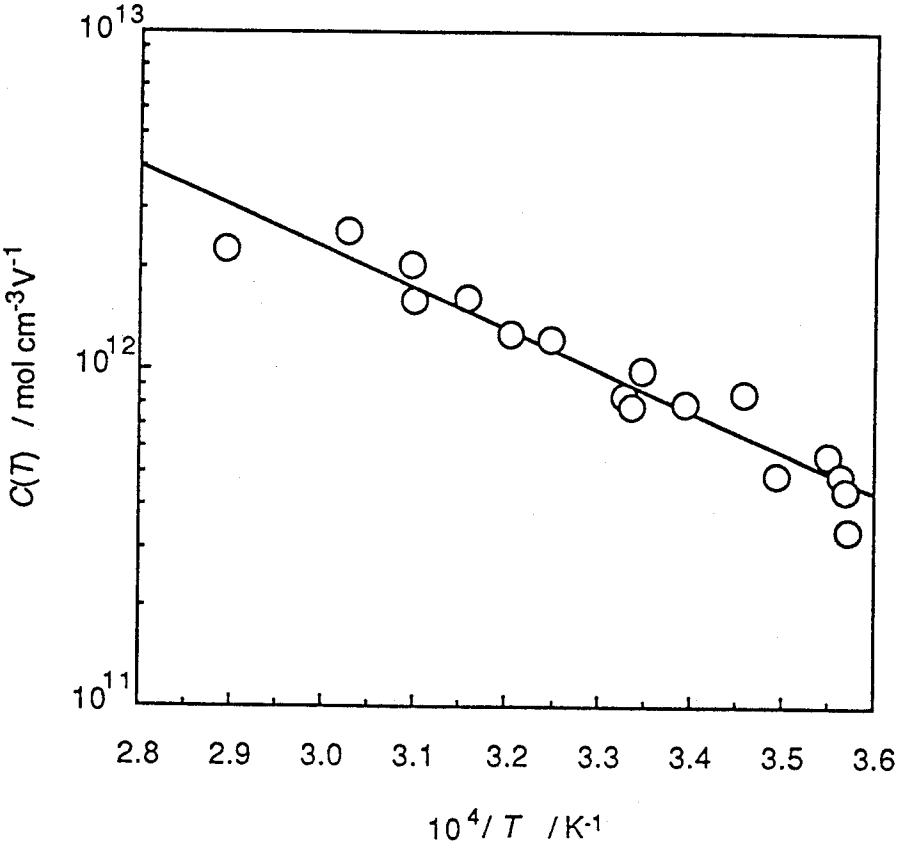

Figure 1. Temperature dependence of the sensitivity coefficient for the calibration between the CN emission intensities and the concentrations.

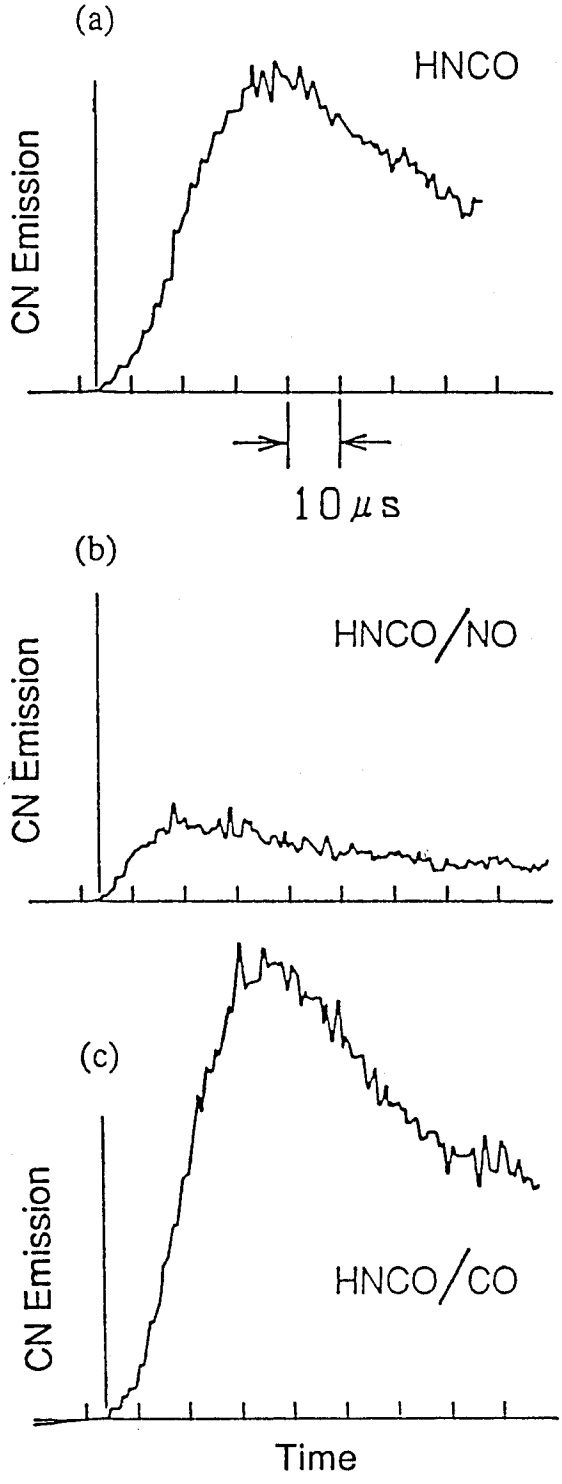

Figure 2. CN emmision-time profiles obtained from the HNCO/Ar experiment (a), and the effect of addition of NO (b) or CO (c) on the profile. (a) HNCO : 0.178 %, 3376 K, 659 Torr ; (b) HNCO/NO : 0.181 / 0.364 %, 3351 K, 659 Torr ; (c) HNCO/CO : 0.178 / 0.854 %, 3365 K, 637 Torr.

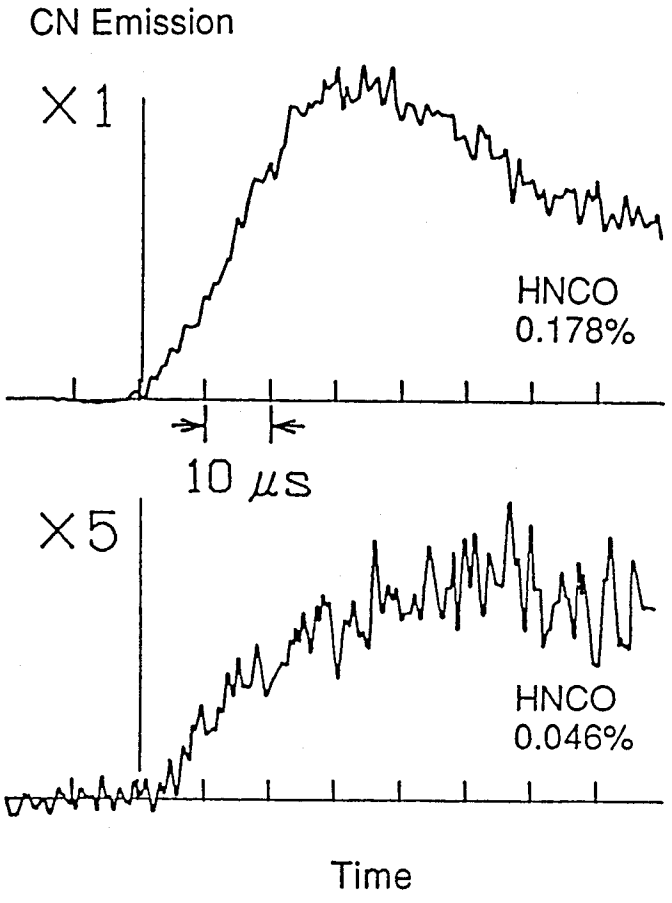

Figure 3. Change of the CN emission profiles by lowering the HNCO concentration. (a) HNCO : 0.178 %, 3246 K, 667 Torr ; (b) HNCO : 0.046 %, 3260 K, 672 Torr.

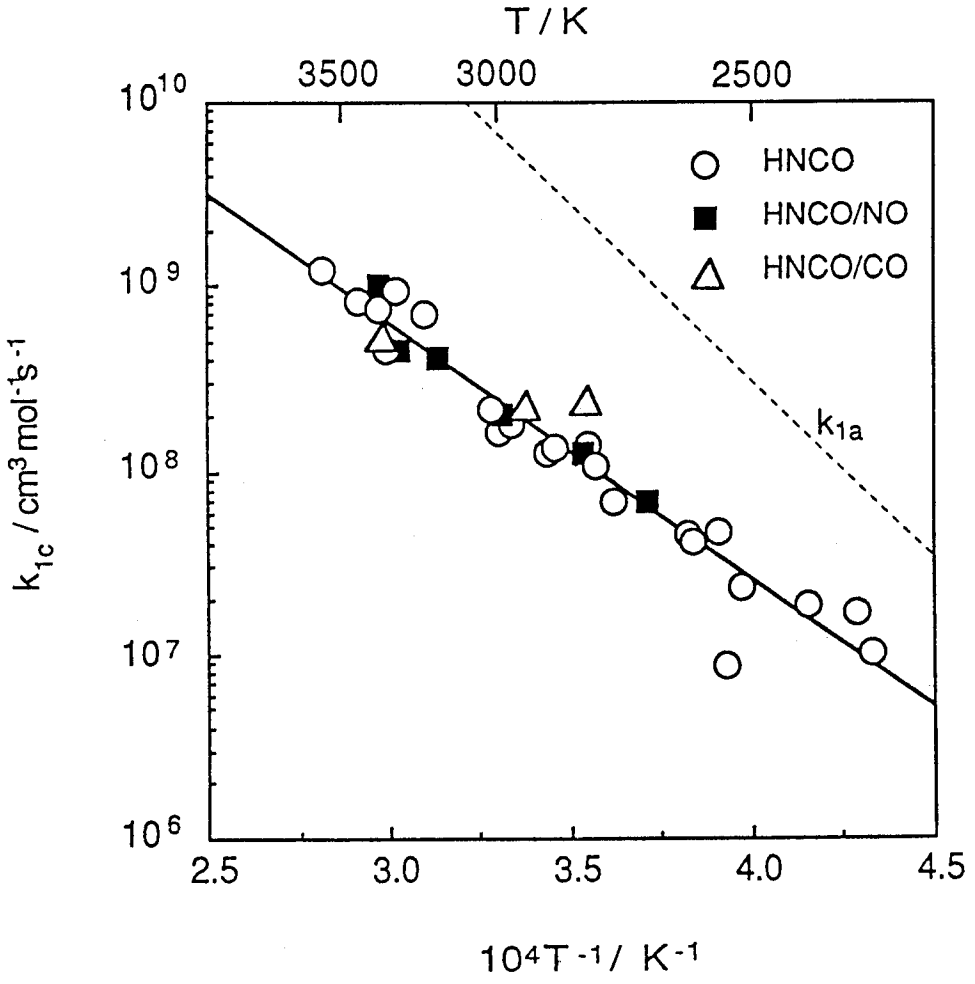

Figure 4. Arrhenius plot of k_{1c}, HNCO + Ar ⟶ CN + OH + Ar (1c).

The data plotted with the circle, the filled square and triangle have been obtained in the HNCO/Ar, HNCO/NO/Ar and HNCO/CO/Ar experiments, respectively. The dashed line provides the temperature dependence of k_{1a}, HNCO + Ar ⟶ NH($^3\Sigma^-$) + CO + Ar (1a), referred from 6).

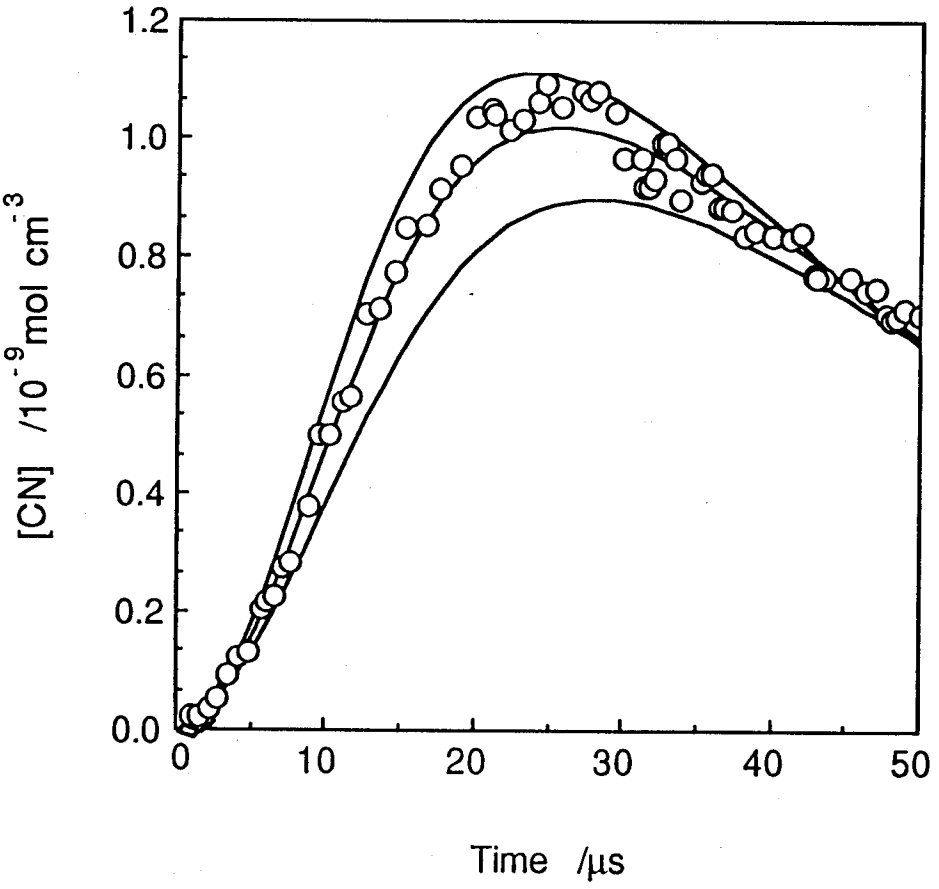

Figure 5. Comparisons of the CN concentration profile computed with the observed. Upper and lower curves show the effects of ± 30 % deviations on k2. T2= 3254 K,P2= 676 Torr, x_{HNCO}= 0.288 %.

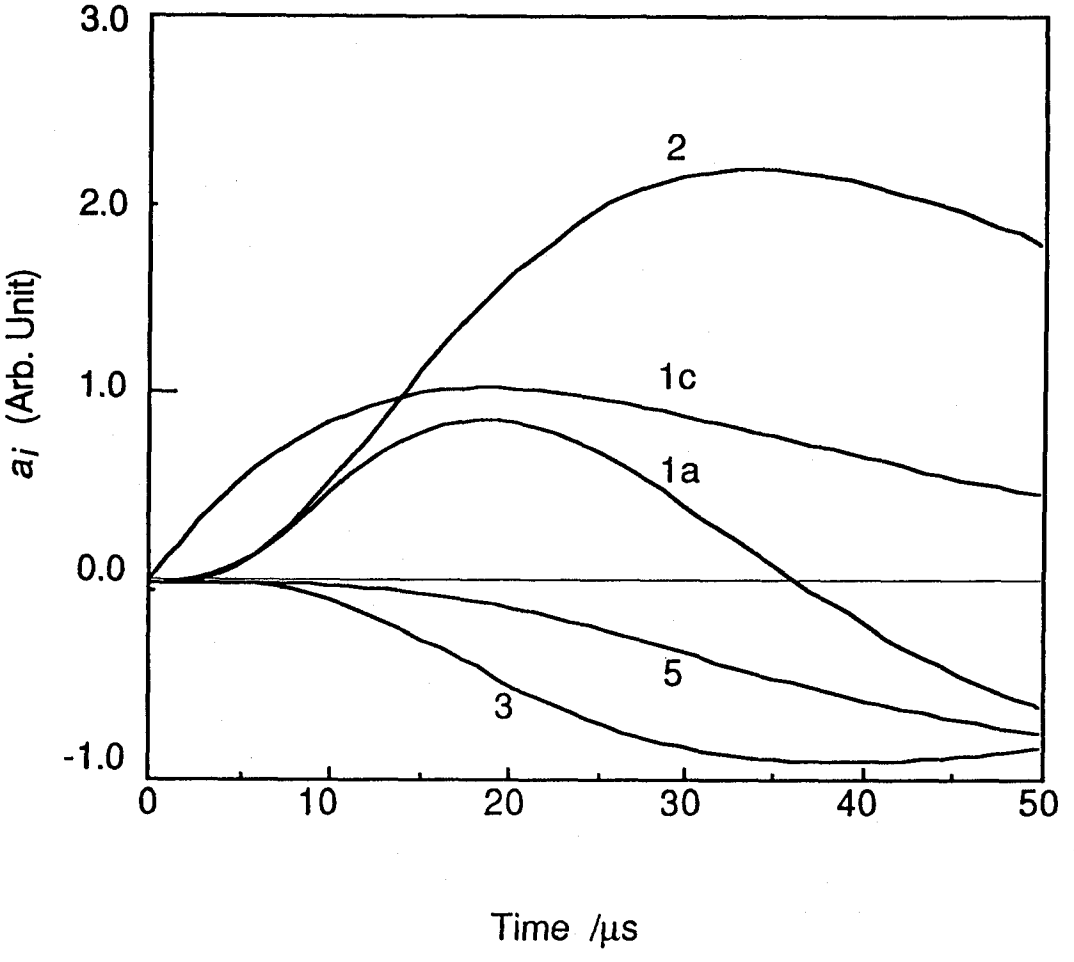

Figure 6. Sensitivity analysis for values of the rate constants for several important reactions used in the simulation mechanism. T_2= 3382 K, P_2= 644 Torr, x_{HNCO}= 0.090 %.

Chapter 6

Computational Studies of the Isomerization Reactions Between the CHNO Isomers

With respect to the energetics of several CHNO isomers with their excited states, transition states for isomerization reactions, and fragmented species were investigated by ab initio MO calculations with the MRDCI method for correlation energy. Geometry optimizations were accomplished with the 6-31G** basis set at the RHF, UHF, or CASSCF level of theory. As a result it was found that the isomerization from isocyanic acid HNCO to cyanic acid HOCN can proceed via two 1,2-hydrogen migration steps rather than by a single 1,3-hydrogen migration. The overall barrier height on the potential energy surface for this isomerization reaction , which was determined to be 427 kJ/mol, lies near the threshold energy for the main decomposition channel, HNCO $\longrightarrow$ $NH(^3\Sigma^-)$ + CO. The isomerization is thus expected to compete with the decomposition reaction. The conclusion is compatible with our previous experimental results.

1. Introduction

Isocyanic acid HNCO decomposes mainly into $NH(^3\Sigma^-)$ + CO in the temperature region above 2000 K.[1-3] Another bond dissociation channel to produce NCO + H has been reported to contribute by less than 5% to the HNCO total consumption.[3] In addition to these two dissociation channels, we observed some evidence for the occurence of reaction (1c),[4]

		ΔH_{3000}(kJ/mol)	
HNCO + M	$\rightarrow NH(^3\Sigma^-) + CO + M$	359	(1a)
	$\rightarrow NCO + H + M$	496	(1b)
	$\rightarrow CN + OH + M$	366	(1c)

a direct decomposition into CN + OH. This last process must involve isomerization to form HOCN or HONC. On the basis of the temperature dependence of the rate constants k_{1c} measured, we concluded that the suddle point of the isomerization lies below the energy threshold for reaction (1a).

Potential energy surfaces for the CHNO isomers were first studied by Poppinger et al. using ab initio MO calculation at the RHF/4-31G level of theory.[5] Their study has revealed that the surface is so complicated with many potential wells corresponding to five chain isomers a ring isomer and a branched isomer. Thus, more than one isomerization pathway must be taken into account for reaction (1c). They include the following:

HNCO $\rightarrow$ $\overline{OCHN}$	$\rightarrow$ HOCN	(2a)
	$\rightarrow$ HONC	(2b)
HNCO $\rightarrow$ $\overline{HNCO}$	$\rightarrow$ HOCN	(2c)
HNCO	$\rightarrow$ HOCN	(2d)

where both $\overline{\text{OCHN}}$ and $\overline{\text{HNCO}}$take ring structures named oxazirine and oxaziridinylidene, respectively.

In the present study, we will report results of calculation around the isomerization reaction paths, and compare the theoretical results with the experimental.

2. Method

Geometry optimizations for the minimum energy structures and the saddle point structures were accomplished by the restricted hartree fock procedure (RHF) for singlet closed shell species in their ground state, by the unrestricted hartree fock procedure (UHF) for open shell species and transition states, and by the complete active space SCF procedure (CASSCF) for the oxazirin intermediate in its ground state and two transition states connected to oxazirin. At each stationary point, the multi-reference single- and double-excitation configuration-interaction (MRDCI) calculation was carried out to obtain the electronic correlation energy. The configurations whose contributions $|c_i|^2$ to a state exceed 0.25% were regarded as the main (reference) configurations for singlet states. In the case of triplet states, especially in OCHN(^{3}A"), we could not afford to take all the configurations with $|c_i|^2 > 0.25$ % as the reference configurations because of too many configurations to be selected with appropriate threshold values. Tripet state energies might thus be somewhat overestimated. The lowest configuration-selection threshold T was deliberately assigned a value between 1 and 30 μhartree, so that the maximal dimension of the configurational space fell in the region 7000-9000. Four successive threshold values increasing stepwise by 5 μhartree each were used to obtain the CI energy extrapolated to T=0 hartree. The generalized Langhoff-Davidson approximation [6,7] was used to correct for possible errors which might arise from the use of a limited number of reference configurations. The CI energies thus corrected are regarded as estimates of full CI

values [7,8] which will be denoted as E_{CI}. The iterative natural orbital CI method was applied occasionally with two or three cycles at each state. All calculations were done by using the 6-31G** basis set. The Gaussian 86 [9] and HONDO7 [10] programs were used for SCF optimization calculations, and the TABLE MRDCI program furnished by Bunker [11,12] was used for CI calculations.

Prior to these calculations, we carried out the perfect-pairing multi-configuration SCF calculation (PPMC) [13] with STO-3G basis to obtain possible reaction paths. The active space included 8 orbitals and 6 electrons (8,6) with only double excitation permitted.

3. Results

(A) Chain isomers

The geometries optimized for four chain isomers are shown in Fig. 1. Their energies are listed in Table 1 at PPMC/STO-3G, RHF/6-31G**, and MRDCI/6-31G**//6-31G** levels. The notation '//' means "at the geometry of". The basis set dependence seems to be large on the energies, especially, with respect to HNCO. Thus searching for saddle points needs large basis sets. HNCO and HCNO (fulminic acid) are stable in the gas phase, by contrast, HOCN and HONC (isofulminic acid) have been observed only in the rare gas matrices.[14,15] The low value of the energy calculated for HOCN indicates the possibility of detecting gaseous HOCN. CCD (coupled-cruster double-excitation) energies reported by Teles et al.[14] agree with our present MRDCI energies (Table 1).

The dissociation energies, D_0, calculated for HNCO in particular are listed in Table 2, together with the experimental enthalpy change, ΔH, referred from [16] for $NH(^3\Sigma^-)$ + CO, $NH(^1\Delta)$ + CO, and CN + OH. Zero point energies were calculated on the basis of the experimental vibrational frequencies.[16] The enthalpy changes are listed both at 0 K and 3000 K. Theoretical dissociation energis are in fairly good agreement with the experimental data, ΔH_0.

(B) Ring and branced isomers

Figure 2b shows the structure for OCHN in its electronic ground state optimized by the CAS(4,4) procedure assuming Cs symmetry. The remarkable feature is that the OCN angle is 94.1°, with the O-N bond index of ca. 0.5. These values indicate that the ground-state OCHN has a "half ring structure". The normal ring species called oxazirine, which was proposed as a reaction intermediate in matrix experiments,[17,18] has still been unknown. We will call this structure as "oxazirine".

In the RHF/6-31G** optimization the stable ring isomer has not been found. All initial guess geometries we tried led to the HNCO potential well. This tendency is similar to that reported by Poppinger et al. using the 4-31G bais set.[5] On the other hand, UHF/6-31G** optimization has given a ring-opened structure with the OCN angle being 123.5°. This branched isomer is strongly spin-polarized and its eigenvalue of $\hat{S}^2$operator is $s^2 = 1.16$, which implies a strong diradical character. The two odd electrons are localized mainly on the O and N atom in-plain orbials. By contrast, it is interesting that, in the PPMC/STO-3G optimization, the initial guess molecular orbital (MO) coefficients prepared from a UHF solution (diradical type MOs) gives the branched isomer minimum while the RHF MOs does not lead to the branched minimum but to the ring minimum. Although there was a doubt whether different electronic states were optimized, the situation is probably due to an unavoidable incompleteness in configurations generated rather than due to the presence of two hardly distinguishable electronic states.

In order to clarify this point, we performed CASSCF optimization using both the diradical and the closed-shell type MO coefficients as initial guess MOs. As mentioned above, the optimized geometries are identical and have an intermediate structure between the ring and the branched isomers. The electronic structure is described with at least two configurations, which are of the diradical and the closed shell types.

$...(1a'')^2(8a')^2(2a'')^2(9a')^1(10a')^1$,

$...(1a'')^2(8a')^2(2a'')^2(9a')^2$.

Their CI coefficients are 0.84 and -0.46, respectively.

Table 3 lists the geometric parameters and the CI energies for the ground OCHN and three excited states. All these excited states are low-lying and have branched structure with OCN angle ~120 ° unlike ground state. Both the $^3A''$ and $^1A''$ states named formylnitrene have their odd electrons on the N atom in-plain and out-of-plain p orbitals being nearly degenerate.

Another ring isomer $\overline{HNCO}$(oxaziridinylidene) was also found to have a potential well on the RHF surface. It has a nonplanar structure with the HNCO dihedral angle ϕ=94.8 °, as can be seen in Fig.3b. Its geometric parameter and CI energy are listed in Table 3. The high energy value (504 kJ/mol relative to HNCO) makes us suspect that the potential well will be shallow, considering the dissociation energy D_0 = 502 kJ/mol for NH($^1\Delta$) + CO (Table 2). This suspicion will be confirmed with the results of MRDCI calculation for the transition state of the ring opening reaction to form HNCO.

Additionally, for the excited HNCO ($^3A''$), the UHF optimized geometry and the CI energy are also listed in Table 3. This state correlates with NH($^3\Sigma^-$) + CO fragments.

(C) Isomerization

We examined three isomerization pathways (2a), (2b) and (2c) and a recombination of NH($^3\Sigma^-$) + CO to form HNCO ($^3A''$). Table 4 shows the corresponding reactions, calculation methods used in geometry optimizations of the transition state, and MRDCI energies. Fig. 5 shows the potential energy diagram for all isomerization pathways considered here.

It is apparent that the most feasible isomerization pathway is reaction (2a), proceeding through two 1,2-hydrogen migrations via the OCHN(X^1A')

intermediate. The overall TS is TS2. Its barrier height, 427 kJ/mol, is comparable with the threshold energy for reaction (1a); TS2 lies near the level of the intersystem crossing point between the surfaces for HNCO (X^1A') and HNCO (a^3A'') on the course of the NC bond dissociation.

Since neither UHF nor RHF calculation gives a correct OCHN (X^1A') electronic state, we have carried out CAS(6,10) optimization to determine the geometries of TS1 and TS2, which are connected to OCHN (X^1A'). Obtained geometries are shown in Fig.2a and 2c. TS2 on the UHF surface was also examined for the sake of comparison with the CAS geometry. The resulting geometry shown in Fig.2d has more HOCN-like features. This tendency must be a consequence of overestimation of the diradical character in UHF solutions relative to CAS solutions. According to Hammond's postulate,[19] a lowering of the OCHN potential energy makes the TS2 geometry "later", i.e. closer to the HOCN geometry. This postulate is also applicable to the relation between TS1 and TS2. Lower energy and more OCHN-like geometry of TS1 compared to TS2 are attlibutable to the greater stability of HNCO compared to HOCN. Thus the TS2 geometry is sensitive to a degree of assessment of correlation energy. Preciser calculation possibly present more refined TS2 geometries.

Analytical vibrational analysis at the CASSCF level is not available in the HONDO7 program, and numerical procedure consumes CPU time enormously. Thus, we have checked only the symmetry breaking of TS2. Strictly speaking, the TS2 was found to have nonplanar structure at this level. However, the angle between the CH bond and the OCN plane is found to be within 0.5 °. Furthermore, we carried out vibrational analysis of the UHF-TS2, to find a single imaginary frequency being $2362i$ cm^{-1}. Taking the low-lying excited state of OCHN ($^1A''$) into account, we may attribute the small deviation from the Cs symmetry in the CAS-TS2 geometry to the second-order Jahn-Teller effect. As a result, we have assumed TS2 having the Cs symmetry.

Another isomerization path from the OCHN intermediate to HONC was found to proceed via TS3 (Fig.4a). The way of this rearrangement may seem somewhat curious. TS3 can be regard as a saddle point for an intramolecular insertion reaction:[20)]

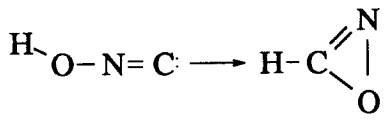

The singlet carbene character of the terminal C atom of HONC enables the C atom to insert into the OH bond in the same molecule.

The third isomerization pathway consists of a ring closure step to form the cyclic- $\overline{\text{HNCO}}$ and a ring-opening step accompanied by the H atom migration from the N to O atom at the SCF level of calculation. The first saddle point, TS4, was found only on the UHF surface and the structure is close to that of the cyclic- $\overline{\text{HNCO}}$ (Fig.3a and 3b), whereas TS5 (saddle point for the second step) were found on the RHF surface (Fig. 3c). Either of TS4 and TS5 was confirmed to have a single imaginary frequency. The MRDCI calculation stabilized TS4; the CI energy of TS4 became only slightly lower than the cyclic- $\overline{\text{HNCO}}$. That is, the cyclic- $\overline{\text{HNCO}}$ may not have a potential well in rearity.

We made an attempt to find the TS for 1,3-hydrogen migration from HNCO to HOCN. However the rectangle TS was not found and the cyclic- $\overline{\text{HNCO}}$ minimum was found alternatively. This situation may correspond to the abscent of cis-HNCO. Thus, we believe TS5 is the only saddle point for 1,3-hydrogen migration step.

Apparently only reaction (2a) will be able to compete with the main decomposition reaction (1a). The potential energy of TS3 and 5 are too high to compete with reaction (1a).

4. Discussion

The main decomposition channel (1a) involves a spin-inversion process. The electronic ground state of HNCO(X^1A') adiabatically correlates to NH($^1\Delta$) + CO. In the prolonged N-C bondlength region, an intersystem crossing must take place between $^1A'$ and $^3A''$ surfaces. The situation is similar to the decompositions of HN_3 and N_2O,[21,22] in which the triplet surfaces are thought to be repulsive.

In the present case, however, we have found a bound state (a^3A'') on the triplet surface connected to NH($^3\Sigma^-$) + CO (Table 3). The NCO angle is 126 ° and its CI energy lies between the NH($^3\Sigma^-$) + CO and NH($^1\Delta$) + CO asymptote. A similar bent triplet state can be seen in the case of CO_2,[23,24] where the intersystem crossing between X^1A' and $^3B_2$ takes place below the dissociation limit for CO + O(^{3}P).[25] Thus, there is a doubt whether the threshold energy for reaction (1a) might reflect the saddle point on the triplet surface, instead of the surface crossing.

TS6 is the transition stat for the decomposition from HNCO($^3A''$) to NH($^3\Sigma^-$) + CO (Table 4). Fairly low energy 476 kJ/mol could not negate the possibility of above-mentioned mechanism. Its geometry is shown in Fig. 4b. If the intersystem crossing occurs at the CN bondlength longer than 1.698, the crossing point corresponds to the barrier top. The crossing bondlengh is not available, but, with respect to the dissociation of HN_3, the corresponding N-N distance was calculated by Alexander et al.[26] to be 1.775. Considering this value together with the bent structure of TS6, we conclude that TS6 is not a barrier top and that the decomposition rate of reaction (1a) is determined by the intersystem crossing.

The threshold energies of reaction (1a) are reported to be 439 and 413 kJ/mol by Kajimoto et al.[1] and Mertens et al.[2] respectively. The threshold energy 427 kJ/mol calculated for the isomerization (2a) has not been corrected with the zero-point energies. The fundamental vibrational frequencies of TS2 are calculated only at the UHF level as mentioned before, resulted in the values; 2361*i*, 482, 543, 1115, 1985 and 2363 cm^{-1}. From these values, the zero-point-corrected threshold

energy has been obtained to be 411 kJ/mol. The result indicates that reaction (2a) is energitically even favorable as compared to reaction (1a).

It is likely for *isomerization (2a)* to compete with reaction (1a), however, the large value of the dissociation energy D_0 for the CN + OH makes *decomposition (1c)* very unlikely (see Table 2). In fact, at room temperature the reaction of $NH(^1\Delta)$ with CO produces NCO radical mainly,[27] and the reaction of NCO with H produces $NH(^3\Sigma^-)$ exclusively.[28] These low temperature results are perfectly conflict our high temperature result that the reaction of $NH(^3\Sigma^-)$ with CO produces sizable amount of CN by a large rate constant of 1×10^{13} $cm^3mol^{-1}s^{-1}$.[4] These defferences could be explained by the temperature dependence of the heat of formation of CN radical listed in the JANAF 3rd ed.[16] Table 2 shows the difference of the enthalpy change between 0 K and 3000 K arising from the temperature dependence of ΔH_f. Thus, the decomposition (1c) is thought to become accessible only in the high temperature region.

The rate constant for reaction (1c) was determined to be $k_{1c} = 5.37\times10^{12}\exp(-250.9kJmol^{-1}/RT)$ $cm^3mol^{-1}s^{-1}$ from our previous shock tube study.[4] This activation energy seems too low to be explained by isomerization (2a) as a rate determining step. We cannot explain this inconsistency with the present results. The unusual temperature dependence of ΔH_f, as can be seen in the case of CN, occur also in the case of TS2.

5. Conclusions

The abinitio calculation involving the MRDCI method reveald the isomerization reaction HNCO ⟶ HOCN to compete with the primaly decomposition channel HNCO ⟶ $NH(^3\Sigma^-)$ + CO. The isomerization consists of two 1,2-hydrogen migrations and an intermediacy of oxazirine. The later transition state is the overall barrier top. These intermediate and transition state is sensitive to degree of assessment of correlation energy.

References

1) O. Kajimoto, O. Kondo, K. Okada, J. Fujikane, and T. Fueno, Bull. Chem. Soc. Jpn., **58**, 3469 (1985).

2) J. D. Mertens, A. Y. Chang, R. K. Hanson, and C. T. Bowman, Int. J. Chem. Kinet., **21**, 1049 (1989).

3) C. H. Wu, H.-t. Wang, M. C. Lin, and R. A. Fifer, J. Chem. Phys., **94**, 3344 (1990).

4) K. Yokoyama and T. Fueno, Bull. Chem. Soc. Jpn, submitted.

5) D. Poppinger, L. Radom, and J. A. Pople, J. Am. Chem. Soc., **99**, 7806 (1977).

6) S. R. Langhoff and E. R. Davidson, Intern. J. Quantum Chem., **8**, 61 (1974).

7) P. J. Bruna and S. D. Peyerimhoff, "Ab initio methods in quantum chemistry," ed. by K. P. Lawley Wiley-Interscience, New York (1987), Part 1, pp. 1-97.

8) R. J. Buenker, Intern. J. Quantum Chem., **29**, 435 (1986).

9) M. J. Frisch, J. S. Binkley, H. B. Schlegel, K. Raghavachari, C. F. Melius, R. L. Martin, J. J. P. Stewart, F. W. Bobrowicz, C. M. Rohlfing, L. R. Kahn, D. J. DeFrees, R. Seeger, R. A. Whiteside, D. J. Fox, E. M. Fleuder, S. Topiol, and J. A. Pople, GAUSSIAN 86, Carnegie-Mellon Quantum Chemistry Publishing Unit. Pittsburgh (1984), IMS version registered by N. Koga, S. Yabushita, K. Sawabe, and K. Morokuma.

10) (a) M. Dupuis, J. Rys, and H. F. King, J. Chem. Phys., 65, 111 (1976).
(b) M. Dupuis, J. D. Watts, H. O. Villar, and G. J. B. Hurst, HONDO 7, QCPE #544, Indiana University, IMS version converted by M. Aoyagi and S. Obata.

11) R. J. Buenker, "Studies in Physical and Theoretical chemistry," R. Carbo, Elsevier, Amsterdam (1982), Vol 21, pp. 17-34.

12) R. J. Buenker and R. A. Phillips, J. Mol. Struct. (Theochem), **123**, 291

(1985).

13) K. Morokuma, S. Kato, K. Kitaura, I. Ohmine, S. Sakai, and S. Obara, IMSPAK, Institute for Moleculer Science (1989).

14) J. H. Teles, G. Maier, B. A. Hess, Jr., L. J. Schaad, M. Winnewisser, and B. P. Winnewisser, Chem. Ber., **122**, 753 (1989).

15) V. E. Bondybey, J. H. English, C. W. Mathews, and R. J. Contolini, J. Mol. Spectrosc., **92**, 431 (1982).

16) M. W. Chase, Jr., C. A. Davies, J. R. Downey, Jr., D. J. Frurip, R. A. McDonald, and A. N. Syverud, "JANAF thermochemical Tables," 3rd ed, National Bureau of Standards, Washington, D. C. (1985).

17) B. K. Carpenter, N. Goldstein, A. Kam, and J. R. Wiesenfeld, J. Chem. Phys., **81**, 1785 (1984).

18) J. N. Crowley and J. R. Sodeau, J. Phys. Chem., **93**, 3100 (1989).

19) (a) G. S. Hammond, J. Am. Chem. Soc., **77**, 334 (1955).
(b) T. Fueno and M. Kamachi, Macromolecules, **21**, 908 (1988).

20) T. Fueno, J. Mol. Struct. (Theochem), **170**, 143 (1988).

21) R. Fisher and E. Bauer, J. Chem. Phys., **57**, 1966 (1972).

22) O. Kajimoto, T. Yamamoto, and T. Fueno, J. Phys. Chem., **83**, 429 (1979).

23) V. Y. Simkin, A. I. Dementev, and V. I. Pupyshev, Russ. J. Phys. Chem., **56**, 1739 (1982).

24) N. W. Winter, C. F. Bender, and W. A. Goddard III, Chem. Phys. Lett., **20**, 489 (1973).

25) M. C. Lin and S. H. Bauer, J. Chem. Phys., **50**, 3377, (1969).

26) M. H. Alexander, H. J. Werner, T. Hemmer, and P. J. Knowles, J. Chem. Phys., **93**, 3307 (1990).

27) W. Hack and K. Rathmann J. Phys. Chem., **94**, 3636 (1990).

28) E. Quinones, J. Chen, and P. J. Dagdigian, Chem. Phys. Lett., **174**, 65 (1990).

Table 1. MRDCI Energy of the HNCO Chain Isomers.

Species	STO-3G	6-31G**			
	ΔE_{PPMC} kJ/mol	E_{RHF} hartree	E_{CI} hartree	ΔE_{CI} kJ/mol	ΔE_{CCD}[a] kJ/mol
HNCO	0	-167.76602	-168.24780	0	0
HOCN	-64	.72902	.21125	96	88
HCNO	[b]	.63260	.12193	331	308
HONC	177	.63273	.10221	382	340

[a], CCD(Coupled-Cluster, Double-Excitation) energy reported by Teles et al.[14]

[b], Not examined.

Table 2. HNCO Dissociation Energies (kJ/mol) Calculated by MRDCI and the Thermochemical Data.

Products	Calcd.			Expt.[b]	
	E_{CI}	ΔE_{CI}	D_0[a]	ΔH_0	ΔH_{3000}
	hartree				
$NH(^3\Sigma^-)$ + CO	-168.11296	354	332	361	359
NCO + H	.06639	476	447	474	496
$NH(^1\Delta)$ + CO	.04531	532	510	512	510
CN + OH	.02094	596	576	574	366

a) MRDCI energy plus zero point energy relative to HNCO.

b) The enthalpy change is refered from "JANAF Thermochemical Tables".[16]

Table 3. Geometries and Energies of the Excited States for OCHN and HNCO and cyclic-HNCO.

State	R_{OC}	R_{CN}	R_{CH}	A_{OCN}	A_{OCH}	E_{UHF}	E_{CI}	ΔE_{CI}
	Å			degree		hartree	hartree	kJ/mol
OCHN								
$^1A'$	1.307	1.247	1.072	94.1	128.7	-167.70142 [a]	-168.11767	342 [b]
$^3A''$	1.236	1.354	1.085	120.8	121.8	.69776	.09085	412
$^1A''$	1.253	1.326	1.083	121.2	121.2	.66954	.08716	422
$^3A'$	1.333	1.251	1.086	126.2	111.7	.66866	.06582	478
HNCO								
$^3A''$(trans)	1.165	1.419	1.010 [c]	126.0	108.5[d]	.66650	.07998	440
Ring [e]	1.261	1.415	1.008 [c]	66.8	109.0[d]	.58786 [f]	.05575	504

[a] CAS(4,4) Energy, [b] Relative Energy to HNCO, [c] NH-Bondlength, [d] HNC Angle, [e] Oxaziridinylidene with HNCO Dihedral Angle 94.8 °, [f] RHF Energy.

Table 4. MRDCI Energies for the Transition States of Various Isomerizations.

TS	reaction	method	E_{SCF}	E_{CI}	ΔE_{CI}
			hartree	hartree	kJ/mol [a]
TS1	HNCO - OCHN	CAS(6,10)	-167.63668	-168.11305	354
TS2	OCHN - HOCN	CAS(6,10)	.62758	.08653	423
TS3	OCHN - HONC	RHF	.50022	.00423	639
TS4	HNCO - $\overline{\text{HNCO}}$	UHF	.58488	.05843	497
TS5	$\overline{\text{HNCO}}$ - HOCN	RHF	.51115	.00929	626
TS6	NH(X)+CO - HNCO(3A")	UHF	.65852	.06646	476

[a] Relative Energy to HNCO.

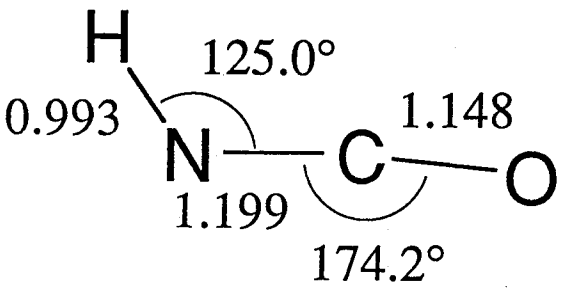

isocyanic acid

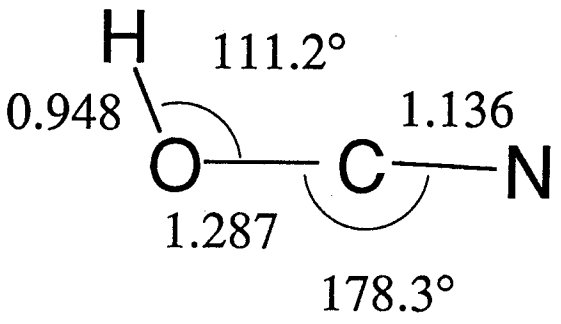

cyanic acid

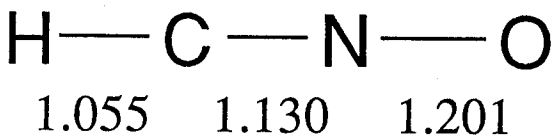

fulminic acid

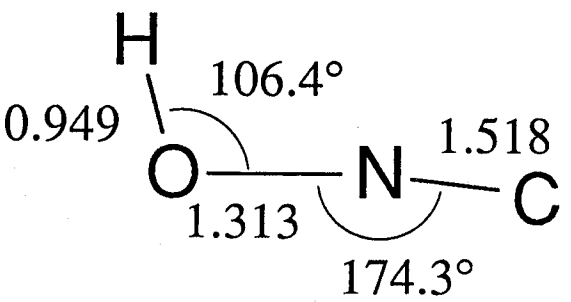

isofulminic acid

Figure 1. Optimized geometries of four chain isomers.

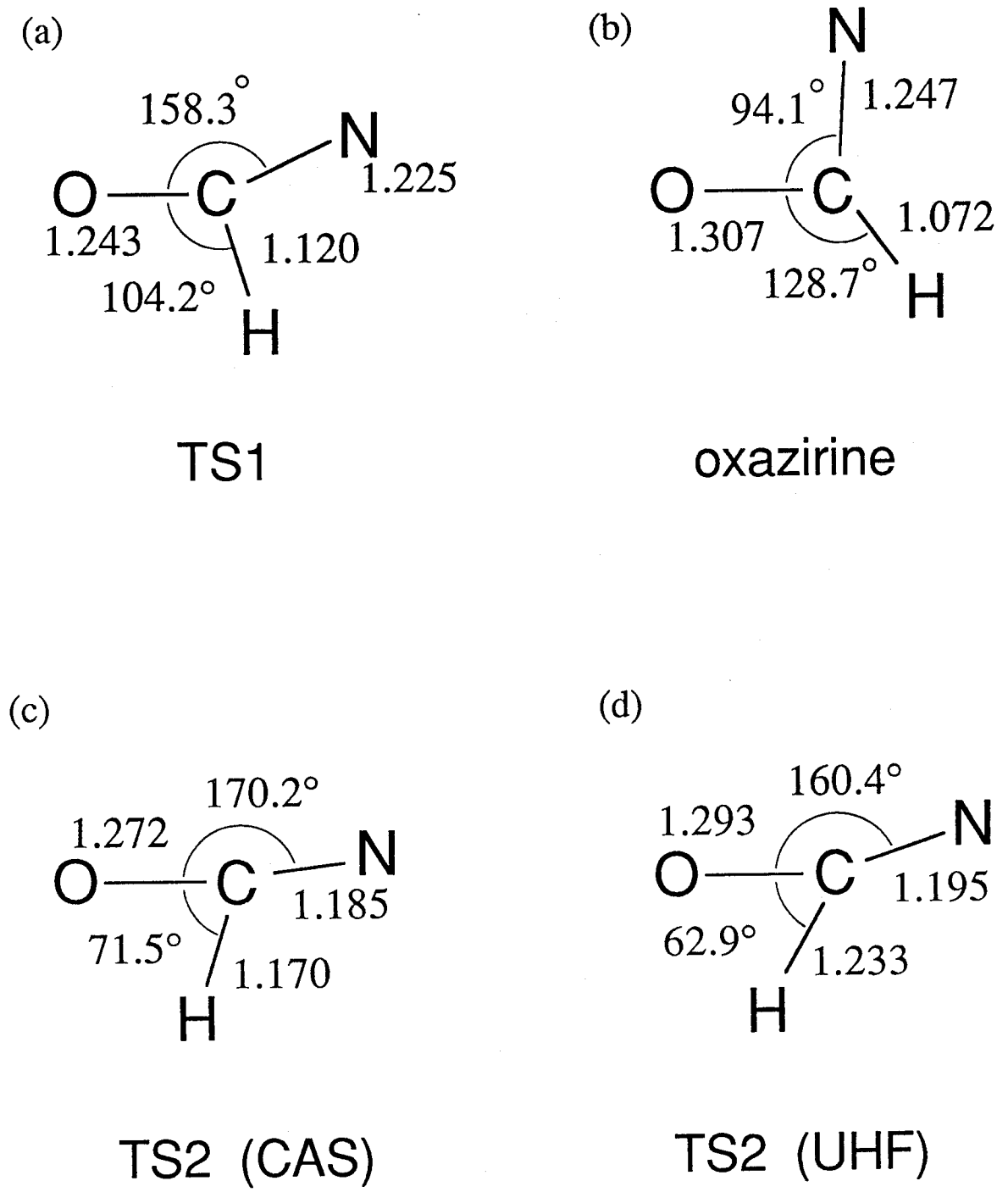

Figure 2. Optimized geometries of the stationary points on the reaction (2a). TS1, the transition state for 1,2 hydrogen migration: HNCO → oxazirine; TS2, that for 1,2 hydrogen migration: oxazirine → HOCN, calculated by CAS or UHF procedure.

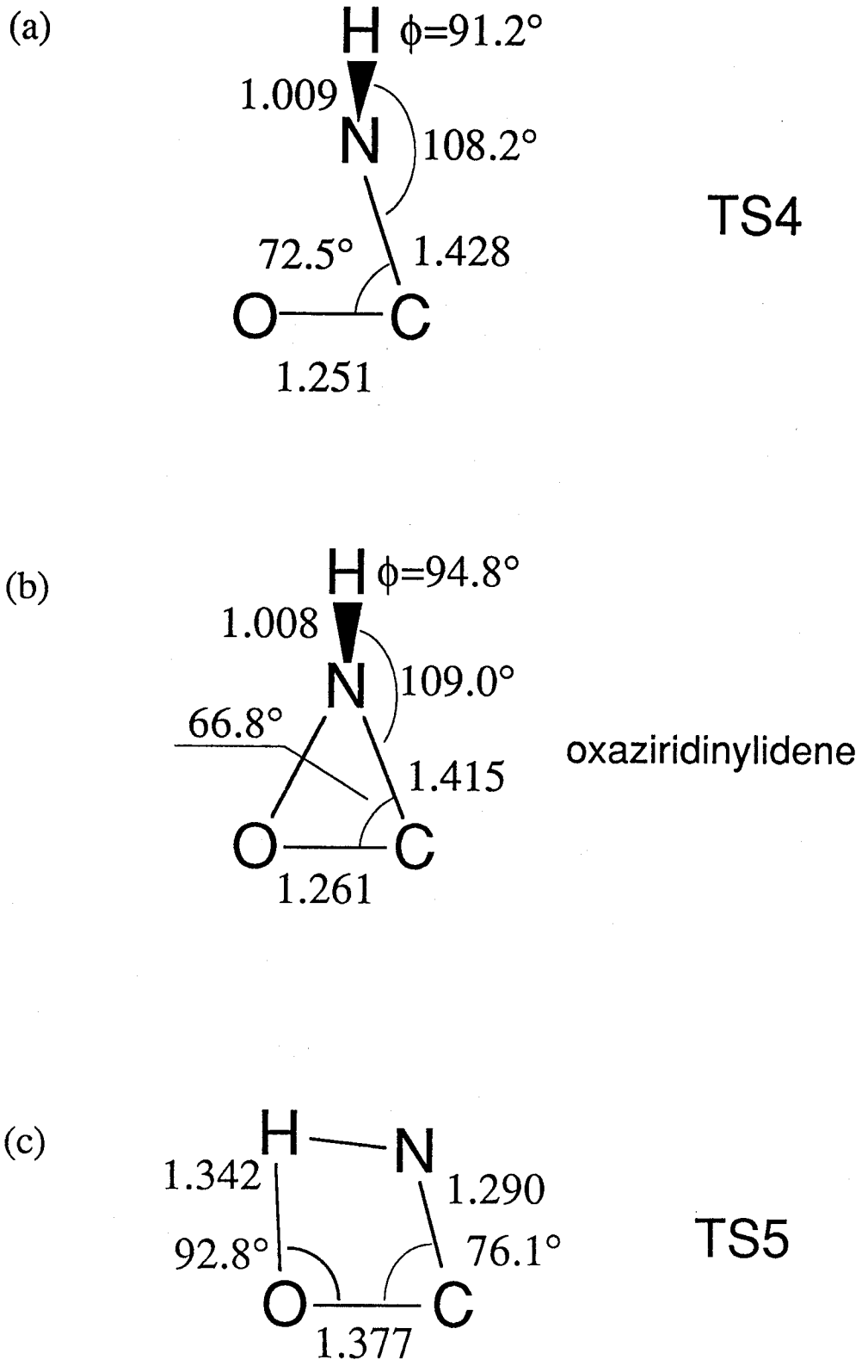

Figure 3. Optimized geometries of the stationary points on the reaction (2c). TS4, the transition state for ring closure reaction: HNCO → $\overline{\text{HNCO}}$; TS5, that for the ring-opening with 1,2-hydrogen migration reaction: $\overline{\text{HNCO}}$ → HOCN.

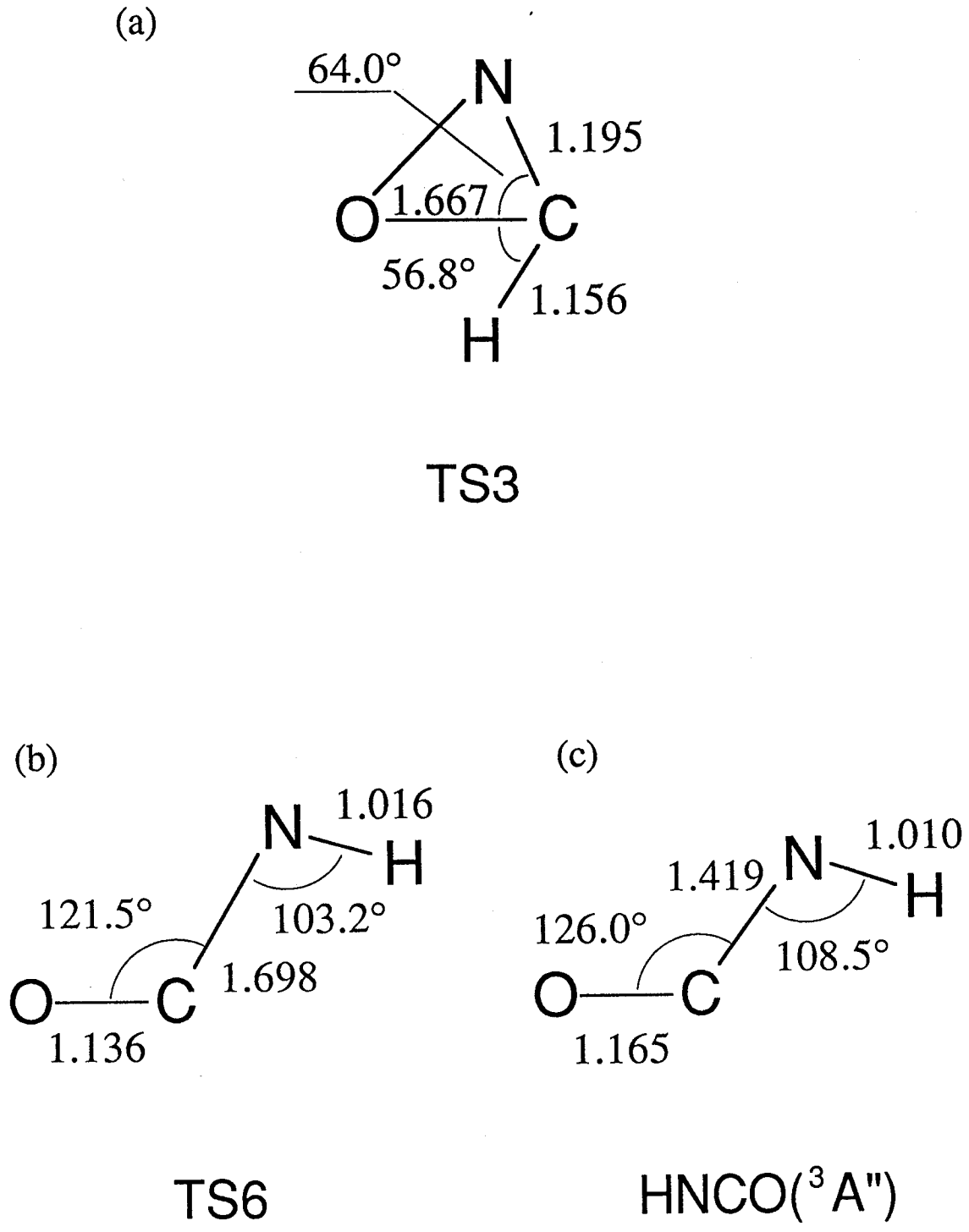

Figure 4. Optimal geometries of TS3, for the intramolecular insertion: HONC → oxazirine, and TS6, for the decomposition: $HNCO(^3A'') \rightarrow NH(^3\Sigma^-)+CO$.

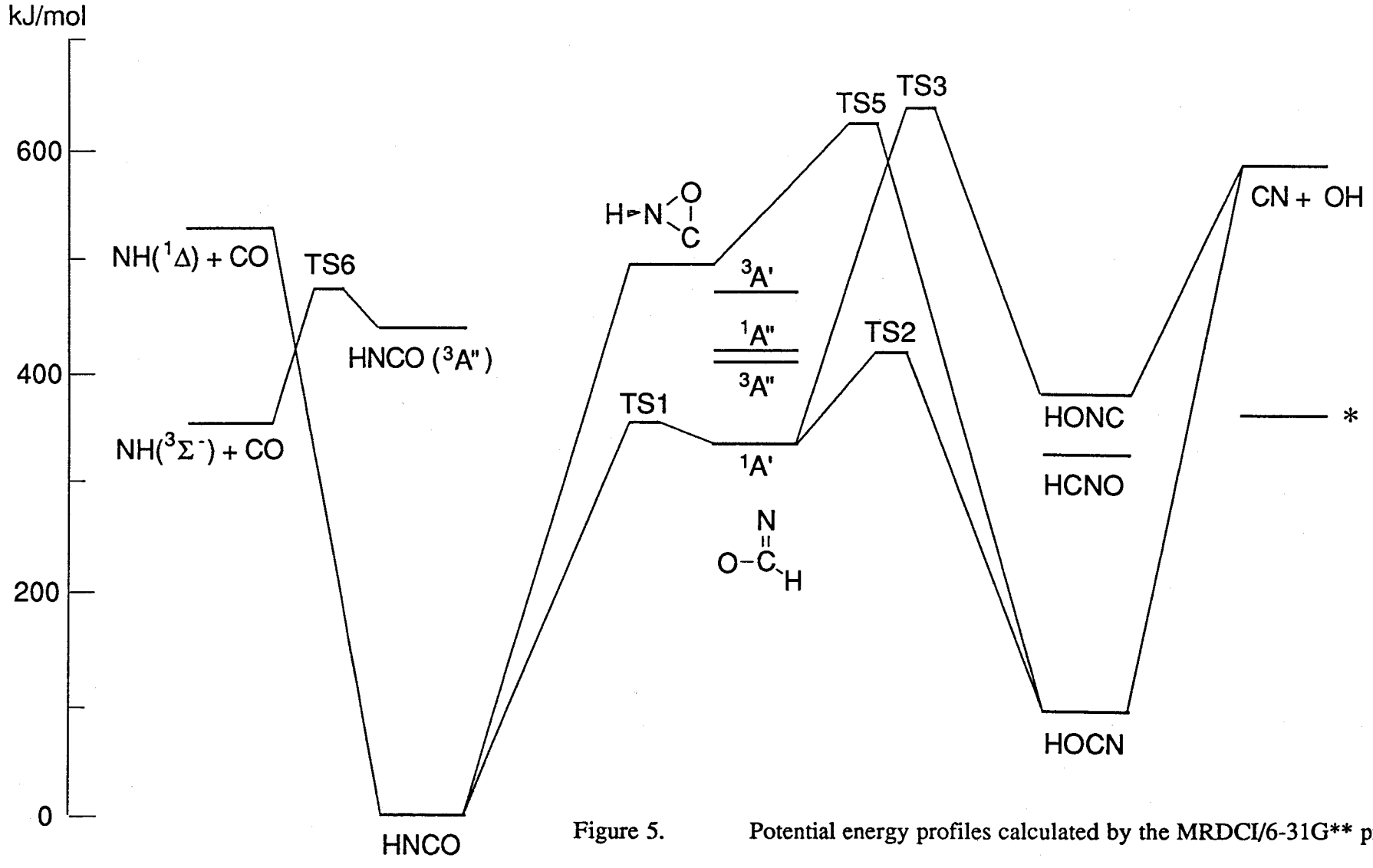

Figure 5. Potential energy profiles calculated by the MRDCI/6-31G** procedure The potential energy value designated by " * " is based on the heat of formation at 3000 K, ΔH_{3000}, referred from JANAF.[16)]

Part II

Mechanism of the Disproportionation Reaction of Nitric Oxide in the presence of the Hydrogen Atom

Chapter 1

Mechanism of the Formation of NO_2 in the Reaction of HNO with NO in the Gas Phase

Formaldehyde, methylnitrate, and ammonia were photolyzed in the presence of nitric oxide by a medium pressure mercury lamp, a low pressure mercury lamp, and a xenon flash lamp, respectively, to investigate the reaction mechanism of nitroxyl hydride HNO with NO. Product analyses based on FTIR absorption spectra exhibited large amounts of nitrogen dioxide, whose yield was estimated to be 5-16 from time-resolved absorption spectra at 420 nm in the flash photolysis of NH_3/NO gas mixtures. A chain mechanism was proposed for the reaction of hydrogen atom in rich NO gas.

1. Introduction

Behavior of the H atom in gasous NO is important in the investigations of the chemistry of gas mixtures involving NO as reactant. The most probable initial reaction is the recombination to form nitrosyl hydride HNO.[1-4)]

$$H + NO + M \longrightarrow HNO + M \qquad (1)$$

HNO is known to be unstable in the presence of excess NO.[5-8)] Stoichiometry as well as the kinetic features of the reaction

$$HNO + NO \longrightarrow \text{product} \qquad (2)$$

has long been a matter of contraversy.

The kinetics of the HNO decay due to reaction (2) was first investigated by Cheskis et al.[5)] by means of a combination of the flash photolysis with the intracavity laser spectroscopy utilizing the HNO absorption. They noted that, in the high pressure region above 600 Torr of NO, reaction (2) followed the pseudo first order decay rate of HNO, while at lower pressures the decay obeyed the second-order law in [HNO]. On the other hand, Wiebe et al.[7)] traced the yields of N2, concluding that at high NO pressures the N_2 yield depends on [NO] while at low pressures it depends on $[NO]^2$. These observations suggest the competetion between the reversible slow reation of HNO with NO (2a) followed by fast subsequent reaction (2b) and the fast bimolecular reaction of HNO (3)

$$HNO + NO \longrightarrow \text{adduct} \qquad \text{slow} \qquad (2a)$$

$$\text{adduct} + NO \longrightarrow \text{products } (N_2, NO_2) \qquad \text{fast} \qquad (2b)$$

$$HNO + HNO \longrightarrow N_2O + H_2O \qquad \text{fast} \qquad (3)$$

The products of the reaction (2) have not been established yet. Cheskis et al.[5] measured [NO_2] growth profiles and mentioned that most likely products were $HO_2 + N_2$ for the reaction (2a) and unlikely chain reactions owing to H atom reproduction.

The present work is aimed at disclosing the products and the stoichiometry of reaction (2) We used formaldehyde HCHO, methylnitrate CH_3ONO, and ammonia NH_3 as the precursors that give rise to HNO upon reactions with NO.

2. Experimental

(A) HCHO/NO

It has been established that HCHO is photolytically decomposed into both H + HCO and H_2 + CO at the spectral region of 250-350 nm.[9] HNO is produced through both the reaction (1) and (5) [10] under excessive [NO] condition.

$$\text{HCHO} \xrightarrow{h\upsilon} \text{H} + \text{HCO} \quad (4a)$$

$$\text{HCHO} \xrightarrow{h\upsilon} \text{H}_2 + \text{CO} \quad (4b)$$

$$\text{HCO} + \text{NO} \longrightarrow \text{HNO} + \text{CO} \quad (5)$$

A cross shaped cylindrical pylex cell of 15 and 11 cm in optical path length and of 35 and 25 mm in internal diameter, respectively, was used for the steady light photolysis. The windows attatched on the both sides of the cylinders were made of NaCl for the longer cylinder to transmit the IR beam and quartz for the shorter one to transmit the UV light, respectively. The UV light source used was medium-pressure mercury lamp (Ushio UM-452). A glass filter was used to transmit the UV light only in the spectral range of 280-400 nm selectively. The light was colimated by a quartz lens and led into the cell. IR absorption spectra of the photolysis gas mixtures were measured by FTIR spectrometer (JASCO FTIR-5000) in a spectral range of 500-4300 cm^{-1} with a resolution of 4cm^{-1} and calculated

from the coaddition of 100 interferograms. Sample gas mixtures composed of HCHO in a fixed pressure of 1.0 Torr and NO varing from 200 to 800 Torr were measured by a capacitance manometer (Vacuum General CMLB-10). Irradiation time was 5, 10, 15, 20, 25, 30, and 35 mins. Concentrations of HCHO, N_2O, CO, and NO_2 were obtained by measuring absorbances at 2806, 2224, 2116, and 1604 cm^{-1}, respectively. The absorption coefficients were determined in separate calibration measurements based on proportionarity between pressures and absorbances. In the calibration for CO and NO_2 absorbances an excessive amount of nitrogen gas in a pressure of ca. 500 Torr was added as a quencher. All experiments were carried out at room temperature.

(B) CH_3ONO/NO

The photolysis of CH_3ONO at 253.7 nm gives rise to NO and CH_3O. In high NO pressures most of the fragments are consumed by the recombination (7). However, a small fraction of CH_3O is converted into HNO through the reaction (8).[6)]

$$CH_3ONO \xrightarrow{h\upsilon} CH_3O + NO \qquad (6)$$

$$CH_3O + NO + M \longrightarrow CH_3ONO + M \qquad (7)$$

$$CH_3O + NO \longrightarrow HNO + HCHO \qquad (8)$$

In the CH_3ONO/NO experiment only the light source used was different from the HCHO/NO experiment. A microwave-discharged low pressure mercury lamp was used as a 253.7 nm source. To prevent the production of NO_2 via photochemical reactions [11)]

$$NO \xrightarrow{h\upsilon} NO^* \qquad (11)$$

$$NO^* + NO \longrightarrow NO_2 + N \qquad (12a)$$

$$NO^* + NO \longrightarrow N_2O + O \qquad (12b)$$

an NO gas filter of 2 cm in thickness at a pressure of 100 Torr was inserted between the lamp and the cell. The sample gases used had the following compositions: $CH_3ONO/NO=1/75$, $CH_3ONO/NO/Ar=1/73/400$, and $CH_3ONO/NO/NO_2=1/225/6$. Concentration of CH_3ONO was determined from the absorbance at 992 cm^{-1}.

(C) NH_3/NO

Photolysis of NH_3 in rich NO mixtures was adapted as the third way to investigate reaction (2). HNO is formed through reaction (1) after the photodissociation of NH_3 below 210 nm.[12)]

$$NH_3 \xrightarrow{h\upsilon} NH_2 + H \qquad (9)$$

The reaction of NH_2 with NO has been investigated thoroughly.[12)] The main products suggested to date is N_2 and H_2O at room temperature in the gas phase.

$$NH_2 + NO \longrightarrow N_2 + H_2O \qquad (10)$$

NO_2 that was produced by reaction (2) seemed to react with NH_3 heterogeniously at high NH_3 pressures, so that the steady light experiments would give incorrect results. Instead, the large dissociation cross section of NH_3 relative to other precursors used here gives a large amount of NO_2, which enabled us to conduct a flash photolysis experiment with transient absorption technique in a very easy way.

A rectangular quartz cell of 4cm × 1cm × 1cm was used for the flash photolysis. The pulse width of the xenon flash lamp was ~100 μs. Absorption at 420 ± 7 nm due to NO_2 absorption band was monitored through the longer axis of the cell using the visible light from a tungsten filament for 100-2000 ms after the pulse. The sample gas pressure was NH_3 40 Torr and NO 300-900 Torr. In order to

estimate the amount of NH_3 dissociated in a single flash a chemical actinometry was conducted with NH_3/ethylene gas mixtures.

$$C_2H_4 + H \longrightarrow C_2H_5 \quad (13)$$

$$C_2H_5 + NH_2 \longrightarrow C_2H_5NH_2 \quad (14)$$

The rate constants available in the literature[11] ensure that the addition reaction (13) dominates the recombination of H with NH_2 to reproduce NH_3. In practice gas mixtures of NH_3 40 Torr and C_2H_4 600 Torr introduced in the same cell that was used in NH_3/NO experiments were photolyzed by 50 pulses. The decrement of NH_3 was measured from the IR absorption due to NH_3 υ_1 band (3338 cm^{-1}) which came into observable spectral region of quartz window

3. Results and Discussion

(A) Photolysis of HCHO/NO and CH_3ONO/NO

It is observed that the UV irradiation of the HCHO/NO mixtures diminishes HCHO with time gives rise to CO, NO_2, N_2O, and HONO. Fig. 1 shows a representative defference spectrum of the IR absorption for the photolyzed sample gas. One of concentration-time profiles for these four species is shown in Fig. 2 where concentration is expressed by pressure. It seems that the decrement of [HCHO] is nearly equal to the increment of [CO]. More precisely, the CO yield which is defined by ϕ_{CO} = -d[CO]/d[HCHO] is found to be 0.8 at the NO pressure P_{NO}= 800 Torr. In a similar way the yield of N_2O yield is obtained to be ϕ_{N2O} = 0.12. Fig. 3 shows the NO pressure dependences of ϕ_{CO} and ϕ_{N2O}. It is evident that ϕ_{CO} approaches unity as P_{NO} increases. Decrease of ϕ_{CO} at lower P_{NO} may be due to the recombination reaction of CO with O atom generated by the NO_2 photodecomposition. A small branching ratio of the N_2O production channel does not seem to be affected by P_{NO}.

The yield of H_2 was measured by mass-spectrometric analysis. From three experiments using HCHO/NO (= 0.5 / 700 Torr) gas mixtures we evaluated ϕ_{H2}= 0.52, indicating that the reactions (4a) and (4b) occur with almost equal probabilities. The result implies that the initial yield of HNO generated from the photolysis of HCHO is about unity, because of two H atom of HCHO.

In contrast to the fairly good linearity in the time profiles of HCHO, CO, and N_2O, [NO_2] shows nonlinear growth curve, which makes us suspect existence of some NO_2-consuming processes, for example, photodecomposition or reactions with active photofragments. However, highly excessive [NO] would convert the photofragmented O atom into NO_2 rapidly through the recombination reaction. Furthermore, the observed growth curve does not look like a usual asymptotic saturation curve which should be seen if photodecomposition affected. It is hard to estimate ϕ_{NO2} from the initial slopes of the [NO_2] profile, but it seems to be more than 2.

Fig. 4 shows similar time profiles for CH_3ONO, HCHO, N_2O, and NO_2 measured in the UV irradiation of CH_3ONO/NO gas mixtures. The yields of HCHO and N_2O were ϕ_{HCHO} (=-d[HCHO]/d[CH_3ONO]) = 1.0 and ϕ_{N2O}= 0.36. Note that HCHO in this experiment plays the same role as does CO in the first experiment. [NO_2] still shows curvature in the time profiles. The value of ϕ_{NO2} estimated from the initial slopes becomes 4 at least. This large yield indicates the possibility of a chain reaction participating in the HNO decay process. Also the curvature of the [NO_2] profile implies the self-inhibition of NO_2.

From the above lines of evidence, we propose a chain mechanism of the over-all reactions (1) and (2) as follows.

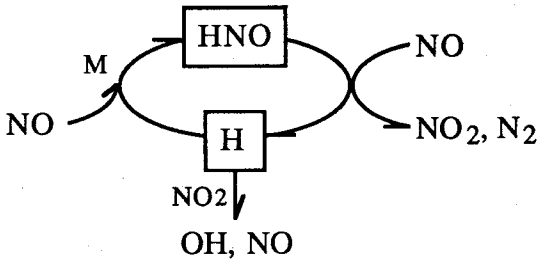

Addition of Ar into the sample gas is expected to accelarate the chain reaction through the recombination (1). On the other hand addition of NO_2 should inhibit the chain reaction through the reaction (15).

$$H + NO_2 \longrightarrow OH + NO \qquad (15)$$

These speculations have been supported by the photolysis of both $CH_3ONO/NO/Ar$ and $CH_3ONO/NO/NO_2$ gas mixtures. As can be seen in Fig. 5 addition of Ar enhanced the production of NO_2. By contrast, the photolysis of $CH_3ONO/NO/NO_2$ mixtures have exhibited decreasings of NO_2 concentration.

(B) Flash Phtolysis

To rule out secondary photochemical processes and heterogenious reactions the flash photolysis was utilized. As the life time of HNO is of the order of 100 ms under present conditions, the pulse width (~ 100 μs) is short enough to investigate the products of the reaction (2). Fig. 6 shows a typical example of the transient absorption spectra at 420 ± 7 nm. Similar absorption profiles were continueously observed up to 700 nm with slightly higher intensity around 420 nm. This feature is consistent with NO_2 absorption band. The rise time is in the same order as Cheskis reported. However, the yields of NO_2 ($\phi_{NO_2} \equiv -[NO_2]_\infty/\Delta[NH_3]$) observed here far exceed unity (see Table 1) in contrast with the results by Cheskis et al.[5] who reported ϕ_{NO_2} being nearly equal unity. The present relsults lend strong support to the chain mechanism proposed above.

4. Summary

Ultimate product analysis for successive reactions caused by hydrogen atom in the presense of nitric oxide NO was conducted by means of FTIR absorption spectroscopy in the photolysis of HCHO/NO and CH_3ONO/NO, using a medium pressure mercury lamp and a low pressure mercury lamp, respectively. In addition time-resolved visible light absorption technique was applied to monitor [NO_2] arising from the flash photolysis of NH_3/NO gas mixtures using a xenon flash lamp. It was found that at the NO pressures of 300-900 Torr the NO_2 yield was found to be large by a factor of 5-16 times relative to the amount of the H atom produced.

References

1) F. C. Kohout and F. W. Lampe, J. Chem. Phys., **46**, 4075 (1967).

2) N. Washida, H. Akimoto, and M. Okuda, J. Phys. Chem., **82**, 2293 (1978).

3) K. Oka, D. L. Singleton, and R. J. Cvetanovic, J. Chem. Phys., **66**, 713 (1977).

4) S. P. Walch and C. M. Rohlfing, J. Chem. Phys., **91**, 2939 (1989).

5) S. G. Cheskis, V. A. Nadtochenko, and O. M. Sarkisov, Int. J. Chem. Kinet., **13**, 1041 (1981).

6) R. R. Baldwin, A. Gethin, J. Plaistone, and R. W. Walker, J. Chem. Soc. Faraday Trans., I, **71**, 1265 (1975).

7) H. A. Wiebe and J. Heicklen, J. Am. Chem. Soc., **95**, 1 (1973).

8) J. L. Holmes and E. V. Sundaram, Trans. Faraday Soc., **62**, 1822 (1966).

9) M. C. Dodge and T. Hecht, Int. J. Chem. Kinet. Symp., **1**, 155 (1975).

10) B. Veyret and R. Lesclaux, J. Phys. Chem., **85**, 1918 (1981).

11) H. Okabe, "Photochemistry of Small Molecules", Wiley-Interscience Publication (1978) pp 171-177.

12) (a) J. A. Silver and C. E. Kolb, J. Phys. Chem., **86**, 3240 (1982).

(b) J. A. Silver and C. E. Kolb, J. Phys. Chem., **91**, 3713 (1987).

(c) L. J. Stiff, W. D. Brobst, D. F. Nava, R. P. Borkowski, and J. V. Michael, J. Chem. Soc. Faraday Trans., 2, **78**, 1391 (1982).

(d) C. F. Melius and J. S. Binkley, 20 th Symp. (Internat.) on Combustion, Combustion Inst., Pittsburgh (1984), p. 575

(e) B. Atakan, A. Jacobs, M. wahl, R. Weller, and J. Wolfrum, Chem. Phys. Lett., **155**, 609 (1989).

13) F. Westley, "Table of Recommended Rate Constants for Chemical Reactions Occurring in Combustion," National Bureau of Standards, Washington, D. C. (1980).

Table 1. Yield of NO_2 in the Fash Photolysis of $NH_3/NO/SF_6$ Gas Mixtures.

No.	P_{NH3} / Torr	P_{NO} / Torr	P_{SF6} / Torr	ϕ_{NO2} / -
061701	43	938	0	16.2
061702	43	924	0	13.0
120901	47	644	0	12.3
120902	39	672	0	8.7
011901	39	336	385	10.3
011902	39	287	434	6.5
011904	39	294	336	4.9
011905	40	280	119	14.6
012601	39	364	378	8.1
012602	40	322	294	6.5
012603	39	329	140	8.4
012604	39	0	70	0.0
012605	43	322	84	9.7
012606	39	336	392	5.5
012607	0	336	434	0.0

$\phi_{NO2} \equiv -[NO_2]_\infty/\Delta[NH_3]$

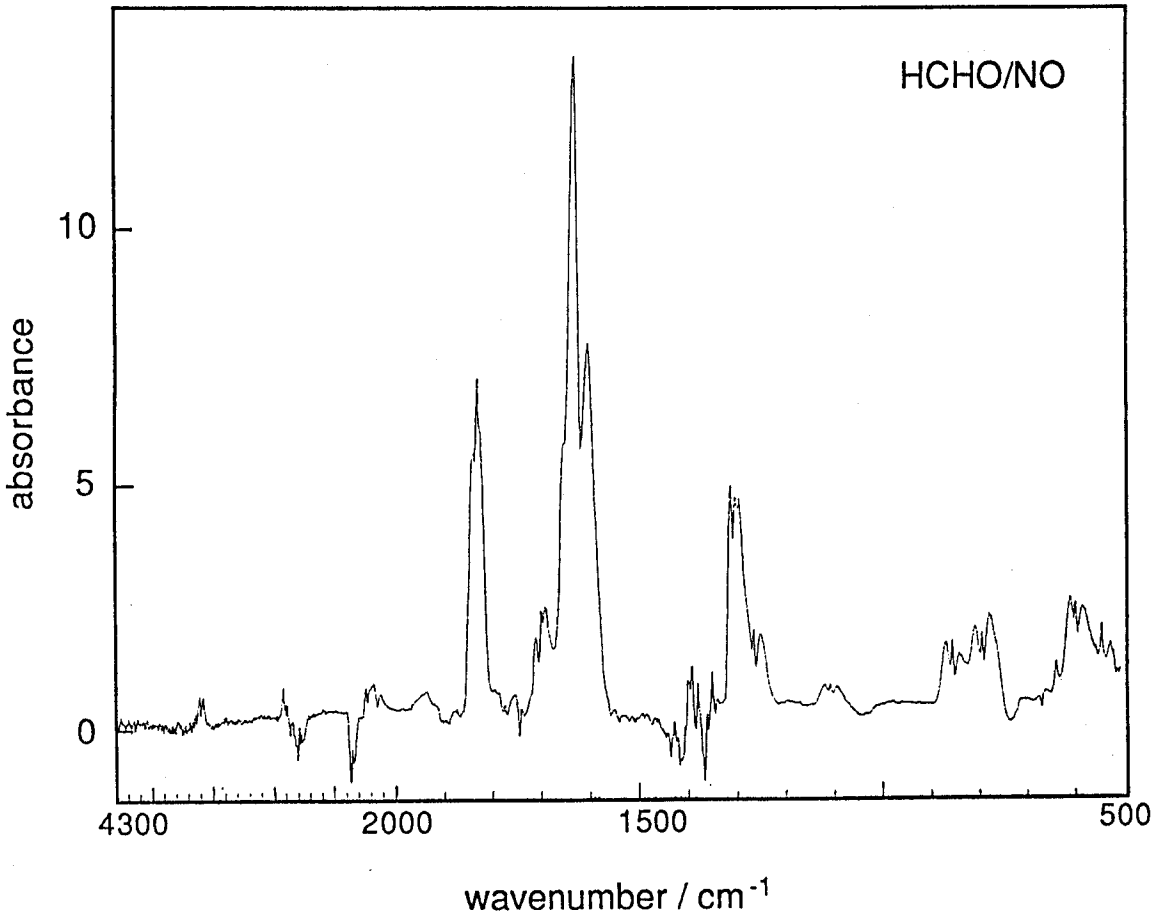

Figure 1. Difference spectrum of IR absorption of the HCHO/NO mixture after 35 mins photolysis.

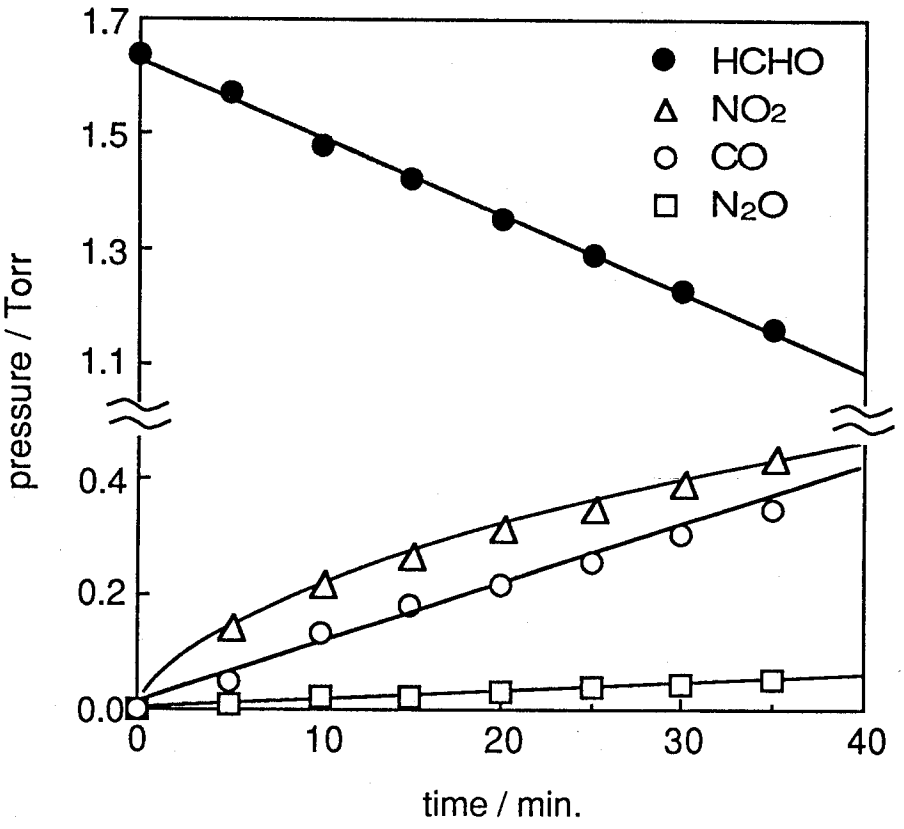

Figure 2. Concentration-time profile in the photolysis of HCHO/NO mixture.

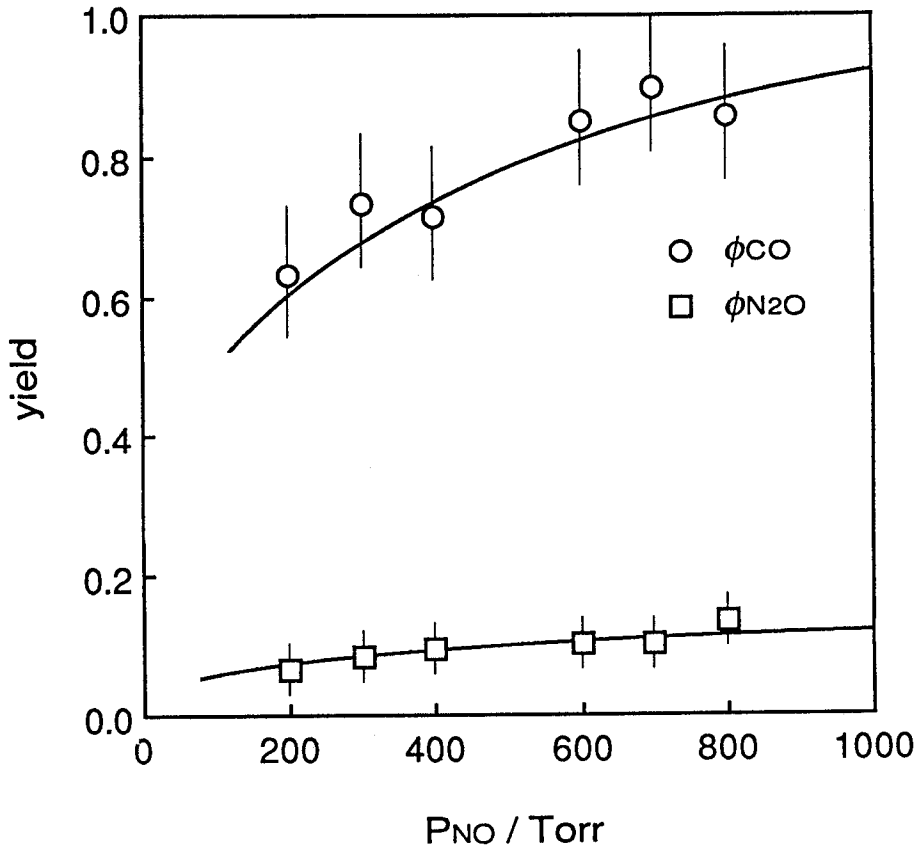

Figure 3. Pressure dependence of the CO and N_2O yield in the photolysis of HCHO/NO mixtures (P_{HCHO}= 1 Torr).

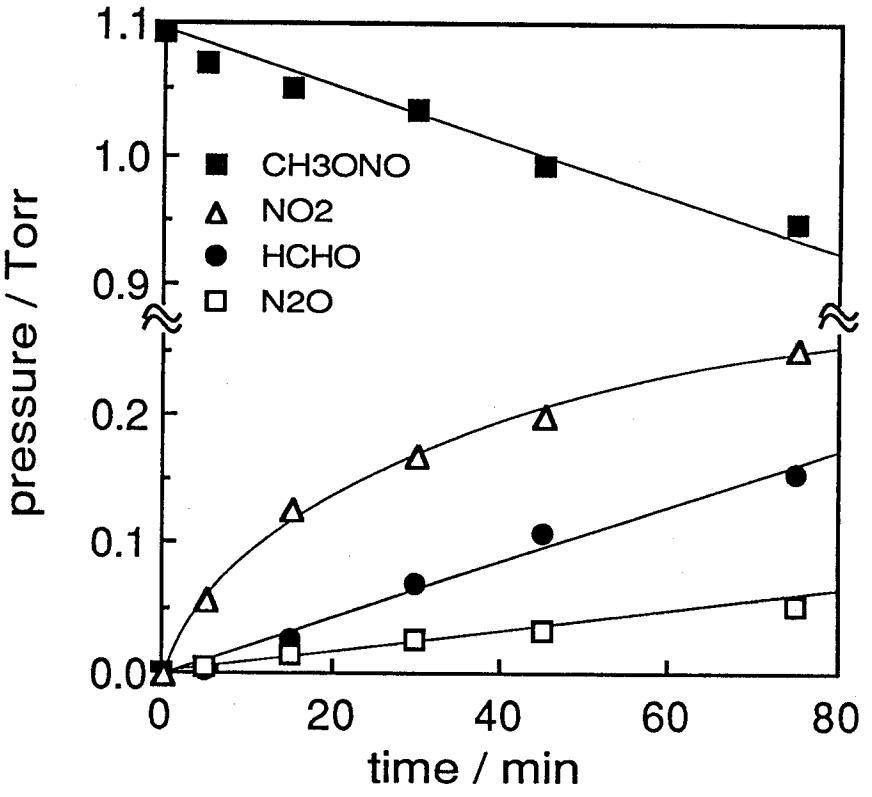

Figure 4. Concentration-time profile of the products in the photolysis of CH_3ONO/NO mixture (1.1 / 600 Torr).

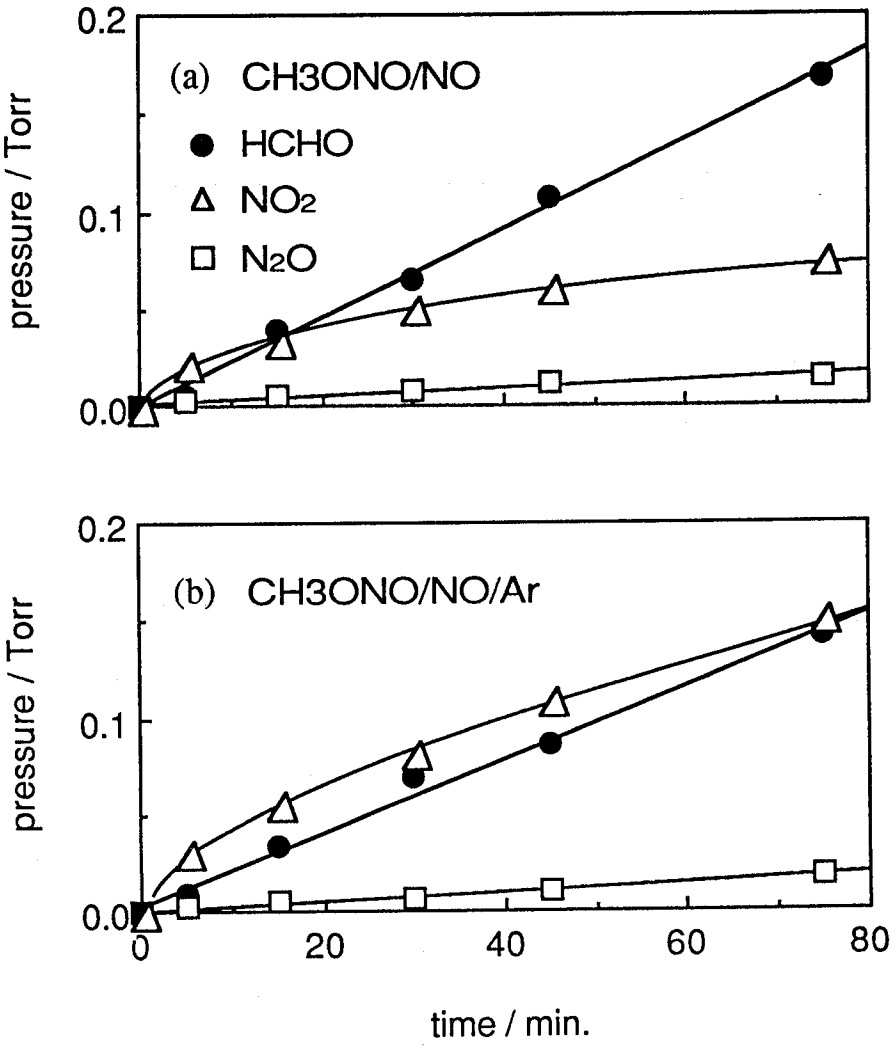

Figure 5. Effect of argon as a quencher on the NO_2 profile.

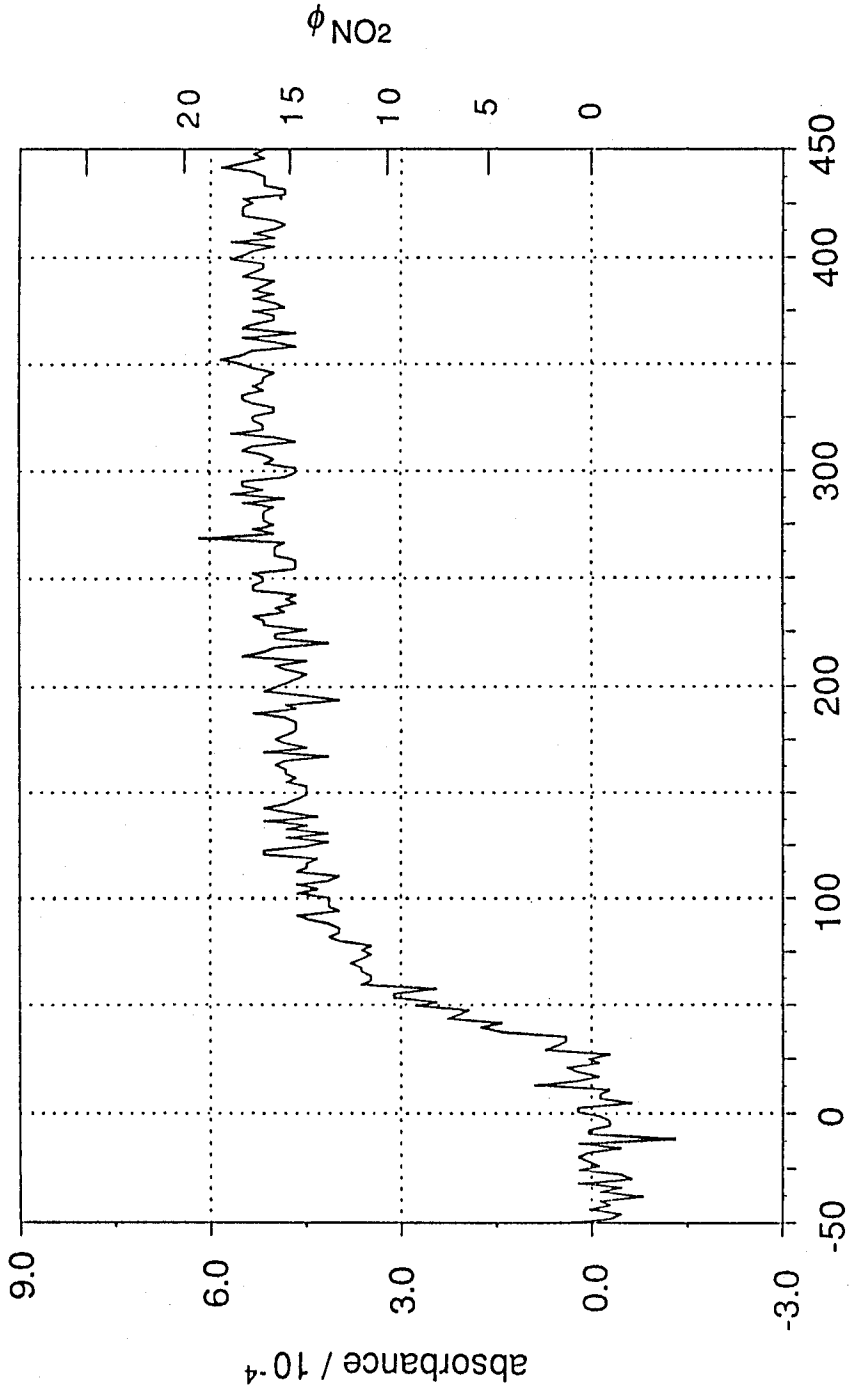

Figure 6. Transient absorption spectrum at 420 nm in the flash photolysis of NH3/NO mixture (43 / 938 Torr).

Chapter 2

Potential Energy Profiles for the Reaction of HNO with NO

Theoretical calculation involving the approximately projected unrestricted Møller Plesset perturbation theory at second order (APUMP2) was performed to investigate the mechanism of the reaction of HNO with NO and the reactions expected to take place subsequently under excess NO conditions. The calculated potential energy profiles have revealed a possiblility of the production of the H atom, which have strongly supported the chain mechanism proposed in chapter 1. The elucidated mechanism would proceed with a stoichiometry of $H + 4NO \longrightarrow H + N_2 + 2NO_2$.

1. Calculations

Main feature of the chain mechanism proposed in chapter 1 is intermediacy of the H atom, which would be consumed by the recombination with NO;

$$H + NO + M \longrightarrow HNO + M \qquad (1)$$

and which would be reproduced by the successive reactions of HNO with some NO to produce NO_2. However the reactions have not been well defined. Thus the mechanism is worth being explored by theoretical calculations to confirm the experimental results.

We have carried out ab initio MO calculations on the energetics relevant to the reaction:

$$HNO + NO \longrightarrow \text{adduct} \qquad (2)$$

in order to explore energetically accessible root for the chain reaction. Geometry-optimization procedures were employed with 6-31G** basis set and correlation energies were estimated by Approximately Projected Unrestricted Møller-Plesset perturbation theory at second order (APUMP2) for open shell species and restrected MP2 (RMP2) for closed shell species. Optimized geometries for 13 stationary points including two saddle points are given in Fig. 1. SCF and APUMP energies for these structures are listed in Table 1. On the basis of these energies we can depict a reaction mechanism where H atom is reproduced.

$$HNO + NO \longrightarrow \mathbf{1} \quad (2a)$$

$$\mathbf{1} + NO \longrightarrow [\mathbf{5}]^* \longrightarrow HNNO + NO_2 \quad (2b)$$

$$HNNO + NO \longrightarrow [\mathbf{11}]^* \longrightarrow N_2H + NO_2 \quad (2c)$$

$$N_2H \longrightarrow N_2 + H \quad (2d)$$

Fig. 2 shows potential energy diagram for HNO + NO system. The first step of the reaction (2) is adduct formation. We examined the lowest electronic state for the adduct **1**, utilizing APUMP2/3-21G** for energy evaluation at the geometry of minimum energy points obtained by UHF/3-21G optimization. Adiabatic excitation energy for three low-lying excited states are listed in Table 2. The electronic ground state has Cs symmetry with 5 π electrons (^{2}A"). Also we examined cis isomers **2** and N-O adducts **3**, where "cis" is defined with respect to ONNO skeleton and "N-O" means addition onto O atom in HNO. Consequently the structure **1** as can be seen in Fig. 1 was found to be the most stable structure with ^{2}A" electronic state. The stabilization energy for the addition (2a) is small (-21 kJ/mol) based on APUMP2 energies. This value may suggest reversibility of the reaction (2a) unless large activation energy is required for the addition-dissociation step.

A transition state structure was found by UHF/6-31G** calculation and designated by **TS1** in Fig. 1. The barrier height relative to HNO + NO level is 82 kJ/mol (APUMP2). TS1 connects HNO(X^1A') + NO with the adduct in its first excited state (^{2}A") while the ground adduct **1** is found to correlate to HNO(a^3A") + NO on the UHF surface. In reality, however, both states should be confused and the ground adduct **1** is thought to be connected with the ground HNO + NO via TS1.

The rate constant of the reaction (2) has been reported to be $k_2 = 3.0 \times 10^5$ $cm^3mol^{-1}s^{-1}$ at room temperature.[1] From this value the activation energy can be estimated to fall into 40 ~ 50 kJ/mol, if the preexponential factor is assumed to be $10^{13\sim14}$ $cm^3mol^{-1}s^{-1}$. The calculated barrier height (82 kJ/mol) is pretty high

relative to that estimated here. Taking it into account that UHF calculation failed in tracing the course of the reaction, the TS1 geometry and energy may be improved by more sofisticated treatment like a CASSCF procedure. Anyway the first step of the reaction (2) forms **1**.

Decompostion of **1** into N_2O + OH or N_2 + HO_2 needs rearrangement of **1** to **4** before dissociation. The potential energy of **4** is slightly higher (18 kJ/mol) than HNO + NO level. It is unlikely that the transition state of this rearrangement comes below that of the first step. On the other hand it is likely that association reaction with another NO molecule proceeds without significant activation energy as can be seen in ordinary radical-radical association reactions.

With respect to the association step we examined three adducts including two N-O adducts and one N-N adduct. The N-N adduct is found to have relatively high energy as compared to N-O adducts. Two lower energy structure relative to **1** + NO level are shown in Fig. 1 (**5** and **7**). Many geometrical isomers and isomerizations are possible, such as **6**, **8**, **9**, and TS2, the transition state between **7** and **9** (see Fig. 3). But we think that the third step is fragmentation of **5** into HNNO(**12**) + NO_2, because, if products levels are energetically accessible, fragmentations tend to require less or no activation energy than isomerizations. Also from the viewpoint of activation entropy fragmentations are advantageous. In addition NO_2 is the species observed in the experiments.

We examined two HNNO isomers (**11** and **12**). Both of them are planer and the ground electronic states are $^2A'$. As can be seen in Fig. 3 **12** is more stable than **11**. We will denote **12** as HNNO. Therefore the third step, i.e. fragmentation from **5** , will give HNNO + NO. Ab initio CI study for HNNO [2] revealed that HNNO would be thermally stable. Thus HNNO is supposed to react with the third NO molecule.

The fourth step is another association of HNNO with NO. This process also expected not to have significant barrier. One of the structure for the adducts is given in Fig. 1 (**10**). As can be expected from the long distance of the center N-O

bond (1.456 Å), the adduct will dissociate to N_2H and NO_2 again (see Fig. 4). This dissociation step will be able to proceed with excess energy in the fourth association step. Finally, it is known that N_2H dissociates to N_2 and H atom.[3] This H atom can form HNO and next cycle starts again.

2. Conclusion

The theoretical calculation was carried out with APUMP2 method. The results indicate that the chain mechanism predicted in chapter 1 will progress as following schemes.

$$H + NO + M \longrightarrow HNO + M$$
$$HNO + NO \longrightarrow HN_2O_2$$
$$HN_2O_2 + 2NO \longrightarrow H + N_2 + 2NO_2$$

In other words, disproportionation of NO effectively occurs in the presence of the H atom.

References

1) S. G. Cheskis, V. A. Nadtochenko, and O. M. Sarkisov, Int. J. Chem. Kinet., **13**, 1041 (1981).

2) T. Fueno, M. Fukuda, and K. Yokoyama, Chem. Phys., **124**, 265 (1988).

3) S. F. Selgren, P. W. Mcloughlin, and G. I. Gellene, J. Chem. Phys., **90**, 1624 (1989).

4) M. W. Chase, Jr., C. A. Davies, J. R. Downey, Jr., D. J. Frurip, R. A. McDonald, and A. N. Syverud, "JANAF thermochemical Tables," 3rd ed, National Bureau of Standards, Washington, D. C. (1985).

Table 1

APUMP2 Energies of Stationary Points.

Compounds	6-31G**		
	SCF	APUMP2	ΔE_{APUMP2}
	hartree	hartree	kJ/mol
HNO + NO	-259.03699	-259.68524	(0)
1	-259.03946	-259.69330	-21
2	-259.03660	-259.69142	-16
3	-259.00285	-259.65463	80
4	-259.03819	-259.67857	18
TS1	-259.00171	-259.59980	82
1 + NO			(0)
5	-388.22776	-389.25226	-4
6	-388.20961	-389.26116	-28
7	-388.21972	-389.26419	-35
8	-388.23979	-389.27475	-64
9	-388.26134	-389.28301	-85
TS2	-388.12742	-389.18279	178
10	-313.42103	-314.27452	-
11	-184.20906	-184.66909	-
12	-184.21210	-184.70192	-

Table 2

Excitation Energies for the Excited States of **1**.

State	3-21G**//UHF/3-21G		
	UHF	APUMP2	ΔE_{APUMP2}
	hartree	hartree	kJ/mol
$^2A''$	-257.70588	-258.34415	(0)
$^2A''$	-257.68879	-258.31887	58
$^2A'$	-257.67218	-258.27867	172
$^2A'$	-257.66463	-258.26153	217

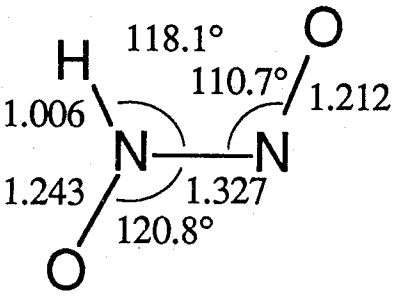

1

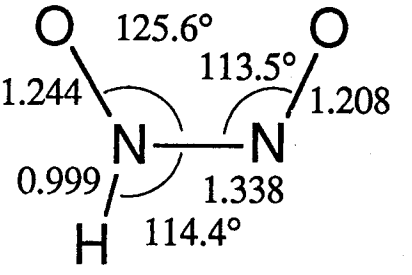

2

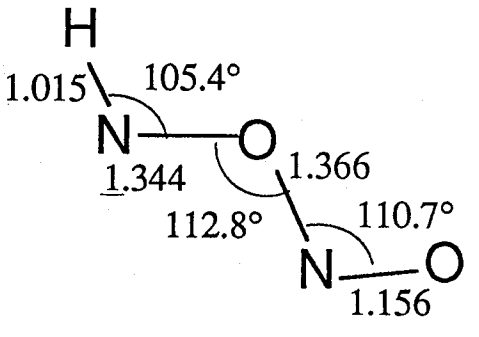

3

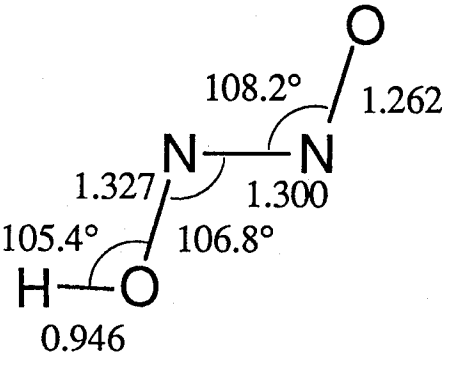

4

Figure 1. Optimized geometries of the stationary points.

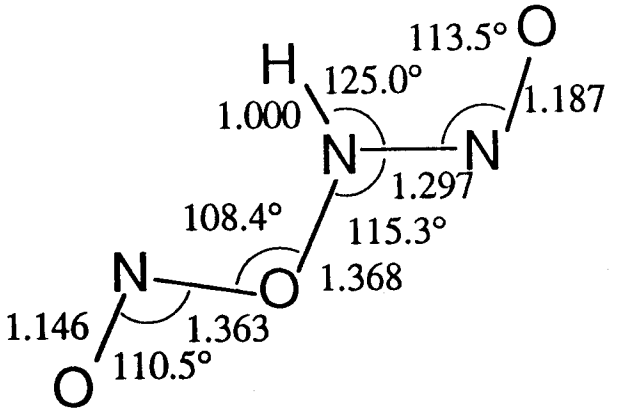

5

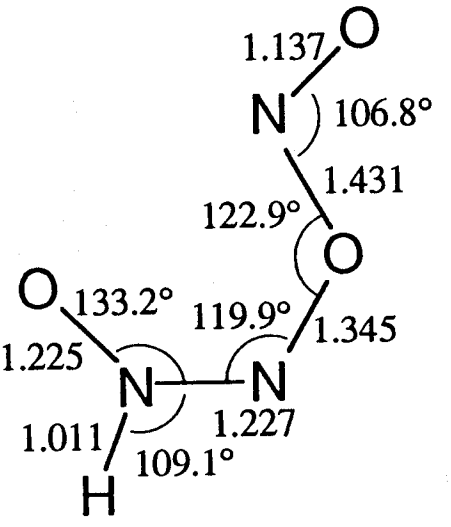

6

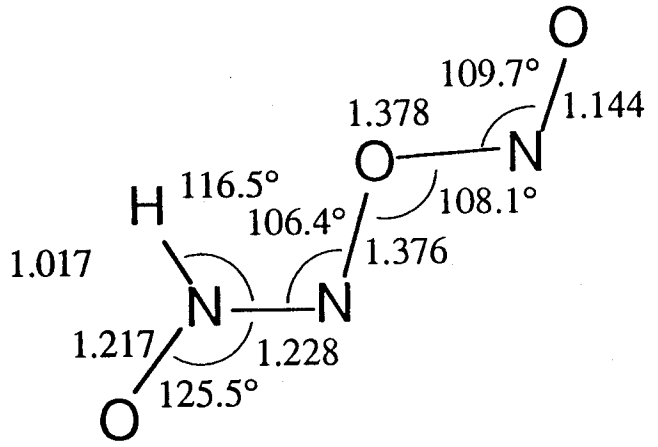

7

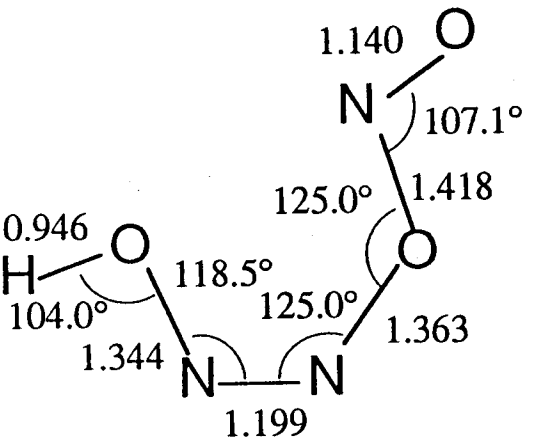

8

Figure 1. (continued)

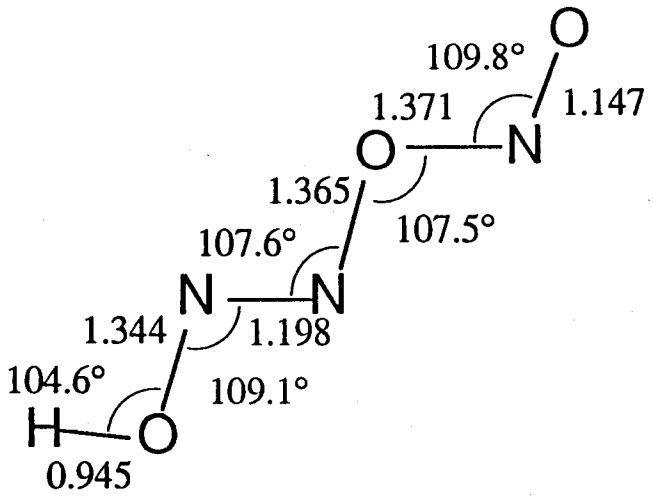

9

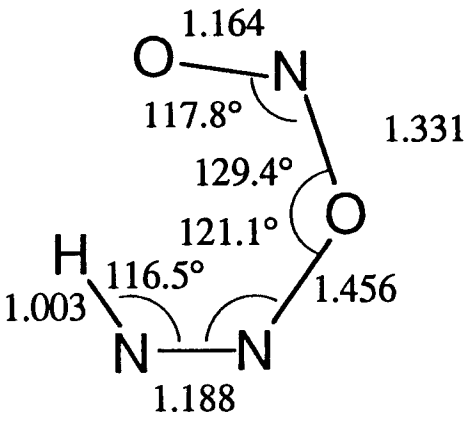

10

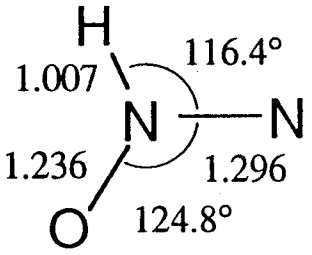

11

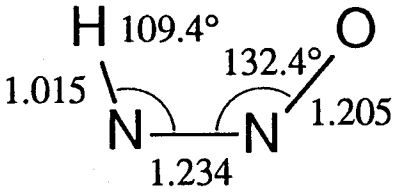

12

Figure 1. (continued)

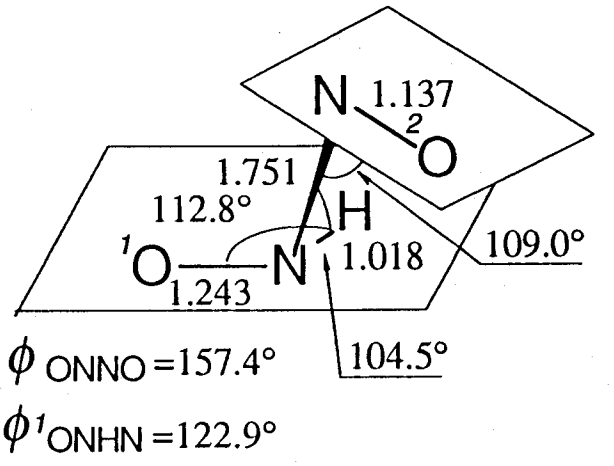

TS1

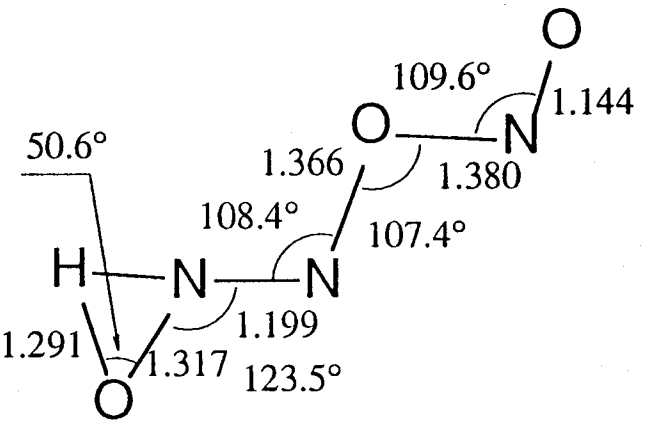

TS2

Figure 1. (continued)

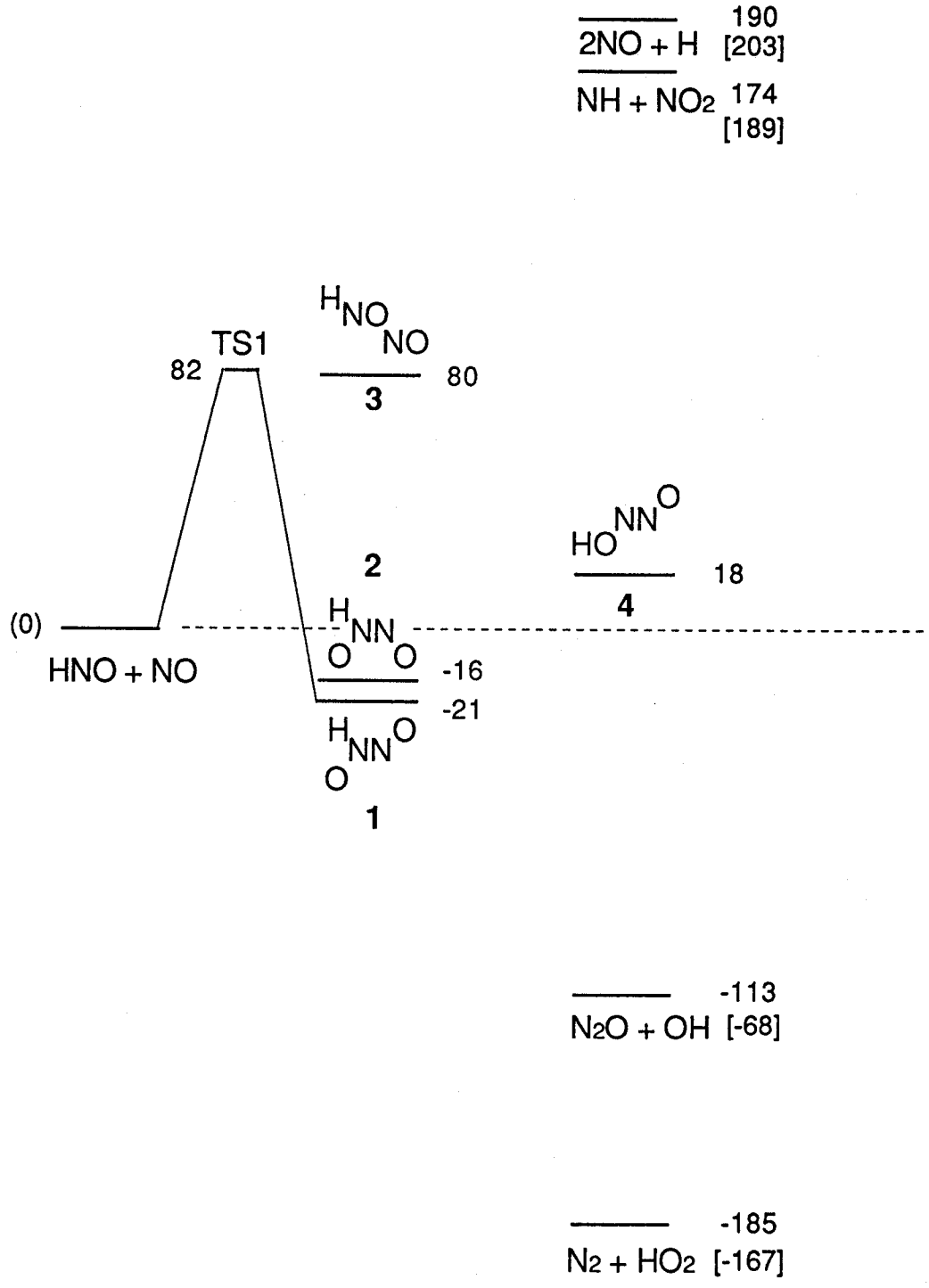

Figure 2. Potential energy diagram for HNO + NO system.

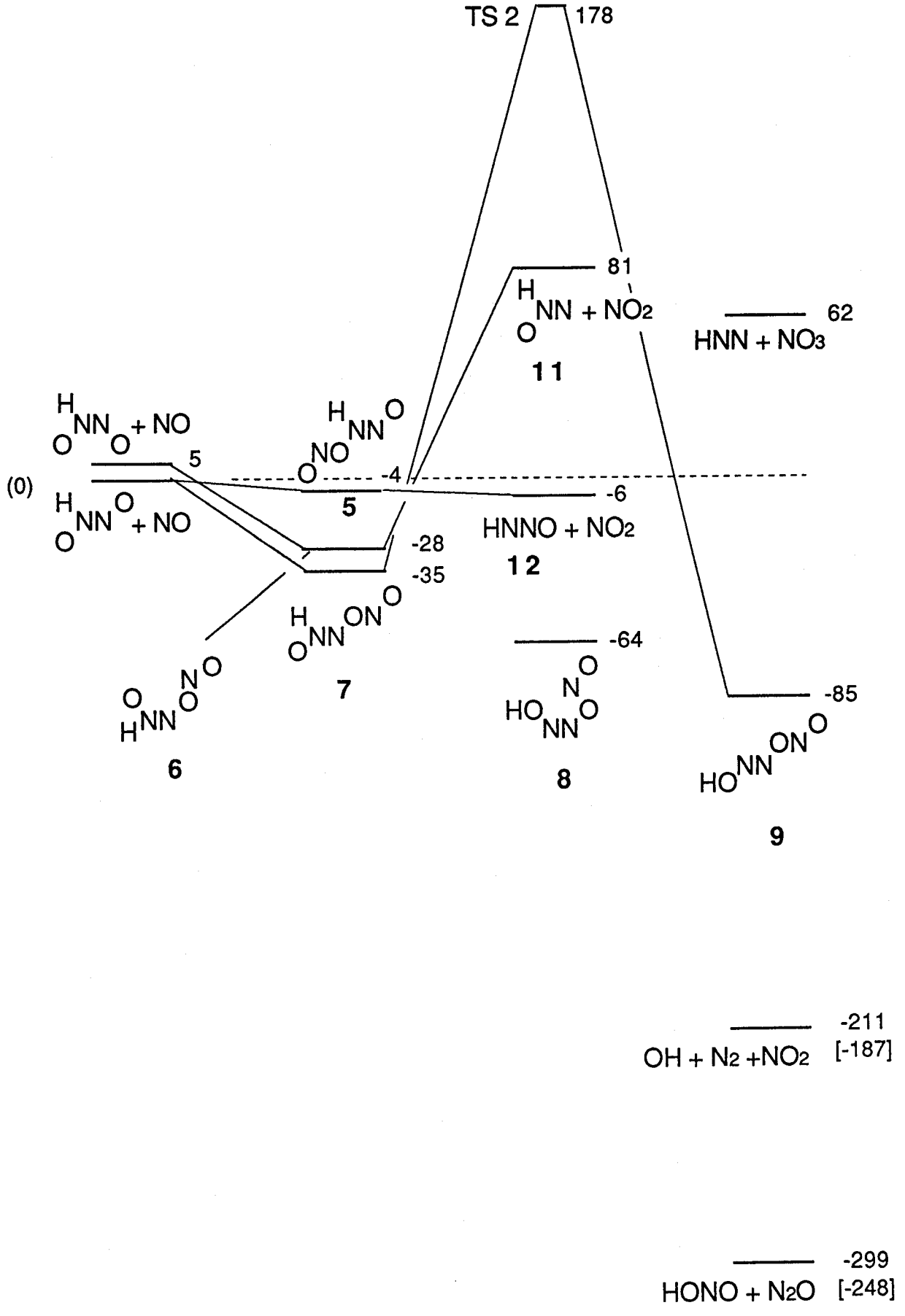

Figure 3 Potential energy diagram for HNO + 2NO system.

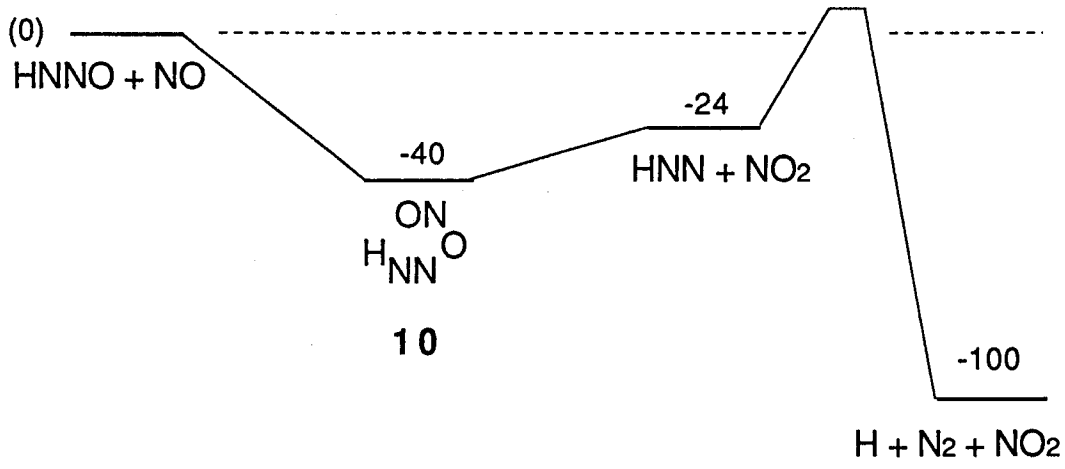

Figure 4. Potential energy diagram for HNNO + NO system.